UNIVERSITÀ DEGLI STUDI DI MILANO

PhD course in Molecular and Cellular Biology

XXXI Cycle

"Two Clade III GLUTAMATE RECEPTOR-LIKE isoforms inversely regulate local and long-distance Ca^{2+} signalling in *Arabidopsis thaliana*"

Fabrizio Gandolfo Doccula

PhD Thesis

Scientific supervisor: Prof. Alex Costa

Scientific tutor: Dr. Maria Cristina Bonza

Academic year: 2018/2019

Index

Abstract (Italian version)

Nel sistema nervoso centrale, i Recettori del Glutammato sono canali tetramerici attivati da ligandi amino acidici. Ad oggi risultano tra i canali meglio caratterizzati perché coinvolti nell'apprendimento, nella memoria e in malattie neurodegenerative come l'Alzheimer. Anche le piante possiedono geni che codificano per Recettori del Glutammato (GLRs) che sono implicati nella regolazione dell'apertura stomatica, nell'accrescimento del tubetto pollinico, nella segnalazione a lunga distanza, nello sviluppo della radice e nella difesa contro patogeno. Tuttavia, poco si conosce riguardo il loro funzionamento, inclusa l'attivazione, il trasporto ionico, la desensitizzazione, la localizzazione sub-cellulare, l'interazione tra diverse subunità etc. Essendo putativi canali attivati da ligando e putativamente permeabili al Ca^{2+}, abbiamo saggiato l'ipotesi che due GLR di Arabidopsis, AtGLR3.3 e AtGLR3.7 (AtGLR3.x), potessero svolgere un ruolo nella genesi/regolazione di transienti di Ca^{2+} intracellulare in seguito a stimolazione con amino acidi. In questo lavoro dimostriamo che piante selvatiche di Arabidopsis mostrano un aumento del Ca^{2+} citosolico nelle cellule dell'apice radicale quando trattate con amino acidi e che questo fenomeno è dipendente dalla presenza del GLR3.3 e regolato dal GLR3.7. La mancanza del GLR3.3 porta all'abolizione dei transienti di Ca^{2+} laddove al contrario mutazioni del GLR3.7 li aumenta. Inoltre, il doppio mutante *glr3.3glr3.7* si comporta come il singolo *glr3.3*, con una totale abolizione della risposta agli amino acidi. Questi risultati permettono di ipotizzare che i AtGLR3.x possano formare un canale eteromerico, in cui il GLR3.3 funzioni da impalcatura e il GLR3.7 ne regoli negativamente le proprietà biofisiche. Abbiamo inoltre appurato che la distruzione di AtGLR3.x influenza la generazione e propagazione delle onde di Ca^{2+} a lunga distanza che esistono tra l'apice fiorale e lo stelo quando questo è soggetto a stress da calore.

Nel prossimo futuro i nostri sforzi saranno finalizzati a comprendere il ruolo funzionale della percezione degli amino acidi da parte di GLR3.x nel meccanismo di segnalazione a lunga distanza.

Abstract (English version)

In the central nervous system, ionotropic Glutamate Receptors (iGluRs) are tetrameric ligand-gated non-selective cation channels. They have been linked to learning and memory as well as to neurodegenerative pathologies such as Alzheimer disease. Thus, they are among the best characterized channels in animals. Animals and plants share this class of proteins. Plant Glutamate Receptors-like (GLRs) have been implicated in stomata movement regulation, pollen tube growth, long-distance signalling, root development and defence against pathogens. However, to date few details are known about their basic properties and functions, such as binding activity, ion transportation, sub-cellular localization, subunits interaction, desensitization etc. My PhD project focused on two GLR isoforms in *Arabidopsis thaliana*, AtGLR3.3 and AtGLR3.7 (hereafter called 'AtGLR3.x'). Being putative amino acids-gated Ca^{2+}-permeable channels, I tested the hypothesis that the two isoforms could handle Ca^{2+} dynamics upon amino acids challenge. Remarkably, Arabidopsis Col-0 plants show a transient elevation of cytosolic Ca^{2+} at the root tip meristematic zone upon amino acids treatment. Ablation of the AtGLR3.3 abolished the increase of Ca^{2+} concentration whereas *loss-of-function* mutants for AtGLR3.7 showed enhanced Ca^{2+} rises in response to amino acids. Additionally, when the double mutant *glr3.3glr3.7* was challenged with amino acids, mirrored the *glr3.3* null-response. These results strongly suggested that the two AtGLRs could assemble in a channel where GLR3.3 would act as main scaffold and GLR3.7 would negatively regulate the biophysical properties. Being AtGLR3.x also expressed in the vascular tissues and in the cells of the floral abscission zone, we also assayed the role of AtGLR3.x in the generation/propagation of long-distance Ca^{2+} waves that occurs between stems and inflorescence apexes of Arabidopsis plants subjected to flaming.

In the future, our efforts will be aimed at understanding whether the predicted amino acid sensing of GLRs is also required for the long-distance signalization.

Chapter I. Bibliographic introduction

I1. Electrical signals in higher plants

I.1.1 Three different electrical signals have been reported to occur in plants

Being sessile, it is essential for a plant to perceive external cues (locally) and trigger long- intercellular signals (systemically) with the final aim to adapt to the new environmental condition (Peña-Cortés, Fisahn and Willmitzer, 1995; Schilmiller and Howe, 2005). Plant cells have evolved sophisticated signals to transfer information throughout the plant body, such as Calcium ion (Ca^{2+}), Reactive Oxygen Species (ROS), Nitric Oxide (NO) and Electrical Signals (ES) (Gilroy *et al.*, 2016; Choi *et al.*, 2017). Three different electrical signals have been reported to occur in plants: Action potential (AP), Variation potential (VP) and System Potential (SP) (Vodeneev, Akinchits and Sukhov, 2015).

i) AP have been linked to non-damaging cues such as cold and touch. AP relies on a single transient depolarization of the plasma membrane (Fisahn *et al.*, 2004) and shows different dynamics when compared to the VP (Fromm and Bauer, 1994) (Fig. 1).

ii) VP is a transient depolarization of the plasma membrane with unpredictable shape, which could last for several minutes. VP has been proved to be activated by damaging external stimuli such as wounding and flaming (Dziubinska *et al.*, 2003).

iii) SP is activated by a plethora of external stimuli. In contrast to AP and VP, SP consists of a transient hyperpolarization of the plasma membrane most likely driven by H^+-ATPases activation (Zimmermann *et al.*, 2009).

It has been shown that ES could modulate physiological processes in plants such as gene expression, root absorption, photosynthesis regulation, phloem transport, hormones synthesis and activation of respiration (Filek and Kościelniak, 1997; Sukhov *et al.*, 2012; Vodeneev, Akinchits and Sukhov, 2015). Differently from AP, VP is not subjected to the 'all-or-not-law', i.e. the VP parameters can directly have effects on plant physiological events (Vodeneev, Opritov and Pyatygin, 2006; Felle and Zimmermann, 2007). Flaming is the most common external cue known to induce VP in a great variety of higher plants such as cucumber, barley, wheat, sunflower, tomato, fava bean, tobacco, soybean, pumpkin and pea (Vodeneev, Akinchits and Sukhov, 2015). Wounding injury or cutting can also induce VP in pea, sunflower and maize, but not in other species such as tomato and wheat (Vodeneev *et al.*, 2012; Vodeneev, Akinchits and Sukhov, 2015). For this reason, flaming is the most conmmonly

used stress to trigger VP. VP is a long-term depolarization of the plasma membrane that could remain sustained for several minutes, it reaches high amplitudes (tens of mV) with a propagation speed rate of $mm \cdot s^{-1}$ (Vodeneev *et al.*, 2011, 2012). VP can include two different components: the first one, that is always present, is a sustained depolarization while the second one is the presence of spikes similar to AP (Dziubińska, Trębacz and Zawadzki, 2001) (Fig. 1). However, VP can occur also without AP-like spikes (Stahlberg and Cosgrove, 1997). The generation of sustained depolarization and or AP-like spikes may occur in the same plant and it depends on the intensity of the damage and on the distance from the local zone of injury. Amplitude and speed propagation of VP are inversely proportional to the distance from the local damage site (Vodeneev, Akinchits and Sukhov, 2015). In wheat and pumpkin, it has been estimated that the decrement in amplitude is 10% cm^{-1} (Vodeneev *et al.*, 2011). In fact, the amplitude of VP is directly proportional to the intensity of the damage (Vodeneev *et al.*, 2012). Moreover, VP has been shown to propagate even through dead injured tissues (Evans and Morris, 2017).

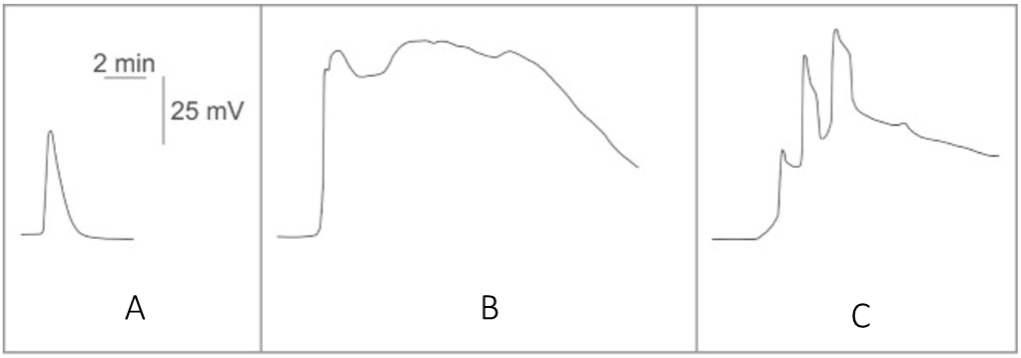

Fig. 1. Action and variation potentials in hypocotyl of pumpkins seedlings induced by different external stimuli. A. Action potential recorded upon ice treatment. **B.** Variation potential recorded upon leaf flaming. **C.** Variation potential showing AP-like spikes upon leaf flaming. Electrical signals were recorded 7cm far from the local site of stress. Pictures from Vodeneev *et al.*, 2015 (Vodeneev, Akinchits and Sukhov, 2015).

I.I.2 Variation potential generation: how is generated?

Pharmacological studies support the hypothesis that plasma membrane H^+-ATPases inactivation is essential for VP generation (Frachisse, 1992). Sodium orthovanadate treatment, an inhibitor of H^+-ATPases, decreased both VP amplitude and depolarization/ripolarization rates (Katicheva *et al.*, 2014). Conversely, VP amplitude increased upon fusicoccin administration (a proton pump activator) (Vodeneev, Akinchits and Sukhov, 2015). Additionally, external and internal pH changes modulate VP generation. In fact, VP generation is accompanied with apoplast pH alkalinization (magnitude of 0.2-0.7 change in pH unit) (Grams *et al.*, 2009; Sukhov *et al.*, 2014). Similarly, a decrease of 0.3-0.6 pH unit was monitored in the cytoplasm during VP generation (Grams *et al.*, 2009; Sukhov *et al.*, 2014). Indeed, pharmacological increase of the plasma membrane permeability by administrating the protonophore carbonyl cyanide m-chlorophenyl hydrazone (CCCP) decreased VP amplitude (Frachisse, 1992). These evidences are in accordance with the involvement of H^+-ATPases inactivation during VP generation (Vodeneev, Akinchits and Sukhov, 2015). Proton pump inactivation leads to depolarization of the plasma membrane. Ca^{2+} is another player in the VP generation/regulation. Dissipating the electrochemical gradient for Ca^{2+} or inhibiting Ca^{2+}-permeable channels decreases VP amplitude or blocks VP generation in pumpkins, wheat, burley and tomato (Frachisse, 1992; Zimmermann *et al.*, 2009; Katicheva *et al.*, 2014). The activation of Ca^{2+}-permeable channels is predicted to be the first step required for the plasma membrane depolarization and H^+-ATPases inactivation (Vodeneev *et al.*, 2011; Sukhov *et al.*, 2013; Katicheva *et al.*, 2014). Moreover, Ca^{2+} influx could in turn activate Cl^- and K^+ channels (Sukhov *et al.*, 2013). This would generate AP-like spikes and fast depolarization of the plasma membrane. H^+-ATPases inactivation, instead, would be responsible for a long-sustained plasma membrane depolarization (Sukhov *et al.*, 2013). Remarkably, Ca^{2+} influx would be responsible for both proton pump's inactivation and K^+ and Cl^- channels' activation (Vodeneev, Akinchits and Sukhov, 2015) (Fig. 2).

I.I.2 Variation potential generation: how is propagated?

As presented above, one of the characteristics of VP is its fast propagation within plant tissues which can also overcome injured tissues (Evans and Morris, 2017). Two main different explanations have been proposed for VP propagation. These hypotheses argue for VP propagation *via* specific factors, that is or hydraulic wave or a chemical agent (Mancuso, 1999; Vodeneev, Akinchits and Sukhov, 2015; Evans and Morris, 2017). Some studies would also support a combination of the two signals (Malone, 1994). Evidences in favor of the hydraulic wave would be a change in stem or leaves thickness elicited

by local damage which mirror a change in hydraulic pressure in the plant body (Malone, 1992; Stahlberg and Cosgrove, 1997; Mancuso, 1999; Vodeneev *et al.*, 2012). In fact, the local damage would increase locally the hydraulic pressure and then propagate as hydraulic wave (Vodeneev, Akinchits and Sukhov, 2015). However, the speed propagation of the hydraulic wave is similar to the speed rate propagation of sound in a water solution (*circa* 1500m·s^{-1}), i.e. at least hundred thousand higher than VP propagation rate (in the range of mm·s^{-1}) (Vodeneev, Akinchits and Sukhov, 2015). Some authors suggested that the lower speed propagation of VP would be linked to a lag-phase which would anticipate the starting point of VP propagation (Stahlberg and Cosgrove, 1997). The chemical hypothesis, instead, is based on chemical synthesis or leaking which would move through the xylem triggering locally depolarization of the membrane (Malone, 1996; Vodeneev, Akinchits and Sukhov, 2015). The nature of this chemical is still unknown. The chemical should be synthesised/released rapidly upon the damage, easily propagated in the xylem tissues and should trigger depolarization of the plasma membrane (Vodeneev, Akinchits and Sukhov, 2015). It has been suggested that cell wall constituents such oligosaccharides, hormons such as jasmonate, ethylen and abscisic acid could work as depolarizing chemicals (Vodeneev, Akinchits and Sukhov, 2015). Recently, hydrogen peroxide (H_2O_2) has been shown to be released at the local damaged site and trigger an ES (Mittler *et al.*, 2011). H_2O_2 could active Ca^{2+}-permeable channels which could depolarize the membrane, leading to VP generation and propagation (Demidchik, 2003; Kwak, Nguyen and Schroeder, 2006; Mazars *et al.*, 2010) (Fig. 2). Water soluble substances such as fluorescent dyes can be propagated through the plant body with a speed propagation similar to VP (Rhodes, Thain and Wildon, 1999; Vodeneev *et al.*, 2012). Molecular diffusion of these compounds has to be discarded (slow rate). However, the increase in the hydraulic pressure could sustain the relatively fast movement of the chemical, thus supporting VP propagation as a combination of hydraulic wave and depolarizing factor (Malone, 1994) However, according to the Evans and Morris model, mass flow could explain chemical agent transportation rate through the xylem more than pressure wave or chemical diffusion (Evans and Morris, 2017) (Fig. 2).

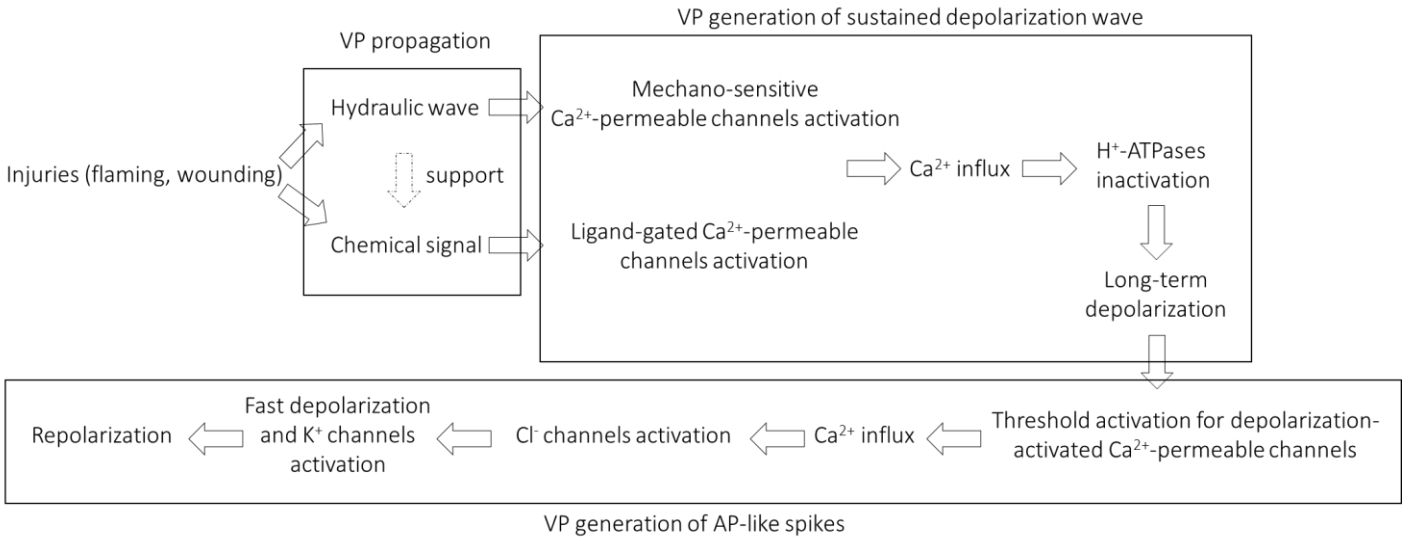

Fig. 2. Hypothetical representation of variation potential propagation and generation. Local damage may induce hydraulic wave propagation and/or chemical agent leaking which would activate mechano-sensitive and ligand-gated Ca^{2+} permeable channels, respectively. Plasma membrane depolarization due to Ca^{2+} influx would in turn lead to H^+-ATPases inactivation, with a following long-term depolarization of the plasma membrane and depolarization-activated Ca^{2+} channels activation. Cl^- and K^+ channels activation would re-polarize the membrane potential to the pre-stimulus resting level. Edited from Vodeneev *et al.,* 2015 (Vodeneev, Akinchits and Sukhov, 2015).

I.2. Shaping the 'Ca^{2+} signature'

I.2.1. Calcium as a widespread second messenger

Ca^{2+} shows two positive charges in its most external orbital. These two positive charges can be coordinated by free phosphate molecules present in a cell as inorganic phosphate (P_i) and eventually precipitate as Ca^{2+} phosphate which could be cytotoxic. Moreover, for a cell, phosphate sequestration and starvation would in turn result in energetic deficit and eventually cell death. For this reason, Ca^{2+} must be maintained in a concentration range which is not potentially dangerous for a cell (nM range) (Dodd, Kudla and Sanders, 2010). It has been estimated that whenever the Ca^{2+} concentration is maintained for a sustained time window higher than 10^{-4}M this would be sufficient for irreversible cellular injury (Costa, Navazio and Szabo, 2018). Cytosolic free Ca^{2+} concentration must be tightly regulated in a cell. Remarkably, environmental or endogenous stimulus can trigger an elevation of the cytosolic Ca^{2+} concentration (Monshausen, 2012). Thus, in almost all physiological systems a transient elevation of cytosolic Ca^{2+} concentration can be used as a message to decode

cues. A toolkit of proteins which are directly or indirectly activated by Ca^{2+} then activate downstream responses, including regulation of gene expression, that is essential for a long-term plant acclimation (Xiong *et al.*, 2006). As outlined above the nature of a Ca^{2+} increase has to be transient and relatively fast (within minutes) to prevent toxic effects (Evans, McAinsh and Hetherington, 2001). On a single cell level, external and internal stimuli have to be perceived and integrated to trigger fast responses or long-term acclimation. Dynamic changes in free Ca^{2+} concentration play a key role in transducing environmental cues and endogenous signals. Several external cues have been reported to induce in different cell types oscillationts of the cytosolic Ca^{2+} concentration that vary in amplitude, frequency and duration. This Ca^{2+} fingerprint associated to each stimulus has been called 'Ca^{2+} signature'. Channels, pumps, transporters and receptors ensure, together with a plethora of Ca^{2+}-binding proteins, Ca^{2+} homeostasis, signal perception and transduction (Trewavas *et al.*, 1996; DeFalco, Bender and Snedden, 2010).

I.2.2. General players of plant Ca^{2+} signalling

In plants, the transient nature of the Ca^{2+} elevation is mediated by transmembrane and cytosolic proteins which mediate the influx and efflux of Ca^{2+} ions (Behera *et al.*, under second round of revision in TPC; Dodd, Kudla and Sanders, 2010). Ca^{2+}-permeable channels establish an hydrophilic path for Ca^{2+} diffusion which move down its electrochemical gradient. Nearby a patch of membrane cytosolic Ca^{2+} elevation can move from 10^{-7}M cytosolic Ca^{2+} resting concentration to 10^{-6}M within milliseconds (McAinsh and Pittman, 2009). These Ca^{2+}-permeable channels localized at the plasma membrane would facilitate Ca^{2+} influx from the apoplast. However, channels can be also resident at the inner membranes, such as those surrounding the endoplasmic reticulum (ER), Golgi apparatus, mitochondria, chorolopasts, peroxisomes and vacuole (Stael *et al.*, 2012). So far, channels selective only for Ca^{2+} have not been identified in plant yet (Swarbreck, Colaco and Davies, 2013). In fact, in most of the cases channels which mediate Ca^{2+} fluxes are also permeable to other ions thus considered non-selective cation channels. However, homology-based analyses (with known animal Ca^{2+}-permeable channels) and experimental available data allows to identify plant Ca^{2+}-permeable channel candidates which belong to the Glutamate Receptor-like gene (GLRs) (Wudick *et al.*, 2018a), Cyclic Nucleotide Gated Channels (CNGCs) (DeFalco, Moeder and Yoshioka, 2016), Mechanosensitive channels (MSCs) (Hamilton, Schlegel and Haswell, 2015) and the Annexin gene families (Davies, 2014).

Whereas channels allow Ca^{2+} influxes into the cytosol, cytosolic buffers (Navazio *et al.*, 2002) and Ca^{2+} efflux systems are necessary to maintain the low resting cytosolic Ca^{2+} concentration before and after a stimulus-triggered cytosolic Ca^{2+} increase (Bose *et al.*, 2011). Ca^{2+}-ATPases (ACA and ECA) are the major active transport systems which ensure the compartmentalization of this cation (Geisler *et al.*, 2000; Frei dit Frey *et al.*, 2012; Costa *et al.*, 2017). Again, apoplast, vacuole and ER are the major extra and intra-cellular compartments which act as a Ca^{2+} storage, respectively. Cation/proton exchangers (CAX) (Pittman and Hirschi, 2016) and Cation/Ca^{2+} exchangers (CCX)(Corso *et al.*, 2018) are other molecular players involved in cytosolic Ca^{2+} efflux and homeostasis. Additionally, nucleus, mitochondria and chloroplasts can also accumulate and release Ca^{2+} in the cytosol generating their own 'Ca^{2+} signature' (Costa, Navazio and Szabo, 2018). In this context, Two Pore Channel 1 (TPC1) (Peiter *et al.*, 2005; Choi *et al.*, 2014; Kiep *et al.*, 2015; Vincent *et al.*, 2017; Hedrich *et al.*, 2018) and the Mitochondrial Calcium Uniporter (MCU) (Wagner *et al.*, 2015; Teardo *et al.*, 2017) have an impact on organelle Ca^{2+} dynamics and, more in general, in cytosolic Ca^{2+} homeostasis.

Once Ca^{2+} has entered into the cytosol its rises and the consequent Ca^{2+} signatures have to be perceived and potentially decoded by sensors. In plants, Ca^{2+}-dependent protein kinases (CDPKs) are primary decoders together with the Ca^{2+}-and calmodulin-dependent protein kinases (CCaMKs), while Calmodulin (CaM), Calmodulin-like proteins (CML), Calcineurin B-like proteins (CBL) act as Ca^{2+} signal relays. These sensors directly bind Ca^{2+} through EF-hand motifs and activate a cascade of events which eventually result in a change of gene expression and adaptation to environmental cues (Tang and Luan, 2017; Charpentier, 2018; Kudla *et al.*, 2018; Lenzoni, Liu and Knight, 2018) (Fig. 3).

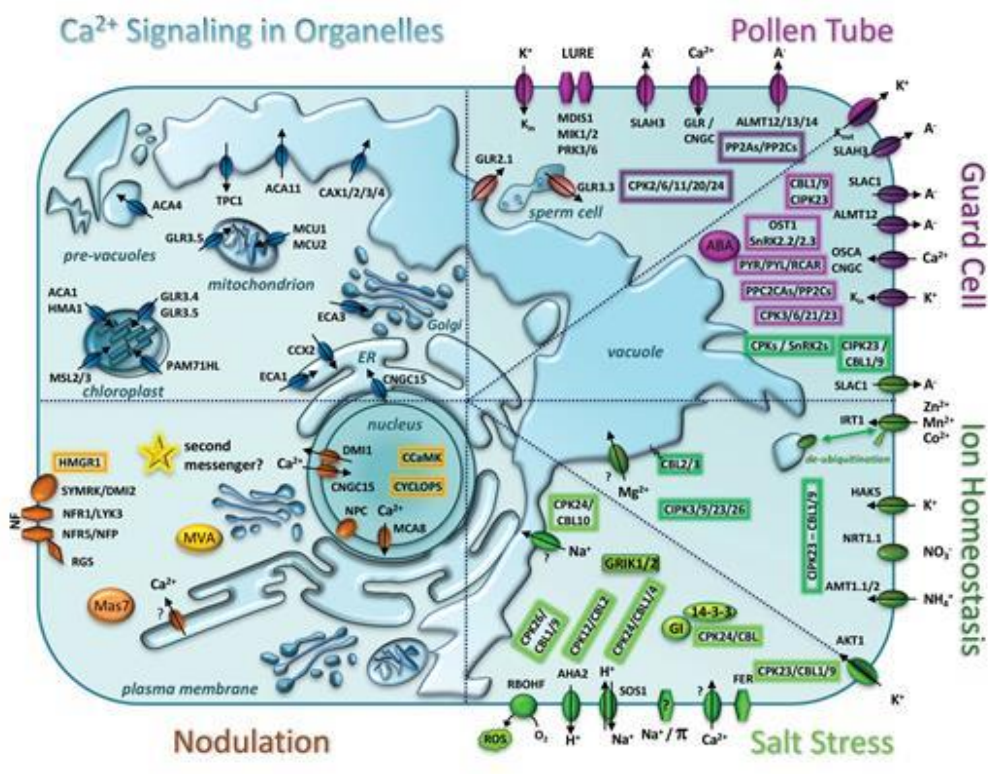

Fig. 3. Schematic representation of Ca^{2+} signalling in a plant cell. The main molecular components involved in Ca^{2+} handling are shown. Vacuole, ER, Golgi apparatus, chloroplast, mitochondrion and nucleus can orchestrate Ca^{2+} dynamics, thence shape the cytosolic Ca^{2+} signature upon stimulus perception. Picture from Feijo and Wudick, 2018 (Feijó and Wudick, 2018).

I.2.3. The main intracellular Ca^{2+} stores: the vacuole

The vacuole occupies 80-90% of the entire volume of a mature plant cell. It temporarily accumulates primary metabolites and permanently secondary metabolites, which are most of the time toxic compounds (Krüger and Schumacher, 2018). However, the vacuole is also the main intracellular Ca^{2+} store (free Ca^{2+} concentration ranges from 0.5mM to 2-5mM) that makes it the principal suspect to contribute, together with the apoplast, to the generation of the cytosolic Ca^{2+} elevation (Felle, Justus-liebig-universitat and Giessen, 1989). A pioneering work where the Ca^{2+} reporter aequorin was anchored to the cytosolic face of the tonoplast proved that vacuolar Ca^{2+} is involved in Ca^{2+} signalling upon cold treatment (Knight, 1996). A Ca^{2+} sensor, specifically localized to the vacuole lumen, would be an extremely useful tool to unravelling the contribution of vacuolar Ca^{2+} to the overall cytosolic Ca^{2+} dynamics (Costa, Navazio and Szabo, 2018). However, the low pH and the high Ca^{2+} concentration of the lumen represent strong limitations for Ca^{2+} detection with the available

372 fluorescent sensors (Shinoda, Shannon and Nagai, 2018). Albeit the *in vivo* analysis of Ca^{2+} dynamics
373 at the vacuole is difficult, direct patch clamp measurements of isolated vacuoles opened the way to
374 recognize and isolate a plethora of Ca^{2+} transporters acting at the tonoplast (Martinoia *et al.*, 2012).
375 The CaM-regulated autoinhibited Ca^{2+}-ATPases (ACA) is a gene family of ten members in Arabidopsis
376 (Geisler *et al.*, 2000). AtACA4 and AtACA11 have been reported to localize at the tonoplast and to be
377 involved in plant cell death (PCD) upon salicylic acid production (Lee *et al.*, 2007; Boursiac *et al.*,
378 2010)(Boursiac *et al.*, 2010). AtCAX1-AtCAX4 are instead tonoplast-localized cation/proton
379 exchangers and have been linked to Ca^{2+} homeostasis regulation (Pittman, Shigaki and Hirschi, 2005).
380 Indole-2-acetic acid (IAA) induced inhibition of abscisic acid (ABA)-induced stomatal closure, resulted
381 impaired in single *cax1*, *cax3* mutants and *cax1cax3* double mutant (Cho *et al.*, 2012). It has been
382 shown that chemicals such as inositol-1,4,5-trisphosphate ($InsP_3$) and inositol-hexakisphosphate
383 ($InsP_6$) can induce Ca^{2+} release from the vacuole (Alexandre and Lassalles, 1990; Lemtiri-Chlieh *et al.*,
384 2003). The two pore channel 1 (TPC1), one of the most characterized channels in plant, localized at
385 the tonoplast and it has been suggested to mediate Ca^{2+} release from the vacuole (Peiter *et al.*, 2005;
386 Carpaneto and Gradogna, 2018) (Fig. 3). Disruption of AtTPC1 impaired the ABA-induced repression
387 of germination and the stomatal response to extracellular Ca^{2+} (Peiter *et al.*, 2005). The structure of
388 TPC1 has been recently solved leading to new possible strategies to understand the impact of TPC1
389 in plant physiology (Guo *et al.*, 2016). However, the Ca^{2+} permeability of TPC1 has been questioned
390 for a long time (Costa, Navazio and Szabo, 2018). Recently, conclusive proof of Ca^{2+} permeability of
391 TPC1 has been reported, even if K^+ is the major cation transported by it (Carpaneto and Gradogna,
392 2018). TPC1 is also implicated in long-distance Ca^{2+} signalling upon salt stress and wounding (Choi *et*
393 *al.*, 2014). Interestingly, TPC1 was recently found to genetically interact with the defense-related co-
394 receptor Brassinosteroid insensitive-associated kinase1 (BAK1) and the Glutamate Receptor-like
395 GLR3.3 and GLR3.6 in a complex relationship necessary for cytosolic Ca^{2+} increase upon aphid
396 infection (Vincent *et al.*, 2017). However, several reports did not support a role for TPC1 in vacuolar
397 Ca^{2+} release (Costa, Navazio and Szabo, 2018). TPC1 *loss-of-function* and overexpressor did not show
398 any differences in the cytosolic Ca^{2+} dynamics when compared to Col-0 and subjected to external
399 abiotic and biotic stresses administration (Ranf *et al.*, 2008). Intriguingly, at least two reports came
400 out where researchers proved that *gain-of-function* mutant of TPC1 (*fou2*) shows a lower cytosolic
401 Ca^{2+} concentration at resting when compared to Col-0 and a higher vacuolar Ca^{2+} content (Rienmller
402 *et al.*, 2010; Wang *et al.*, 2015). Moreover, electrophysiological analysis on TPC1 showed Ca^{2+} influx
403 into the vacuole which suggest a role for TPC1 in cytosolic Ca^{2+} efflux rather than a contribution to

404 the generation of the cytosolic Ca^{2+} rise (Rienmller *et al.*, 2010; Wang *et al.*, 2015). Even if
405 controversial evidences are on the market, TPC1 remains one of the most important targets of
406 research in the Ca^{2+} signaling field (Costa, Navazio and Szabo, 2018).

407

408 ### I.2.4. The main intracellular Ca^{2+} stores: the endoplasmic reticulum (ER)

409 Given the presence of the vacuole, the endoplasmic reticulum (ER) has been for a long time
410 underestimated as a Ca^{2+} store in plants (Costa, Navazio and Szabo, 2018). In animals, ER has been
411 studied for decades and it is essential for Ca^{2+} release during events that require availability of free
412 Ca^{2+} such as muscle contraction (Sammels *et al.*, 2010). The amount of total Ca^{2+} in the animal ER has
413 been estimated as 2mM, with 50µM to 500µM free Ca^{2+} concentration. Experimental evidences
414 suggested that the same amount of free Ca^{2+} concentration can be found in the ER of a plant cell
415 (Stael *et al.*, 2012). Calreticulin is a protein localized in the ER lumen and it behaves as a low-affinity
416 high-capacity Ca^{2+}-binding protein and together with calnexin has been shown to act as a chaperone
417 for glycoproteins and protein folding in general (Jin *et al.*, 2009). Moreover, a genetically encoded
418 Ca^{2+} sensor expressed in pollen tubes has revelead the important role of ER played in the contribution
419 of the tip-focus Ca^{2+} gradient essential for pollen tube elongation (Iwano *et al.*, 2009). Plant cells have
420 four P(IIA)-type Ca^{2+}-ATPases, ECA1-4, which localize at the ER endomembranes (Costa, Navazio and
421 Szabo, 2018). ECA1 has been shown to be important in Ca^{2+} and Mn^{2+} homeostasis when plant grow
422 in low Ca^{2+} and high Mn^{2+} media. In fact, ECA1 actively transports these two cations into the ER when
423 Ca^{2+} is scarcely present in the milieu and Mn^{2+} is abundant (Wu *et al.*, 2002). *In vivo* measurements
424 of luminal ER Ca^{2+} dynamics in a plant root cell revealed that, plant ER seems to act mainly as a Ca^{2+}
425 sink instead of a source (Bonza *et al.*, 2013). In fact, several stimuli such as L-Glutamate, salt, mannitol
426 and external ATP triggered an elevation of cytosolic Ca^{2+} concentration which result in a following
427 accumulation of Ca^{2+} in the ER lumen which thus works as a sink (Bonza *et al.*, 2013; Corso *et al.*,
428 2018). However, cyclopiazonic acid (CPA), an ECAs specific inhibitor, lead to the increase of cytosolic
429 Ca^{2+} and a decrease of ER lumen Ca^{2+}, suggesting that the plant ER may also have a role as a Ca^{2+}
430 store which can be important in signalization events (Bonza *et al*., 2013). In support of this idea it has
431 been recently shown that in Arabidopsis, the hydrotropic stimulation induced a cytosolic Ca^{2+}
432 increase in the cells of the root elongation zone (EZ), which was required for the following root
433 bending toward water (hydrotropism). This mechanism was demonstrated to be dependent on a
434 reduced activity of ECA1 determined by its interaction with MIZ1. The key role played by ECA1 in

hydrotropism was also confirmed by the demonstration that the *eca1* knock out showed a deeper bending toward water as well as an increased cytosolic Ca^{2+} concentration (Shkolnik *et al.*, 2018). This latter evidence suggests that the ER as a compartment for Ca^{2+} storage and that an impaired ER Ca^{2+} homeostasis may have remarkable physiological effects. Recently another work has shed light on the importance of ER in the regulation of Ca^{2+} signaling. Besides ACAs and ECAs AtCCX2 (a member of Calcium/Cation exchanger family) has been shown to localize at the ER and regulate cytosolic and ER Ca^{2+} concentration upon osmotic stress. Lower cytosolic Ca^{2+} concentration and higher ER lumen Ca^{2+} concentration was measured in the absence of CCX2 activity, showing that this co-transporter is a key regulator of Ca^{2+} fluxes between cytosol and ER upon osmotic stress (Corso *et al.*, 2018) (Fig. 3).

As regards Ca^{2+}-permeable channels localized at the ER, biochemical experiments have revealed that voltage-gated channels may exist at the ER endomembranes (Klüsener *et al.*, 1995). Moreover, pyridine nucleotide derivatives nicotinic acid adenine dinucleotide phosphate (NAADP) and cyclic ADP-ribose (cADPR) have been proposed to activate ER Ca^{2+} release into the cytosol (Navazio *et al.*, 2000; Navazio *et al*., 2001). Additionally, in the legume species the nitrogen-fixing symbiosis-triggered nuclear Ca^{2+} oscillations seem to depend on release of Ca^{2+} from the nuclear envelope (NE) (Charpentier *et al.*, 2016). Remarkably, in *Medicago truncatula* the MtCNGC15 has been reported to localize at the NE (which is known to be in continuity with the ER) (Brandizzi, Fricker and Hawes, 2002) and is involved in the generation of these transient Ca^{2+} signals (Charpentier *et al.*, 2016).

I.2.5. The main extracellular Ca^{2+} stores: the apoplast

The apoplast is the main extracellular Ca^{2+} store. Together with the vacuole this represents the main source and store for Ca^{2+}. Apoplast Ca^{2+} concentration ranges from 0.33mM to 1mM (Stael *et al.*, 2012). Evidences support that apoplast is the first source for Ca^{2+} influx upon the perception of external stimuli. In fact, by chelating external Ca^{2+} by means of EGTA or BAPTA (Ca^{2+} cheleators), or by blocking the plasma membrane cation channels with non-selective blockers (La^{3+} or Gd^{3+}), cytosolic Ca^{2+} increases are strongly impaired (Lamotte *et al.*, 2004; Ali *et al.*, 2007). *In vivo* analysis of apoplast Ca^{2+} dynamics is tempered by the high Ca^{2+} concentration and the low pH (as for the vacuole) (Gao *et al.*, 2004). However, the use of a Ca^{2+} dye reported that the Arabidopsis *cngc2* and *cax1cax3* mutants overaccumulated apoplastic Ca^{2+} compared with wild type, when grown in high Ca^{2+} media (Mahmood, Ashraf and Shahbaz, 2009; Wang *et al.*, 2017). This is interesting since CAX1

and CAX3 are vacuolar proteins. This report would suggest a potential fascinating link between apoplast Ca^{2+} and vacuolar Ca^{2+} homeostasis (Costa, Navazio and Szabo, 2018).

I.2.6. Other intracellular Ca^{2+} stores: Golgi apparatus

In a plant cell the Golgi apparatus is formed by endomembrane pockets embedded into the cytoplasm which move along the ER (Robinson *et al.*, 2015). Cell-wall matrix polysaccharides, such as pectins and hemicellulose, are formed at the Golgi apparatus and protein glycosylation also occurs at the Golgi level (Vitale, 2001; Mravec *et al.*, 2017). Golgi vesicles are important for exocytosis which is promoted by Ca^{2+} (Cucu *et al.*, 2017). Free Ca^{2+} in the Golgi apparatus of plants has been estimated to be as low as 0.70µM, much lower compared to the animal Golgi apparatus (130-250µM) (Pizzo *et al.*, 2011; Ordenes *et al.*, 2012). The presence of calreticulin in the Golgi working as a Ca^{2+} buffer may explain such low free Ca^{2+} concentration (Navazio *et al.*, 2002). Little information is available about Ca^{2+} handling and signalling by Golgi. Increase of the Golgi Ca^{2+} concentration has been measured in response to several stimuli while the auxin analogue 2,4-diclorophenoxy acetic acid (2,4-D) decreased the Ca^{2+} level (Ordenes *et al.*, 2012). The decoding proteins CML4 and CML5 localize at the Golgi apparatus endomembranes in Arabidopsis. However, their CaM domains which bind Ca^{2+} lay on the cytosplasmic side. This would suggest that CML4 and CML5 would be regulated by cytosolic Ca^{2+} rather than by Golgi luminal Ca^{2+} (Ruge *et al.*, 2016). Lastly, AtECA3 has been proposed to pump Ca^{2+} into the Golgi lumen, even if more evidences are necessary (Mills *et al.*, 2007).

I.2.7. Other intracellular Ca^{2+} stores: Peroxisomes

The intraperoxisomal lumenal Ca^{2+} concentration has been estimated to range from 150nM to 2µM. Mammalian and plant peroxisomes in fact show increase in the Ca^{2+} concentration upon external stimuli challenge (Drago *et al.*, 2008). Only few reports are present in the plant field. Essentially, the dynamics of Ca^{2+} increase and decrease in plant peroxisomes mirror the cytosolic Ca^{2+} dynamics (Costa *et al.*, 2010; Costa et al 2013).

I.2.8. Shaping their own Ca^{2+} signature affecting cytosolic Ca^{2+} dynamics: Chloroplasts

493 It has been proposed that chloroplasts can act as a Ca^{2+} capacitors (Nomura *et al.*, 2012). In the last
494 years, however, evidences have revelead that chloroplasts have their own Ca^{2+} signals. This, could in
495 turn have an effect on the modulation of cytosolic Ca^{2+} transients (Loro *et al.*, 2016; Sello *et al.*, 2018).
496 A large amount of chloroplastic Ca^{2+} is bound to proteins or to thylakoid membranes (15mM *circa*),
497 while chloroplast free Ca^{2+} concentration has been estimasted to be as high as 150µM (Hochmal *et*
498 *al.*, 2015). Light to dark transition and photosynthesis can affect/modulate stromal Ca^{2+}
499 concentration. Biosensors targeted to the chloroplastic stroma have in fact reported Ca^{2+} increase
500 upon light to dark transition. This observation lead to the hypothesis that Ca^{2+} influx mechanisms
501 exist on the envelope membranes of the chloroplast. Ca^{2+} spikes have been detected in single guard
502 cell chloroplasts which are dependent on cytosolic Ca^{2+} (Loro *et al.*, 2016). It has been suggested that
503 Ca^{2+} channels may mediate the influx of Ca^{2+} from the cytosol. Electrophysiological analysis revealed
504 that voltage-dependent Ca^{2+} channels (fast-activating cation channel FACC) exist in the inner
505 envelope of pea chloroplast, but thier identity is still missing (Pottosin, Muñiz and Shabala, 2005). In
506 this scenario, the new reported BICAT transporters (BICAT1 and BICAT2) have been shown to regulate
507 darkness-induced Ca^{2+} signal in the chloroplast stroma. In fact, BICAT2 transports Ca^{2+} across the
508 chloroplast envelope whereas BICAT1 stores Ca^{2+} into the thylakoid's lumen (Frank *et al.*, 2018).
509 Recently, two Glutamate Receptor-like channels have been found in chloroplasts, AtGLR3.4 and
510 AtGLR3.5 together with the mechano-sensitive MLS2/3 channels (Haswell and Meyerowitz, 2006;
511 Teardo *et al.*, 2011, 2015). ACA1 and HMA (P-Type ATPase) are also among the candidates to pump
512 Ca^{2+} in the chloroplast stroma, even if definitive evidences are still lacking (Huang, 1994; Ferro *et al.*,
513 2010) (Fig. 3). Another candidate is one of the six mitochondrial Ca^{2+} unipoters (MCU). Even if there
514 are no proofs that suggest the localization of MCU at the chloroplast, the N-terminus of this protein
515 would argue for a targeting to both mitochondria and chloroplasts (Stael *et al.*, 2012). However, other
516 transporters can affect Ca^{2+} dynamics at the chloroplast level. This is the case of KEA1 and KEA2, two
517 K^+/H^+ co-transporters. The double mutant *kea1kea2* shows reduced cytosolic Ca^{2+} level upon osmotic
518 stress. This would suggest that a complex mechanism involving the two K^+/H^+ co-transporters and
519 Ca^{2+} mobilization systems could actually have an effect on the cytosolic Ca^{2+} homeostasis under
520 osmotic stress conditions (Stephan *et al.*, 2016). The case of the thylakoid-attached Ca^{2+}-sensing
521 receptor CAS is interesting. *Loss-of-function* mutant for CAS affected stomatal movement as well as
522 plant growth, even if the molecular mechanism is still well not understood (Wang *et al.*, 2012; Fu *et*
523 *al.*, 2013).

524

I.2.9. Shaping their own Ca^{2+} signature affecting cytosolic Ca^{2+} dynamics: Mitochondria

Similar to animal, plant mitochondria can modulate cytosolic Ca^{2+} dynamics (Costa, Navazio and Szabo, 2018). The extremely negative matrix (-180/220mV) promotes the uptake of cations, such as Ca^{2+}, through cation channels. The free Ca^{2+} concentration ascribed to the plant mitochondria ranges from 100 to 600nM (Wagner *et al.*, 2016). *In vivo* measurements have shown that mitochondria accumulate and release Ca^{2+} when challenged with external stimuli (Loro *et al.*, 2012; Wagner *et al.*, 2015). The mitochondria Ca^{2+} accumulation and release are dependent on cytosolic Ca^{2+} elevation and show a slower dynamic when compared to the cytosol. This would suggest that mitochondria may behave like Ca^{2+} capacitors and are implied in shaping cytosolic Ca^{2+} dynamics (McAinsh and Pittman, 2009). The molecular identification of the mammalian MCU was a fundamental step for the comprehension of how mitochondria accumulate Ca^{2+} and potentially modulate the cytosolic Ca^{2+} dynamics (Baughman *et al.*, 2011; De Stefani *et al.*, 2011). In Arabidopsis five out six MCU members are predicted to localize at the inner mitochondria membrane (Stael *et al.*, 2012). MCU1 and MCU2 when expressed in heterologous system show Ca^{2+} conductivity. However, possibly due to the high redudancy, a mild Ca^{2+} phenotype was ascribed to the *mcu1* knock out mutant (Teardo *et al.*, 2017). Instead, the *mcu2 loss-of-function* showed a pollen tube (PT) phenotype even though the mutation also affected cytosolic Ca^{2+} dynamics, making it difficult to predict whether the PT phenotype was dependent or not on mitochondria Ca^{2+} (Selles *et al.*, 2018). Disruption of the MCU regulator protein MICU lead to the increase, even at resting conditions, of mitochondria Ca^{2+} uptake as well as the speed of the accumulation. This suggested that MICU acts as a negative regulator of the MCU (Wagner *et al.*, 2015). The Arabidopsis Glutamate Receptor-like channel 3.5 was shown to localize both at the chloroplasts and at the mitochondria. A reduction of the Ca^{2+} accumulation rate in mitochondria was apparent in the silenced mutant *glr3.5* (Teardo *et al.*, 2015) (Fig. 3). Other proteins such as the Actin Related Protein ARP2, the transcription factor WRKY15, the two EF-hand Ca^{2+} binding proteins LETM1 and LETM2 have been shown to regulate mitochondria Ca^{2+} dynamics (Vanderauwera *et al.*, 2012; Zhang *et al.*, 2012; Zhao *et al.*, 2013).

I.2.10. A plethora of tools to measure Ca^{2+} signals *in vivo*

Ca^{2+}-sensitive dyes have been originally employed for measurement of Ca^{2+} dynamics in plants (McAinsh and Pittman, 2009). Even though they paved the way for a deeper understanding of Ca^{2+}-dependent mechanisms *in planta*, dyes are associated with several drawbacks. Dyes have to be

556 loaded or injected. Moreover, dye analysis is prone to artifacts and it is affected by low throughput
557 and high variability (Costa, Navazio and Szabo, 2018). For these reasons, the use of Genetically
558 Encoded Ca^{2+} Indicator (GECI) in plants was actually seen as a revolution (Pérez Koldenkova and
559 Nagai, 2013). GECI allows to monitor Ca^{2+} dynamics in a non-invasive way, in real time, with spatial
560 and temporal resolution. Additionally, targeting GECIs to different compartments allowed to dissect
561 Ca^{2+} dynamics in organelles as well as to specific tissues/cells (Stael *et al.*, 2012; Costa and Kudla,
562 2015). In plants, the two sensors of choice are aequorin and Cameleon (Mithöfer and Mazars, 2002;
563 Costa and Kudla, 2015). Both of them can report Ca^{2+} increases in a physiologically relevant range
564 (Palmer *et al.*, 2006). Aequorin-based sensors have been largely used and can report absolute
565 concentration for Ca^{2+}. Moreover, aequorin is low pH and Mg^{2+} sensitive and can be potentially used
566 to report Ca^{2+} level in acidic compartments. Aequorin is based on photon acquisition upon the
567 reconstitution of the aequorin holoenzyme with the prostethic group coelentrazine when the latter
568 is exogenously administered. The high signal-to-noise ratio and the no need for excitation of the
569 sensor are great advantages for long-time measurements (Knight *et al.*, 1991; Marti, Stancombe and
570 Webb, 2013). Aequorin-based sensors have been targeted to different compartments such as the
571 tonoplast, the nucleus, Golgi apparatus, chloroplasts and mitochondria as well as at the extracellular
572 apoplast level (Costa, Navazio and Szabo, 2018).

573 Recently, a bioluminiscent resonance energy transfer (BRET)-based aequorin sensor has been
574 developed which allows higher emission of photons compared to the aequorin (one the major
575 limitations of aequorin is in fact the low light emitted) (Xiong *et al.*, 2014).

576 GFP-based ratiometric sensors such as Yellow Cameleon 3.6 (YC3.6) has greatly enhanced the spatio-
577 temporal resolution and the Ca^{2+} sensitivity of the analysis. Cameleon sensors are based on the
578 phenomenon of the Forster Resonance Energy Transfer (FRET) and harbour two fluorescent proteins
579 (FPs), a Cyan Fluorescent Protein (CFP) and a Yellow Fluorescent Protein (YFP) or their derivatives,
580 linked by a bridge made by the Ca^{2+}-binding protein CaM and a flexible CaM-binding peptide called
581 M13. When the Ca^{2+} concentration rises up, the four EF hands of CaM bind a Ca^{2+} ion each. The
582 following conformational change driven by the Ca^{2+} binding to the CaM allows the two FPs to come
583 closer leading to a FRET increase. A FRET increase reports an increase in Ca^{2+} concentration,
584 calculated as the ratio between YFP and CFP emission intensity over CFP excitation. Interestingly,
585 since the calculated Ca^{2+} increase relies on ratio increase only, Ca^{2+} analysis by ratiometric sensor is
586 not affected by protein abundance. Moreover, Ca^{2+} acquisitions by means of Cameleon sensors do

not suffer from focus change (i.e. it is possible to correct them). In addition, Cameleon-based sensors have been successfully targeted to different intracellular compartments (Miyawaki *et al.*, 1997; Nagai *et al.*, 2004; Krebs *et al.*, 2012; Costa and Kudla, 2015).

Besides ratiometric sensors, the succesfull use of intentiometric sensors based on GFP has been reported for cytosolic and nuclear Ca^{2+} detection. Among them, GCaMP3, GCaMP6 and the two green and the red variant of R-GECO1 (G-Geco and R-Geco1) have been employed *in planta* (Keinath *et al.*, 2015; Waadt *et al.*, 2017; Kelner *et al.*, 2018). The greater advantages of these sensors are the high sensitivity and the signal increase upon Ca^{2+} detection compared to YC3.6 sensors (Costa, Navazio and Szabo, 2018). Moreover, the high fluorescent yield of GCaMP sensors make them suitable for whole-tissue imaging (Vincent *et al.*, 2017; Nguyen *et al.*, 2018; Toyota *et al.*, 2018). The new development of red-shifted sensors opens the possibility to simultaneously monitor Ca^{2+} dynamics in at least two different compartments. Nuclear and cytosolic Ca^{2+} dynamics have been followed upon treatment with nod factors of *Medicago truncatula* root hairs (Kelner *et al.*, 2018). However, a severe drawback of single FP-Ca^{2+} sensors is that they can not report absolute Ca^{2+} concentration as easily as ratiometric sensors. Additionally, sensor abundance can affect the measurement of Ca^{2+} when comparing mutant and wild-type Ca^{2+} dynamics (Costa, Navazio and Szabo, 2018).

I.2.11. Calcium waves propagation

Abiotic and biotic stimuli trigger cytosolic Ca^{2+} elevations at the local site of stress perception which in several cases then spread systemically as a propagating wave. Choi *et al.* (2014) have shown that NaCl induced increase in cytosolic Ca^{2+} at the root elongation zone which spread shootward through endodermis and cortex at 400µm/s through a mechanism which involves the vacuolar channel TPC1 (Choi *et al.*, 2014). Additionally, disruption of the respiratory burst oxidase homolog D RBOHD, drastically decreases the speed propagation of the Ca^{2+} wave, supporting a positive feedback mechanism involving Ca^{2+} (*via* TPC1) and ROS production (*via* RBOHD) (Evans *et al.*, 2016). Recently, Toyota *et al.* (2018) reported that upon leaf caterpillar chewing and/or mechanical wounding, cytosolic Ca^{2+} increase locally occurs which is then propagated through the phloem and plasmodesmata to undamaged distal leaves. Ca^{2+} wave through the phloem moves at 1000±200µm/s *circa*, more than twice the speed propagation in root tissues (Toyota *et al.*, 2018). The low resistance path given by the phloem, which does not have vacuoles, could explain this speed rate increase. In addition to TPC1, plant GLRs have been shown to play a fundamental role in both electrical and Ca^{2+}

systemic signalling (Mousavi *et al.*, 2013; Salvador-Recatalà, 2016; Toyota *et al.*, 2018). However, being putative Ca^{2+}-permeable gated channels, it remains to be defined whether the ligand binding might play a role in such long distance communication (Gilroy *et al.*, 2016; Toyota *et al.*, 2018). Besides ROS and Ca^{2+} waves, electrical signals can move through vessels. The integration of ROS, Ca^{2+} and ES could explain long travelling systemic signals which induce change in gene expression and eventually environmental adaptation (Gilroy *et al.*, 2016; Choi *et al.*, 2017). However, the molecular identity of the channels involved in electrical signal propagation are still unknown, even though disruption of GLR genes altered electrical signal propagation (Mousavi *et al.*, 2013; Gilroy *et al.*, 2016; Salvador-Recatalà, 2016).

I.3. Plants and animals Glutamate Receptors: a comparison

I.3.1. Animals and plants Glutamate Receptors, an overview

Glutamate Receptors belong to the super-family of the ligand gated channels (Price, Jelesko and Okumoto, 2012). Based on agonist selectivity and topology, as well as ionic selectivity and desensitization kinetics mammals Glutamate Receptor have been sub-grouped in four different clades: the N-Methyl-D-Aspartate (NMDA) receptors, the α-amino-3-hydroxy-5-methyl-4-isoxazolepropionic acid (AMPA), the Kainate Receptors and the Delta (δ) Receptors, which share the same topology with iGluRs but are not activated by L-Glutamate (Price, Jelesko and Okumoto, 2012; Traynelis *et al.*, 2014; De Bortoli *et al.*, 2016). Animals and plants share this class of proteins (Wudick *et al*., 2018a). Plant GLRs and animal iGluRs diverged before the diversification of animal iGluRs in different clades (Turano *et al.*, 2001; Chiu *et al.*, 2002; De Bortoli *et al.*, 2016; Wudick *et al*., 2018a). Mainly based on sequence alignment, plant GLRs have been divided in three different clades. Clade III includes gymnosperm (*Ginkgo biloba*), mosses (*Physcomitrella patens*) and liverwort GLRs (*Mercanthia polymorfa*), while clade I and II only contain angiosperm GLRs (Price, Jelesko and Okumoto, 2012; De Bortoli *et al.*, 2016) (Fig. 4). So far, few functional reports came out about plant GLR making them difficult to study (Wudick *et al*., 2018a). Since the relatively high sequence similarity between plant GLRs and iGluRs (16 to 63%) (Lam *et al.*, 1998) it is possible to predict GLR structural information based on available data regarding iGluRs (Chiu *et al.*, 2002). However, profound differences between animal and plant Glutamate Receptors will be highlighted in the following paragraphs both at the structural and the functional levels.

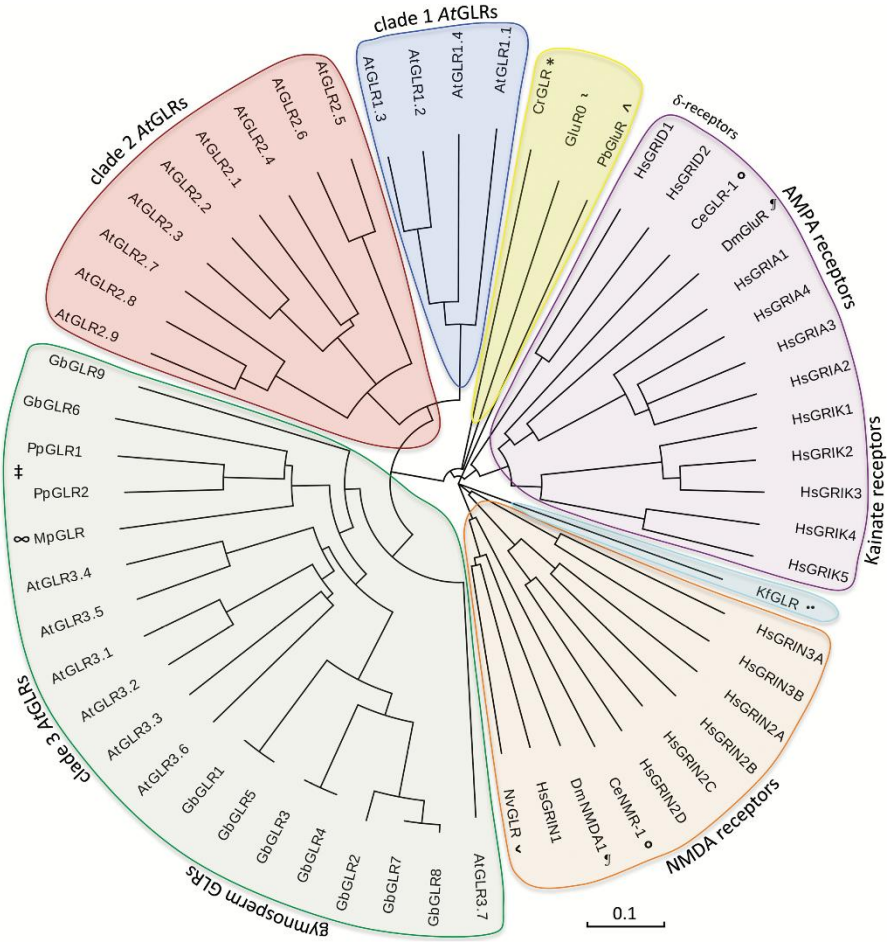

Fig. 4. Phylogetic relationship of Glutamate Receptors. In this cartoon are shown selected Glutamate Receptors belonging to *Arabidopsis thaliana* (At), the nematode *Caenorhabditis elegans* (Ce, °), the unicellular green alga *Chlamydomonas rheinhardtii* (Cr, *), the fruit fly *Drosophila melanogaster* (Dm, ¶), the gymnosperm *Ginkgo biloba* (Gb), *Homo sapiens* (Hs), the filamentous green alga *Klebsormidium flaccidum* (Kf, ¨), the liverwort *Marchantia polymorpha* (Mp, ∞), the sea anemone *Nematostella vectensis* (Nv, ˇ), the moss *Physcomitrella patens* (Pp, ‡), the ctenophore *Pleurobrachia bachei* (Pb, ^), and the cyanobacterium *Synechocystis sp*. (GluR0, ~). Cartoon from Wudick *et al.* (2018a)

I.3.2 Channel stoichiometry and subunit interaction

Glutamate Receptors are homo or hetero-tetramers. In particular, subunits which belong to the same clade can exclusively form a functional channel. GluN1, GluN2A-2D, GluN3A and GluN3B belong to the NMDA receptor class. For instance, functional NMDA receptors are formed by two dimers of GluN1 and a combination of GluN2 dimers or a subunit of GluN2 and GluN3. NMDA receptors are

gated by simultaneous binding of L-Glutamate and Glycine, and each subunit gives ligand binding specificity (Traynelis *et al.*, 2014). In plants few data are available about channel stoichiometry and subunit interaction. A putative interaction was suggested for AtGLR3.2-AtGLR3.4 in the phloem as well as for AtGLR3.1-AtGLR3.5 in guard cells (Vincill *et al.*, 2013; Kong *et al.*, 2016). AtGLR3.3 expressed in mammalian cells, when co-expressed with regulatory proteins, mediated cationic currents suggesting that AtGLR3.3 homomeric channels are functional (Wudick *et al.*, 2018).

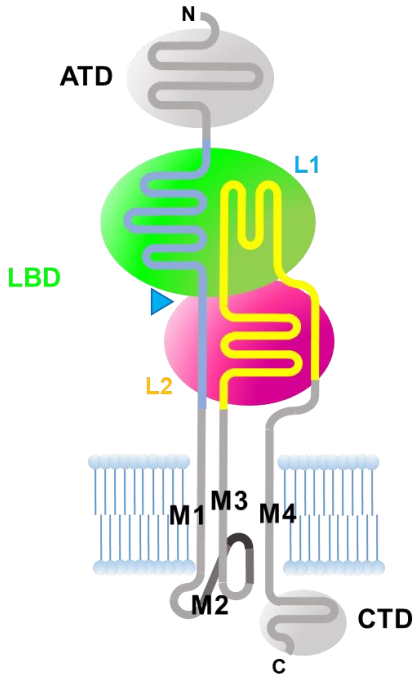

Fig. 5. General scheme of a single subunit of eukaryotic iGluR/GLR. Each channel is a homo or heterotetramer of this subunit. S1 and S2 segments are shown in light blue and yellow, respectively. Ligand binding domain LBD is formed by L1 (green) and L2 (purple) lobes. L1 lobe is mainly formed by S1 segment, whereas L2 lobe is mainly formed by S2 segment. Amino acidic ligand (blue triangle) accommodates between L1 and L2. ATD, amino terminal domain; M1-4 transmembrane domains; CTD C-terminus domain. Cartoon made by Dr. Andrea Alfieri.

I.3.3 The amino terminal domain (ATD)

Thanks to the presence of a N-terminal transmembrane anchor, a vast majority of animal iGluRs enter the secretory pathway. The signal peptide is then eventually cleaved off (Traynelis *et al.*, 2014). Sixteen out twenty plant GLRs have been suggested to harbour a N-terminal transmembrane domain which would act as a signal peptide (He *et al.*, 2016) (Fig. 5). So far, a plasma membrane localization

682 has been reported only for AtGLR1.4, AtGLR3.2, AtGLR3.3 and AtGLR3.4 (Vincill, Bieck and Spalding,
683 2012; Tapken *et al.*, 2013; Wudick *et al.*, 2018). However, informatic analysis and published data
684 suggested that not all the 20 GLRs enter the secretory pathway (Wudick *et al*., 2018a). For instance,
685 AtGLR3.4 has been reported to be also resident on plastids membrane (Teardo *et al.*, 2015).
686 Accordingly, among AtGLRs, AtGLR3.5 resulted with low probability to enter the secretory pathway
687 and localizes at the mitochondria even if a report predicts its presence also at the plasma membrane
688 (Kong *et al.*, 2015). AtGLR2.1 is instead the first GLR with a tonoplast localization in pollen tube
689 together with AtGLR3.6 which localizes at the vacuoles of xylem contact cells (Nguyen *et al.*, 2018;
690 Wudick *et al.*, 2018).

691 The amino terminal domain (ATD) localized to the N-terminus of Glutamate Receptors (Fig. 5). ATD
692 has been deeply studied and structures of this domain has been solved for several clades of iGluRs
693 (Sobolevsky, 2015). ATD shows a clamshell-like conformation which mirrors the bacterial
694 leucine/isoleucine/valine binding domain (LIVBP). Remarkably, ATD plays an active role in allosteric
695 regulation of the NMDA receptors. Indeed, Zn^{2+} and other ligands such as polyamines can bind ATD
696 adding another level of regulation. ATD, together with the ligand binding domain, plays a crucial role
697 in oligomerization and trafficking of the channel. It also contributes to desensitization event, i.e. the
698 time where the channel remains insensitive to external ligands (Sobolevsky, 2015; Zhu and Gouaux,
699 2017; Wudick *et al*., 2018a). However, phylogenetic analysis suggested that ATD of clade III (including
700 Physcomitrella, Mercanthia and Ginkgo) is closer to metabotropic GluR and GABA receptors (G
701 protein couple receptors (GPCR)) than iGluRs. AtGLR3.5 shows a conserved consensus motif found in
702 GPCRs necessary for ligand binding. Hence, it is not feasible to rule out a different/additional
703 regulation of clade III GLRs compared to clade I and II GLRs (Wudick *et al*., 2018a).

704

705 ### I.3.4. The ligand binding domain (LBD)

706 The ligand binding domain (LBD) is an extracellular domain highly conserved in all iGluRs classes. As
707 the ATD, LBD is a clamshell-like domain made of two different segments referred to as S1 and S2
708 which made the two lobes (L1 and L2) of the clamshell (Fig. 5). The binding pocket bears in the middle
709 of the two lobes (Traynelis *et al.*, 2014; Sobolevsky, 2015; Zhu and Gouaux, 2017). Crystal structures
710 of the LBDs, i.e. the two segments S1 and S2 joined by a short artificial linker, carried the same
711 information than LBD in a full-length iGluR structure (Traynelis *et al.*, 2014). In animals, residues that
712 directly interact with α-carboxil and α-amino group of iGluRs ligands are highly conserved among all

713 the iGluRs. Upon the binding of an agonist, the clamshell domain adopts a closed conformation. This
714 conformational change is enough to trigger a wider movement of the transmembrane M3 thus
715 allowing the opening of the pore (Fig. 5). Depending on the subunits composition, NMDA and δ
716 receptors can bind Glutamate/Aspartate or Glycine/D-Serine, while AMPA and kainate receptors can
717 only bind Glutamate/Aspartate (Traynelis *et al.*, 2014). The high specificity of the ligand binding is at
718 the basis of the fast excitatory post synaptic transmission played by iGluRs. Their binding affinity shifts
719 from 0.1 to 3µM (dissociation costant, K_d) for endogenous agonists and is dependent on the S1 and
720 S2 residues composition (Traynelis *et al.*, 2014). Interestingly, AtGLRs do not show conservation of
721 the LBD residues. This would explain the reason behind the low ligand selectivity of plant GLRs (Qi,
722 Stephens and Spalding, 2006; Michard *et al.*, 2011; Vincill, Bieck and Spalding, 2012; Li *et al.*, 2013;
723 Tapken *et al.*, 2013). However, only indirect proofs have been reported so far about ligand binding
724 activity in plant GLRs (Wudick *et al*., 2018a). In plants, AtGLR1.4 mediated plasma membrane
725 depolarization upon L-Methionine administration and site specific mutagenis proved that this was
726 dependent on AtGLR1.4 LBD (Tapken *et al.*, 2013). AtGLR3.4, instead, when expressed in HEK cells
727 was activated by L-Serine, L-Asparagine and Glycine (Vincill, Bieck and Spalding, 2012). Micromolar
728 and millimolar concentrations of external amino acids have been used in these two works to activate
729 GLRs-dependent currents (Vincill, Bieck and Spalding, 2012; Tapken *et al.*, 2013). Moreover, AtGLRs
730 currents may be blocked or inhibited by iGluRs antagonists (e.g. DNQX, CNQX, AP5) only at high
731 concentration (Dubos *et al.*, 2003; Meyerhoff *et al.*, 2005; Michard *et al.*, 2011; Teardo *et al.*, 2011;
732 Li *et al.*, 2013; Traynelis *et al.*, 2014; Iwano *et al.*, 2015a; Ortiz-ramírez *et al.*, 2017). This would suggest
733 that these inhibitors are specific for animal Glutamate Receptor but not for plant GLRs and should be
734 at least used with awareness (Traynelis *et al.*, 2014; Wudick *et al*., 2018a). Lastly, three different
735 reports by the Feijo laboratory appeared in the last years which supported plant GLR activation
736 independently by external agonists (Michard *et al.*, 2011; Ortiz-ramírez *et al.*, 2017; Wudick *et al.*,
737 2018). These evidences would suggest that more studies about the ligand binding activity of plant
738 GLRs are needed for a better comprehension of GLRs activity in plants (Wudick *et al*., 2018a).

739

740 ### I.3.5 The pore and the gate domain

741 Animal Glutamate Receptors are tetrameric channels formed by four subunits. M2 transmembrane
742 domain is a relatively short domain, which lies between transmembranes M1 and M3 (Fig. 5). The
743 transmembrane domains M2 of the four subunits assemble in the formation of the pore domain

744 (Traynelis *et al.*, 2014). Bacterial iGluR0 contains the 'GYGD' filter motif which allows iGluR0 to
745 selectively transport potassium. The same motif is shared with the rotifer *Adineta vaga* AvGluR1.
746 Animal iGluRs are non-selective cation channels and lost this motif (Traynelis *et al.*, 2014; Wudick *et*
747 *al.,* 2018*)*. NMDA receptors are Ca^{2+}-permeable channels, however plant and animal Glutamate
748 Receptors pore domains do not share the same residues (Traynelis *et al.*, 2014; De Bortoli *et al.*,
749 2016). This means that prediction of ions selectivity for plant GLRs based on sequence similarity with
750 iGluRs is hard (Wudick *et al*., 2018a). Moreover, the residues that confer Ca^{2+} selectivity in NMDA
751 receptors are not conserved in plant GLRs, suggesting differences in ionic selectivity of plant GLRs
752 (De Bortoli *et al.*, 2016). In a pivotal paper, AtGLR1.1 and AtGLR1.4 pore domain were swapped in
753 AMPA and Kainate receptors and expressed in HEK cells. Patch clamp measurements suggested
754 cation permeation of the two pores, without any selectivity (Tapken and Hollmann, 2008). D-Serine
755 triggered an increase of cytosolic Ca^{2+} in pollen tube when exogenously administered at 5mM final
756 concentration (Michard *et al.*, 2011). AtGLR3.4 when expressed in HEK cells resulted in a Ca^{2+}-
757 permeable non selective cation channel, as well as AtGLR1.4 when expressed in Xenopus oocytes
758 (Vincill, Bieck and Spalding, 2012; Tapken *et al.*, 2013). The Physcomitrella PpGLR1 as well as AtGLR3.2
759 and AtGLR3.3 mediated Ca^{2+} influx which was blocked by the broad cation channel inhibitor
760 Gadolinium (Ortiz-Ramírez *et al.*, 2017; Wudick *et al.*, 2018). Albeit this represents a good panel of
761 information, many questions about plant GLRs selectivity are still largely unsolved (Wudick *et al*.,
762 2018a).

763 A large conformational change has been proved to occur in animal iGluRs upon ligand binding. ATD
764 moved outward, while the clamshell of the LBD moved from an open configuration to a closed state.
765 As a consequence, large rearrangements of the transmembrane domains occur, including to a series
766 of residues of the gating domain which normally sterically blocks the pore domain. This assures the
767 opening of the channel only upon ligand binding (Traynelis *et al.*, 2014; Twomey and Sobolevsky,
768 2018). The gate region in iGluRs is extremely conserved and is formed by the 'SYNTANLAA' motif
769 (Traynelis *et al.*, 2014). When compared, the plant GLRs do not show the same conservation of iGluRs
770 at the residues level of the gate region (Wudick *et al*., 2018). In fact, Tyrosine, Alanine and Leucine in
771 position 3, 4 and 6 are conserved while residue in position 5 is the most variable. Intriguingly, clade
772 III GLRs, except for AtGLR3.7, show the most conservative scheme of residues. In fact, the gating
773 region of clade III is 'SYTASTLS', which is also conserved in the two Physcomitrella GLRs and in all
774 Ginkgo GLRs, while the most promiscuous motif is shown by the clade I GLRs in Arabidopsis (Wudick
775 *et al*., 2018a).

I.3.6. The C-terminus domain (CTD)

The last transmembrane domain, made of M4 transmembrane domain and the C-terminal domain (CTD), is present in both iGluRs and plant GLRs, while it is missing in bacterial iGluR0 (Chen and Roche, 2010). This domain has been shown to be involved in both gating (AMPA and NMDA) and desensitization (AMPA), and it is necessary for post-translational regulation (Traynelis *et al.*, 2014) (Fig. 5). AtGLR3.3 and AtGLR3.4 showed desensitization-like events *in planta*, but desensitization phenomenon was absent when AtGLR1.4 and AtGLR3.4 were expressed in heterologous systems (Stephens, Qi and Spalding, 2007; Vincill, Bieck and Spalding, 2012; Tapken *et al.*, 2013).

The C-terminus of iGluRs is a soluble cytosolic domain and results as the most divergent both in the amino acids composition and in length. It bears regulatory motifs such as ER retention domain and consensus sequence for interaction with other proteins (Traynelis *et al.*, 2014; Wudick *et al*., 2018a) which harbour the PDZ-domain such as GRIP, GRIP2 A and PICK1. These proteins are involved in trafficking and recycling of the receptors (Traynelis *et al.*, 2014). Interestingly, PDZ-harbouring domain proteins evolved only in higher organisms and thus they were not found in Arabidopsis (Wudick *et al*., 2018). The CTD domain also shows consensus motif for 14-3-3 proteins binding. In NMDA receptors, this interaction has been shown to have an impact on trafficking, channel export, subunits interaction and expression of the channel at plasma membrane (Chen and Roche, 2010; Chung, Wu and Chen, 2015). Interestingly, AtGLR1.4, AtGLR2.9 and AtGLR3.7 have been shown to interact with 14-3-3 *in vitro*. In fact, AtGLRs CTD of six AtGLRs show 14-3-3 consensus binding motif (Chung, Wu and Chen, 2015). In animal, the interaction is dependent on CTD residues phosphorylation and may occur in plant GLRs as well, even if such a regulation has not reported yet (Wudick *et al*., 2018a).

I.4. Biophysical properties and sub-cellular localization of plant GLRs

I.4.1. GLRs, not only plasma membrane resident channels

Glutamate Receptors-like, as their animal counterpart, have been suggested to be resident at the plasma membrane. However, several reports suggested that at least some of them localize at the secretory pathway and also at the organelle membranes. Teardo *et al.* (2015) reported a dual localization for AtGLR3.4, present both at the plasma membrane and at the chloroplasts/plastids.

Knock-out mutant for AtGLR3.4 showed a subtle photosynthetic phenotype (Teardo *et al.*, 2011). The same authors found out a dual localization also for AtGLR3.5. AtGLR3.5 localized both in mitochondria and chloroplasts. Silenced mutants for AtGLR3.5 showed mitochondria with altered morphology and a slightly reduced mitochondrial Ca^{2+} uptake (Teardo *et al.*, 2015). Lastly, it has been recently reported that AtGLR2.1 and AtGLR3.6 localize at the tonoplast in pollen tube and at the vacuole of the xylem contact cells in leaves, respectively (Nguyen *et al.*, 2018; Wudick *et al.*, 2018b).

I.4.2. GLRs isoforms assembly: who is interacting with who?

As reported above, iGluRs are tetrameric channels that can be either homo- or heterotetramers. As regard subunits interaction, few are known in plants. A putative heteromeric channel was suggested by Vincill *et al.* (2013) The authors proposed a AtGLR3.2-AtGLR3.4 isoforms interaction, with both subunits expressed at the phloem. Mutations in both GLRs genes led to aberrant placement of lateral root primordia (Vincill *et al.*, 2013). Kong *et al.* reported the existence of a AtGLR3.1-AtGLR3.5 channel in guard cells activated by L-Met (Kong *et al.*, 2016). In an extensive work, Price *et al.* (2012) by means of a modified split ubiquitin assay in yeast and FRET analysis in HEK cells proposed that AtGLR1.1 and AtGLR3.4 could form homomeric channels, while they did not observe interaction between AtGLR3.2 and AtGLR3.4 (Price, Jelesko and Okumoto, 2012).

I.4.3. GLRs trafficking regulation

Another level of regulation for GLRs, besides amino acids activation, is protein-protein interaction and targeting. It is well known that iGluRs trafficking is tightly regulated (Traynelis *et al.*, 2014). Cornichons homolog (CNIH) proteins have been found in Arabidopsis. Wudick *et al.* (2018) showed that this class of proteins regulates AtGLR3.3 trafficking through the secretory pathway (Wudick *et al.*, 2018). Co-expression of CNIHs and AtGLR3.3 in COS cells upregulated non-selective cation fluxes, thus providing evidences for CNIHs-mediated AtGLR3.3 regulation and activation. Additionally, possible interaction between AtGLRs (1.2, 2.1, 2.9, 3.4, 3.7) and 14-3-3 proteins has been suggested by *in vitro* studies (Chung *et al.*, 2015). In fact, putative phosphorylation sites found at the C-terminus of many AtGLRs could be targets of 14-3-3 recognition and interaction, which would putatively regulate GLRs trafficking (Wudick *et al.*, 2018a).

I.4.4. GLRs activation by amino acidic ligands. Is it really necessary?

In the early 2000, Dennison and Spalding reported a fast cytosolic Ca^{2+} increase followed by trasient plasma membrane depolarization in Arabidopsis root upon K^+-Glutamate addition. The Ca^{2+} chelator ethylene glycol-bis(β-aminoethyl ether)-N,N,N',N'-tetraacetic acid (EGTA) and Lanthanum ($LaCl_3$) treatments abolished the Glutamate-induced Ca^{2+} transient and membrane depolarization, suggesting that the pathway for the Ca^{2+} input upon Glutamate addition occurs across the plasma membrane (Dennison and Spalding, 2000). The same group in 2006 showed that a wide variety of amino acids, besides Glutamate, could activate Ca^{2+} currents in Arabidopsis roots and that disruption of the AtGLR3.3 gene abolished these Ca^{2+} transients (Qi, Stephens and Spalding, 2006). Similarly, cytosolic Ca^{2+} increase was impaired in the AtGLR3.4 *loss-of-function* upon L-Asn, L-Cys and Gly administration (Stephens, Qi and Spalding, 2007; Vincill, Bieck and Spalding, 2012). Additionally, the reduced form of the tripeptide Glutathione (GSH_{red}, γ-Glu-L-Cys-Gly) was reported to induce cytosolic Ca^{2+} increase in Arabidopsis roots (Li *et al.*, 2013). L-Methionine seems to activate the GLR3.1-GLR3.5 channel in Arabidopsis guard cells, as well as AtGLR1.4 in hypocotyl (Tapken *et al.*, 2013). Lastly, L-Glutamate stimulation leads to a local increase of cytosolic Ca^{2+} in leaves which in turns triggers the propagation of a Ca^{2+} wave in distal leaves, acting as an alarming molecule (Toyota *et al.*, 2018). D-Serine has been shown to activate Ca^{2+} currents at the tip of pollen tubes necessary to control pollen tube growth (Michard *et al.*, 2011). However, in two distinct papers the Feijo laboratory reported that GLRs can mediate currents in a ligand-independent manner (Ortiz-Ramírez *et al.*, 2017; Wudick et al., 2018a).

I.4.5. GLRs ions permeability

iGluRs at the post-synaptic cleft are non selective cation channels activated by amino acids binding. Na^+, K^+ (mainly non-NMDA-mediated) and Ca^{2+} (mainly NMDA-mediated) influxes depolarize the membrane up to the threshold where depolarized-activated channels become active. A deeper depolarization of the plasma membrane leads thus to an action potential. iGluRs therefore are the main actors that tune membrane potential in order to trigger an action potential and eventually neuron communication (Traynelis *et al.*, 2014). Ca^{2+} currents in plant cells have been documented since decades (Dennison and Spalding, 2000; Very and Davies, 2000; Dodd, Kudla and Sanders, 2010; Michard *et al.*, 2011; Costa *et al.*, 2013; Swarbreck, Colaco and Davies, 2013; Candeo *et al.*, 2017; Edel *et al.*, 2017; Wudick *et al.*, 2018). However, the molecular components that mediate this event

are still under investigation (Dodd, Kudla and Sanders, 2010; Stael *et al.*, 2012). Mutations of plant GLRs affected Ca^{2+} influxes, suggesting that GLRs can handle Ca^{2+} dynamics in plant (Wudick *et al.*, 2018). The first report that GLR works as ion channels dates back to 2008 where Tapken and Hollmann transplanted the M2 transmembrane pore region of AtGLRs into rat AMPA and Kainate receptors. These chimeras were tested in *Xenopus laevis* oocytes for ion channel activity. AtGLR1.1 and AtGLR1.4 pores showed Na^{+}, K^{+} and Ca^{2+} permability when 300µM external L-Glutamate was applied (Tapken and Hollmann, 2008). The same authors showed that AtGLR1.4 mediated cationic current activated by L-Methionine in Xenopus oocytes and that mutation in the LBD residues strongly affected L-Methionine-induced plasma membrane depolarization *in planta* (Tapken *et al.*, 2013). Lastly, the Feijo laboratory has shown that AtGLR3.3, PpGLR1 and GLR2 act as non selective Ca^{2+}-permeable channels (Ortiz-Ramírez *et al.*, 2017; Wudick *et al.*, 2018b).

I.5. From structure to function: physiological implications of plant GLRs

I.5.1. GLRs in evolution

It was a surprising and exciting discovery that plants have their own Glutamate receptors. One of the first papers that came out was focused on the evolution of these putative channels. The authors suggested that a common ancestor of Glutamate Receptors existed before the divergence of animals and plants. Moreover, they showed that the two S1 and S2 segments and the transmembrane domains co-evolved and assembled before plants and animals divergence (Chiu *et al.*, 1999). Moving from the observation that plant GLR N-terminal domain shares similarities with metabotropic GLRs while GLR C-terminus is related with iGluRs, Turano *et al* (2001) provided evidences to sustain that an ancestral plant GLR would be the progenitor of animal iGluRs and mGluRs. Accordingly, the two superfamilies of animal neurotrasmitter receptors then evolved *via* distinct evolutionary mechanisms (Turano *et al.*, 2001).

I.5.2. GLRs in monocots

Monocots such as rice do have GLRs. Li *et al.* (2006) showed that mutation in the *Oryza sativa* GLR3.1 affected root elongation. The authors provided evidences for enhanced programmed cell death (PCD) in the *Osglr3.1* mutant, suggesting that GLR3.1 might be involved in root apical meristem (RAM) maintainance during early root development (Li *et al.*, 2006). It has been shown that Glutamate

induces cytosolic Ca^{2+} rises in rice roots (Behera *et al.*, 2015; Ni *et al.*, 2016). OsGLR2.1 and OsGLR3.2 can mediated ion uptake when expressed in bacteria. OsGLR2.1, moreover, mediates Glu-induced cytosolic Ca^{2+} increases in HEK cells (Ni *et al.*, 2016).

I.5.3. GLRs involvement in light signal transduction, Carbon/Nitrogen metabolism and stomatal movement

The plant GLRs are involved in several physiological processes. In the late 90's, Gloria Coruzzi's laboratory showed that plants challenged with 6,7-dinitroquinoxaline-2,3-dione (DNQX), a specific inhibitor of Kainate/AMPA receptors, phenocopyed the Arabidopsis mutant *hy* (*long hypocotyl*) impaired in light-signal transduction. Additionally, plants grown in light but challenged with DNQX showed a 60% reduction in chlorophyll accumulation. These results suggested that GLRs are involved in light-signal transduction in plants (Lam *et al.*, 1998). The contribution of June Kwak's laboratory in understanding the involvement of GLRs in stomatal physiology is also important. They reported that long-term Ca^{2+}-programmed stomatal closure is impaired when AtGLR3.1 is overexpressed (Cho *et al.*, 2009). Recently, Kong *et al* (2016) revealed the involvement of AtGLR3.1 and AtGLR3.5 in a mechanism which regulates basal Ca^{2+} level in guard cells and ROS production dependent on L-Methionine (Kong *et al.*, 2016). In 2003, Kang and Turano reported for AtGLR1.1 a regulatory role in Carbon/Nitrogen metabolism and in ABA biosynthesis related to seeds germination (Kang and Turano, 2003). In this context, AtGLR3.5 was shown to be involved in Ca^{2+} signalling, which mediates seeds germination, counteracting ABA inhibition in the same process (Kong *et al.*, 2015). It was also shown that ABA accumulated in AtGLR1.1 *loss-of-function* resulting in reduced stomata aperture and water loss compared to Col-0 plants (Kang, Mehta and Turano, 2004).

I.5.4. GLRs in immunity responses

The reduced form of the tripeptide Glutathione (GSH_{red}, γ-Glu-L-Cys-Gly) induces cytosolic Ca^{2+} increase and triggers innate immunity responses after *Pseudomonas syringae* infection through the AtGLR3.3 (Li *et al.*, 2013). A similar result was reported by Manzoor *et al*. (2013). Plants defective in AtGLR3.3 expression were hypersensitive to *Hyaloperonospora arabidopsidis* (Manzoor *et al.*, 2013). GLRs activity was also detected upon the perception of the microbe-associated molecular patterns (MAMPs) such as chitin or flagellin. The subsequent elevation of cytosolic Ca^{2+} which is necessary for

the initiation of the innate immune response has been suggested to be GLRs-mediated (Kwaaitaal *et al.*, 2011).

I.5.5. GLRs propagate long-distance signals

Even if plants lack specialized cells for fast communications such as neurons, they may have a sort of "excitable cells" suitable for long-distance communication. The phloem offers a low-hydraulic resistence due to the loss of vacuoles, nuclei and organelles and results in a perfect environment to transmit electrical signals. The Farmer laboratory, in a milestone paper, showed that upon leaf wounding, jasmonates increased in undamaged distal leaves which correlated with membrane depolarization. Mutants of the AtGLRs clade III, GLR3.2, GLR3.3 and GLR3.6 showed reduction (*glr3.2*) or null plasma membrane depolarization (*glr3.3glr3.6*) in distal leaves as well as impaired jasmonate-induced gene expression (Mousavi *et al.*, 2013). Similarly, a contribution for long-distance electrical signal transmission was recent reported for AtGLR3.1 (Nguyen *et al.*, 2018). It was shown that the electrical signals evoked by wounding and caterpillar chewing move through sieve elements and xylem contact cells, anticipating an increase in the Ca^{2+} concentration (Nguyen *et al.*, 2018). Accordingly, the Gilroy laboratory has recently shown that stimulation with 100mM external L-Glutamate induces Ca^{2+} wave propagating through the phloem and plasmodesmata in distal leaves through AtGLR3.3 and AtGLR3.6 (Toyota *et al.*, 2018). Moreover, Salvador-Recatalà in his report showed that GLR3.3 and GLR3.6 propagated the wound-induced action potential throughout the phloem to neighbour cells and that GLR3.5 prevents the AP transmission to non-neighbour leaves. In addition, this electrical signal generates at the shoot and is propagated to the root in adult plant (Salvador-Recatalà, 2016). A local increase in cytosolic Ca^{2+} concentration was instead monitored upon aphid feeding at the epidermal and mesophyll cells. This elevation was dependent on AtGLR3.3 and AtGLR3.6 which interplay with the defense co-receptor Brassinosteroid insensitive-Associated Kinase (BAK1) and the tonoplast localized Ca^{2+}-permeable channel TPC1 (Vincent *et al.*, 2017).

I.5.6. GLRs in reproduction

GLRs in plants are also involved in reproduction and male-female recognition. In this context, the Feijo laboratory reported fundamental information on GLR-mediated pollen tube growth and guidance towards the female reproductive organ. In a pivotal work, Michard *et al*. (2011) showed

957 that the ablation of AtGLR1.2 strongly affected tip-cytosolic Ca^{2+} gradient in pollen tube thus altering
958 pollen tube growth and morphogenesis. Moreover, wild-type pollen tube did not grow properly on
959 serine-racemase (an enzyme required for the D-serine biosynthesis) mutant pistils. The authors
960 suggested that an amino acid mediated recognition mechanism could exist between male
961 gametophyte and pistil tissues. Here, D-Serine would act as a possible agonist for pollen tube
962 guidance and growth control (Michard *et al.*, 2011). Similarly, the same laboratory reported that
963 disruption of the two GLRs in the moss *Physcomitrella patens*, GLR1 and GLR2, impaired sperm cell
964 chemotaxis and sperm cell guidance towards female reproductive organ. PpGLR1 and PpGLR2
965 encoded non selective Ca^{2+}-permeable channels (Ortiz-Ramírez *et al.*, 2017). In a complex and
966 fascinating work, Wudick *et al*. (2018b) reported that mutations of several AtGLRs (e.g. AtGLR1.2,
967 AtGLR1.4, AtGLR2.1, AtGLR3.3) led to severe pollen tube phenotypes and Ca^{2+} flux impairment
968 (Wudick *et al.*, 2018b). Moreover, a Japanese group reported that elevation of cytosolic Ca^{2+} is
969 essential for self-incompatibility response and that 1mM D-(−)-2-amino-5- phosphonopentanoic acid
970 (AP-5) treatment, an iGluRs competitive inhibitor, impaired this phenomenon. Disruption of AtGLR3.5
971 and AtGLR3.7 partially compromise Ca^{2+} elevation and thus self-incompatibility response (Iwano *et*
972 *al.*, 2015a).

973

Aim of the thesis

Ca^{2+} signaling is known to be a mechanism at the basis of a plethora of plant environmental responses that are required for their survival. In the plant field there is still a lack of information regarding the molecular identity of Ca^{2+} permeable channels involved in the generation of stimuli-induced cytosolic Ca^{2+} increases.

In this context it is worth mentioning that in the early 2000, the laboratory of Gloria Coruzzi identified in the model plant model *Arabidopsis thaliana* genes coding for putative ionotropic Glutamate Receptors and termed Glutamate Receptor-like (AtGLRs), which are putative Ca^{2+}-permeable channels. Arabidopsis has 20 genes coding for GLRs divided into three phylogenetic clades, with Clade III the nearest to animal Glutamate Receptors (iGluRs). Since their discovery, GLRs have been associated with several aspects of plant physiology. In fact, stomata movement, pollen tube tip growth, leaf to leaf communication, lateral root development, resistance against bacteria have been linked to GLRs activity. Additionally, it has been reported that GLRs, being putative Ca^{2+}-permeable channels, can handle Ca^{2+} dynamics in response to a plethora of cues such as amino acids addition, cold, aphids and caterpillar attacks and wounding. iGluRs are tetrameric channels activated by amino acids occupation of the ligand binding domain. Whether amino acids could also activate plant GLRs has to be demonstrated. Furthermore, so far little is known about the basic functional properties of several GLR isoforms, such as ion permeability, sub-cellular localization, subunits interaction, desensitization, channel regulation etc..

In such a scenario, the goal of the present study was to investigate the roles and functions of two distinct Arabidopsis GLRs isoforms, AtGLR3.3 and AtGLR3.7 (hereafter called AtGLR3.x) in the generation of local amino acid-induced cytosolic Ca^{2+} increases and in long-distance Ca^{2+} signalization. Our interest in AtGLR3.x started from the observation of their predicted expression patterns throughout the plant (retrieved from microarray data). In fact, AtGLR3.x are expressed in root meristematic zone in young seedlings (cells that sense external cues) and in vascular tissues (cells involved in long-distance signaling).

In the present work our main aims could be subsumed in the following points:

- to define the role of AtGLR3.3 and AtGLR3.7 in the amino acids-triggered cytosolic Ca^{2+} elevation in root tip cells;
- to define the AtGLR3.3 and AtGLR3.7 expression pattern and their sub-cellular localization;

- to define a possible AtGLR3.3 and AtGLR3.7 interaction;
- to define the role of AtGLR3.3 and AtGLR3.7 in the long-distance Ca^{2+} signaling.

To achieve these main goals, we employed a combination of advanced molecular imaging approach, molecular biology and reverse genetics, coupled with electrophysiology and cell biology approach.

Chapter II. Results and discussion

II.1. Primary amino acids sensing occurs at the root meristematic tissues in *Arabidopsis thaliana*

Different stimuli are known to induce a rise of cytosolic Ca^{2+} concentration in root cells. L-Glutamate triggered a transient, rapid elevation of cytosolic Ca^{2+} at the root meristematic cells of *Arabidopsis thaliana* Col-0 plants when applied exogenously at 1mM final concentration (Fig. 1A). The *in vivo* visualization of Ca^{2+} was made possible thanks to the use of Arabidpsis plants expressing the cytosolic localized FRET-based Ca^{2+} sensor Yellow Cameleon YC3.6 (NES-YC3.6) coupled with fluorescence microscopy (Nagai *et al.*, 2004; Krebs *et al.*, 2012). Based on the available literature (Dennison and Spalding, 2000; Qi *et al*., 2006, Stephens and Spalding, 2006; Li *et al.*, 2013) we also hypothesized that beyond L-Glutamate, other amino acids (AAs) could also trigger an elevation of cytosolic Ca^{2+} concentration in root tip cells when applied exogenously. To this aim, we therefore assayed whether the remaining nineteen L-isomer proteinogenic AAs could trigger a cytosolic Ca^{2+} elevation in root meristematic cells. Six out of nineteen L-AAs, i.e. L-Cysteine, L-Alanine, Glycine, L-Serine, L-Asparagine and L-Methionine were able to induce a transient rise of the cytosolic Ca^{2+} concentration (Fig. 1B). These observations were indeed consistent with previous published data which reported cytosolic Ca^{2+} rises in root cells upon AA addition, however these previous works did not provide information regarding the tissue specificity of the response (Dennison and Spalding, 2000; Qi *et al*., 2006, Stephens and Spalding, 2006; Li *et al.*, 2013). In our experimental conditions, L-Glu, L-Cys, L-Ala and Gly were the most effective AAs to increase the cytosolic Ca^{2+} concentration, ranged from 0.37±0.08 as maximal normalized ΔR ($\Delta R_{max}/R_0$) triggered by the L-Cys to 0.26±0.04 elicited by the Gly. L-Ser and L-Asn triggered a cytosolic Ca^{2+} increase of 0.14±0.03 and 0.12±0.03, respectively ($\Delta R_{max}/R_0$). L-Methionine was the less effective AA, with a Ca^{2+} increase of 4% compared to the one triggered by L-Glu (0.017±0.001**,** as $\Delta R_{max}/R_0$) (Fig. 1B and C; Supp. Mat. Table 2A). D-Serine at high concentration (up to 10mM) was ineffective in triggering a cytosolic Ca^{2+} elevation, albeit it was reported to trigger a cytosolic Ca^{2+} increase at the tip of pollen tube (Michard *et al.*, 2011). L-Tryptophan, which increased currents in a GLR-dependent fashion in *Xenopus* oocytes, did not trigger any cytosolic Ca^{2+} increase in root tip cells of the meristematic zone (Tapken *et al.*, 2013) (Fig. 1B and C; Supp. Mat. Table 2). With the final aim to report an accurate spatial (single cell visualization) and temporal description of AAs-induced Ca^{2+} transients in root tip, we employed the recently developed Light Sheet Fluorescence Microscopy (LSFM)-FRET setup (Costa *et al*., 2013; Candeo *et al*., 2017). In accordance with the previous experiments, 4D acquisitions (*x, y, z, t*) of Col-0 seedling harbouring

NES-YC3.6 reported L-Glutamate-induced cytosolic Ca^{2+} elevation in root tip cells (Fig. 2A and B). In fact, when added exougenously at 1mM final concentration, L-Glutamate triggered a primary and transient cytosolic Ca^{2+} elevation at the epidermal cells of the lateral root cap of the meristematic zone, which then spread into the inner tissues (most likely cortex and endodermis) and propagated shootward along the primary root (Fig. 2B). Our analysis supported previously published results of 3D imaging (*x,y,t*) of primary root tip treated with 1mM L-Glutamate which showed a propagation of cytosolic Ca^{2+} along the root tip cells of the meristematic zone upon the primary perception by outer root tip cells (Costa *et al.*, 2013).

In summary, seven proteinogenic L-AAs triggered a primary transient cytosolic Ca^{2+} increase at the epidermal cells of the lateral root cap of the meristematic zone when added exogenously at a final concentration of 1mM. Then, a shootward Ca^{2+} elevation event occurred.

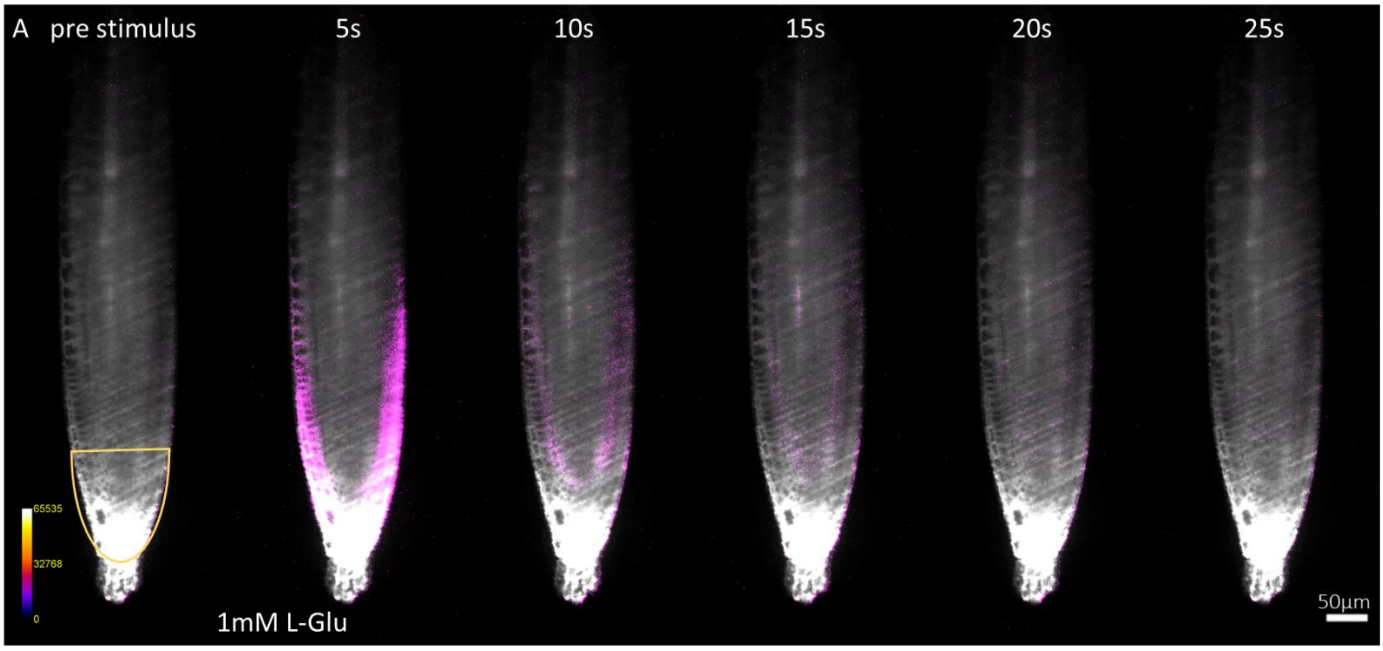

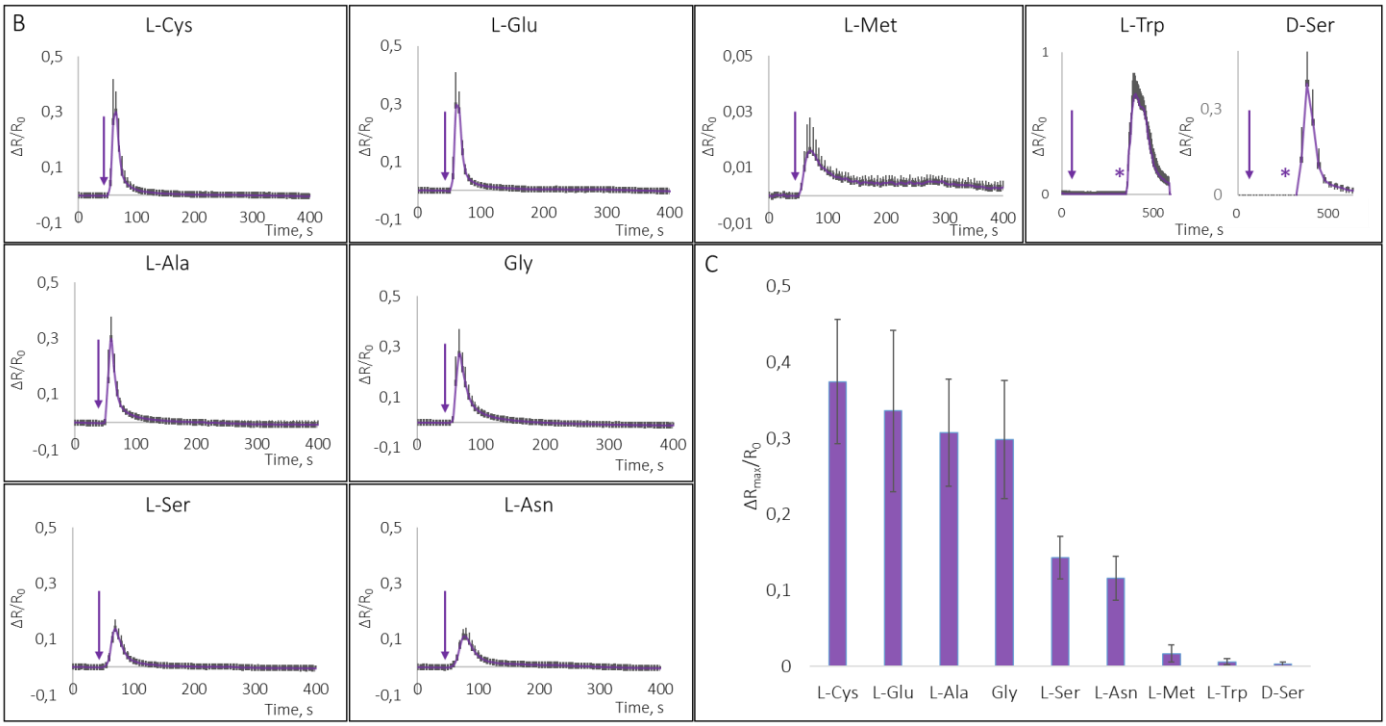

Fig. 1. Amino acids-evoked Ca^{2+} elevation in root cells of the meristematic zone.

A. Time-lapse frames of Col-0 root meristematic zone exposed to external 1mM L-Glu acquired by means of Light Sheet Fluorescence Microscopy. The yellow region of interest (ROI) in 'pre-stimulus' picture represents the ROI used to calculate a change in the cpVenus/CFP ratio reported as trend (plotted against the time) in B or histograms in C, respectively. Increase in the FRET efficiency is reported in false colors (the brighter, the higher the FRET efficiency). **B**. Trend of the normalized cpVenus/CFP ratios ($\Delta R/R_0$) recorded in Col-0 seven-day-old seedlings expressing the FRET sensor NES-YC3.6 and treated with external amino acids at the final concentration of 1mM. Under a wide-field microscope, plantlets were constantly supefused with standard imaging solution and transiently exposed to the selected amino acid (dissolved in imaging solution) for 3min. 100µM ATP was employed after L-Trp and D-Ser treatments to show that seedlings were indeed responsive. Arrows and stars indicate the moment when seedlings faced 1mM AAs or 100µM ATP, respectively. **C.** Maximal normalized cpVenus/CFP ratios ($\Delta R_{max}/R_0$) triggered by 1mM external amino acids. Traces are the average of *n*>4±S.D.

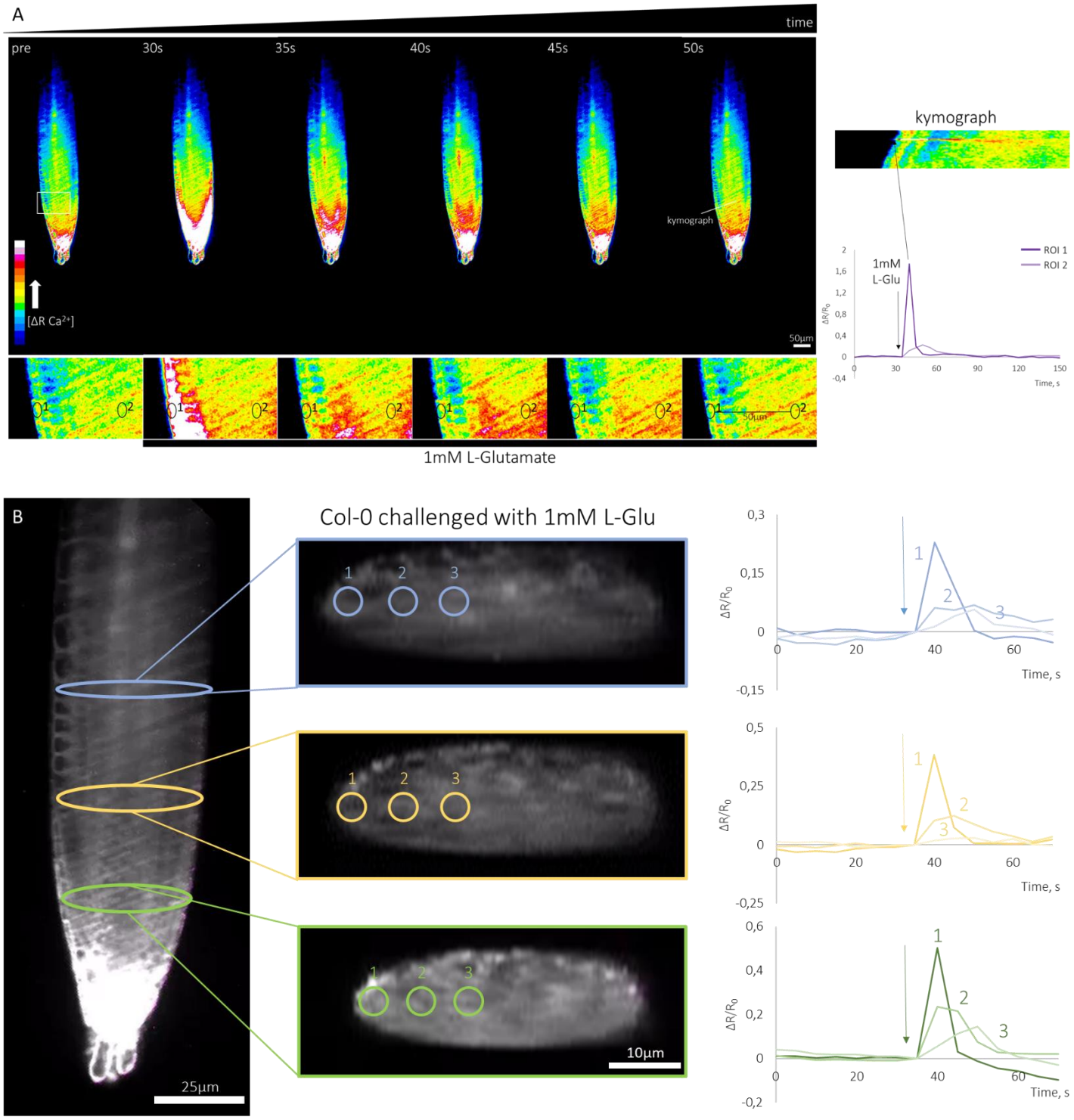

Fig. 2. 4D acquisitions (*x, y, z, t*) of root tip meristematic cells challenged with 1mM L-Glutamate by means of Light Sheet Fluorescence Microscopy.

A. Time-lapse frames of Col-0 root meristematic zone exposed to external 1mM L-Glu. An increase in the cpVenus/CFP ratio primarly occurred at the lateral root cap cells. A region of interest in the root meristematic zone was zoomed and two ROIs corresponding to two different cells were analysed for FRET increase and plotted against the time (right panel, $\Delta R/R_0$). From the cpVenus/CFP frames, a

kymograph was extracted following the temporal evolution of the line drawn on the 50s time lapse frame. The increase in the FRET efficiency is reported in false colors (the brighter, the higher the FRET efficiency). **B**. Volumetric analysis (*x, y, z, t*) of the same Col-0 NES-YC3.6 plant showed in A. Z stacks were acquired every 5sec. Cross section analysis along the root meristematic zone showed a primary increase in the FRET efficiency at the epidermal cells with a centripetal diffusion of the Ca^{2+} signal, from the most external cells to the stele. Three ROIs were drawn in the cross section covering epidermal cells (1), endondermal and cortex (2), and stele (3), respectively. Trends of the normalized cpVenus/CFP ratios ($\Delta R/R_0$) recorded in the three different cross sections were reported in the corresponding graphs (on the far right). Arrows indicate the moment when the seedling faced 1mM Glutamate administration. The experiment reported in Fig. 2 is representative of three independent experiments.

II.2. Two Glutamate Receptor-like isoforms belonging to Clade III are highly expressed in the epidermal cells of the lateral root cap in Arabidopsis

The demonstration that Arabidopsis genome shares with animals a gene family encoding for putative ionotropic Glutamate Receptors (Lam *et al.*, 1998; The Arabidopsis Genome Initiative, 2000) led us to hypothesises that the fast cytosolic Ca^{2+} increase upon AAs addition may be dependent on the activity of this class of channels. We queried the electronic Fluorescent Pictograph (eFP) database (Dinneny *et al.*, 2007; Winter *et al.*, 2007) to determine the mRNA expression level coding for the Glutamate Receptor-like (GLR) isoforms in the tissues of the root meristematic zone of Arabidopsis, with particular attention on the lateral root cap and epidermis (Supp. Mat. Fig 1). In fact, a primary response to AAs (in terms of cytosolic Ca^{2+} increase) occured at the epidermal cells of the lateral root cap (Fig. 2A and B). Members of the AtGLR family belonging to Clade III resulted the highest expressed isoforms in all the tissues analysed, followed by Clade I and Clade II (Fig. 3A). Notably, AtGLR2.1 resulted the most expressed GLR in the whole root with a particular high expression level in the epidermis and lateral root cap, as well as in root hairs (Supp. Mat. Fig. 2). However, GLRs belonging to Clade III showed a more homogenous and wider expression in the tissues of the meristematic zone. Particularly, among Clade III, AtGLR3.3 and AtGLR3.7 were the most abundant isoforms in the epidermal cells of the lateral root cap (Fig. 3A). We therefore focused our attention on these two isoforms and their possible role in the AAs-evoked cytosolic Ca^{2+} increase was further investigated.

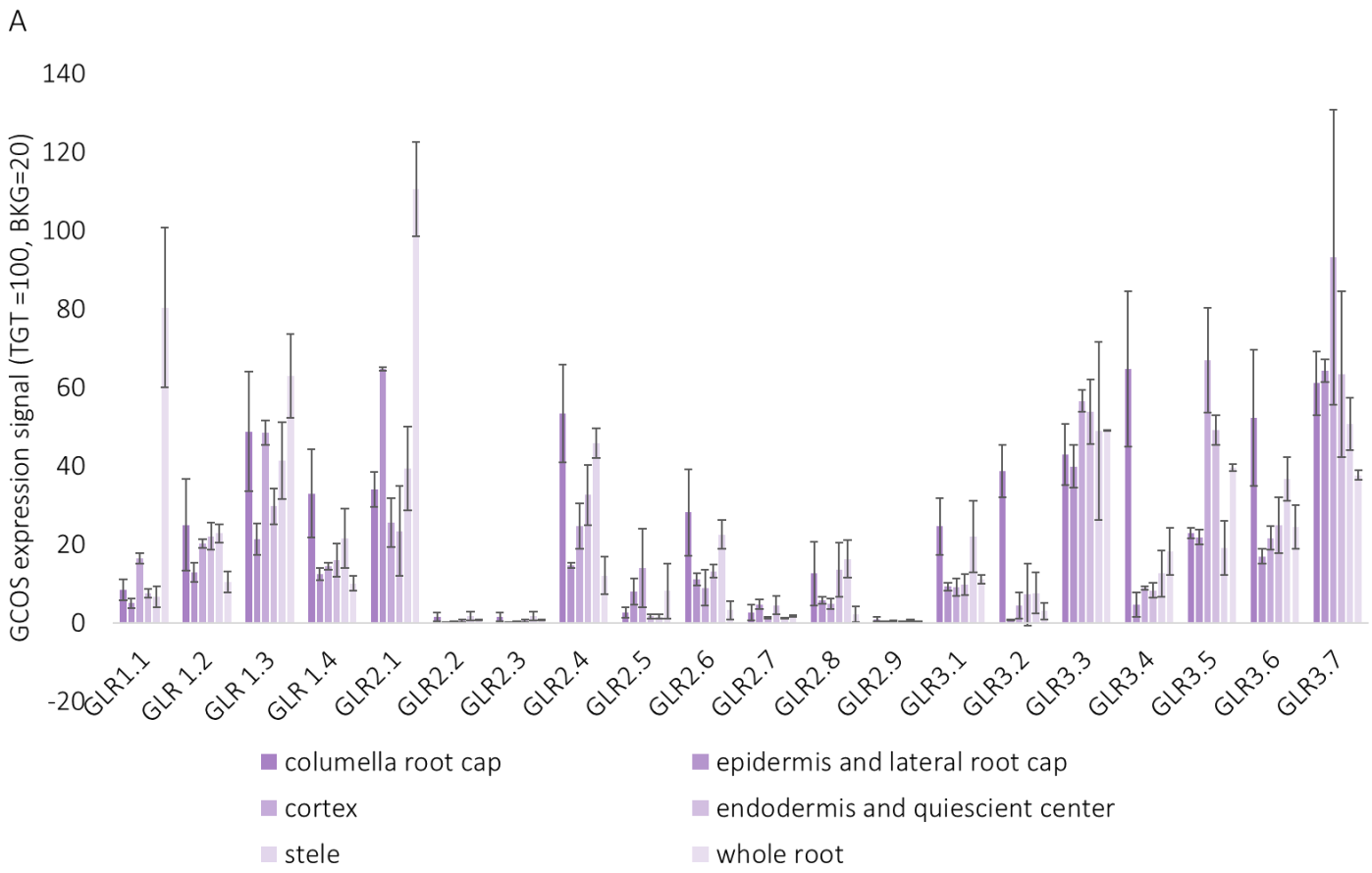
A
GCOS expression signal (TGT =100, BKG=20)
140
120
100
80
60
40
20
0
-20
GLR1.1
GLR 1.2
GLR 1.3
GLR 1.4
GLR2.1
GLR2.2
GLR2.3
GLR2.4
GLR2.5
GLR2.6
GLR2.7
GLR2.8
GLR2.9
GLR3.1
GLR3.2
GLR3.3
GLR3.4
GLR3.5
GLR3.6
GLR3.7
columella root cap
epidermis and lateral root cap
cortex
endodermis and quiescient center
stele
whole root

1106

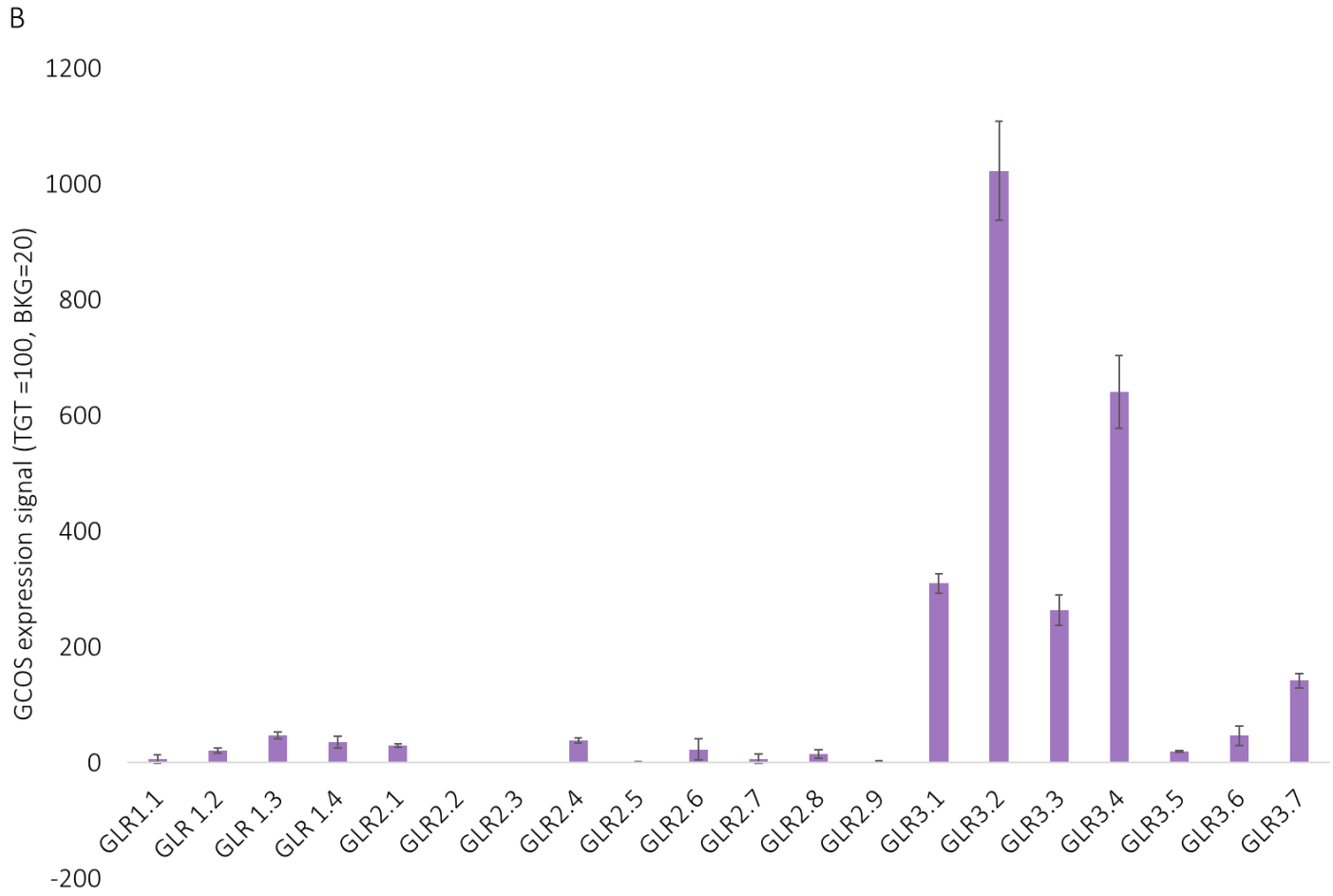

Fig. 3. GLRs expression in root tissues. A. Absolute expression of GLRs in columella root cap, epidermis and lateral root cap, cortex, endodermis and quiescent center, stele and whole root from 6/7-day-old Arabidopsis seedlings. Values were collected from eFP browser(Dinneny *et al.*, 2007; Winter *et al.*, 2007). *n*>2, reported as Gene-Chip Operating Signal expression signal (target intensity TGT=100 and background BKG=20)±S.D. **B**. Absolute expression of GLRs in root protophloem. *n*>2, reported as Gene-Chip Operating Signal GCOS expression signal (target intensity TGT=100 and background BKG=20)±S.D.

II.3. Expression pattern of AtGLR3.3 and AtGLR3.7

In order to better dissect the expression pattern of AtGLR3.3, we pursued a translational fusion protein strategy. Consequently, we analysed a C-terminal eGFP-tagged AtGLR3.3 fusion protein in a *null-allele* for AtGLR3.3 whose expression was driven by the AtGLR3.3 native promoter (Vincill *et al.*, 2013). Confocal analyses of 7-day-od seedling reported a widespread AtGLR3.3 expression along the plant body at seedling stage (Fig. 4A). eGFP fluorescence was detected in cotyledons, guard cells,

hypocotyl and root tissues. AtGLR3.3-eGFP localizes at the stele, epidermal, cortex and endodermal cells in the root elongation and maturation zone. The AtGLR3.3 expression along the vascular tissues, both in root and leaves, was in accordance with published reports that claimed the GLR3.3 was involved in long-distance electrical signalling (Mousavi *et al.*, 2013; Vincent *et al.*, 2017; Nguyen *et al.*, 2018; Toyota *et al.*, 2018). Notably, AtGLR3.3 was highly expressed at the root tip meristematic zone.

As regards GLR3.7 expression, to look at the overall expression of AtGLR3.7, we isolated two different AtGLR3.7 promoters and fused them to the reporter gene β-glucuronidase (GUS). However, both were not functional when expressed in Arabidopsis Col-0 plants (unpublished data). For this reason, we came back to the literature and we found out that Roy *et al.* (Roy *et al.*, 2008) reported GUS-staining of stable plants harbouring a *pAtGLR3.7::uidA* construct (Fig. 4B). They showed an extensive activity of the AtGLR3.7 promoter throughout the plant body. In particular, the transcriptional reporter was active at the root apex, root hairs and in the vascular tissues of 7-day–old seedlings as well as in leaf veins and inflorescences of mature plants (4-6week-old). Unfortunately, the transgenic line reported in that works is no longer available thus not allowing us to confirm their data. Nevertheless, quantitative analysis of transcript abundance revealed that AtGLR3.7 is expressed in 7-day-old seedlings (Supp. Mat. Fig 3C).

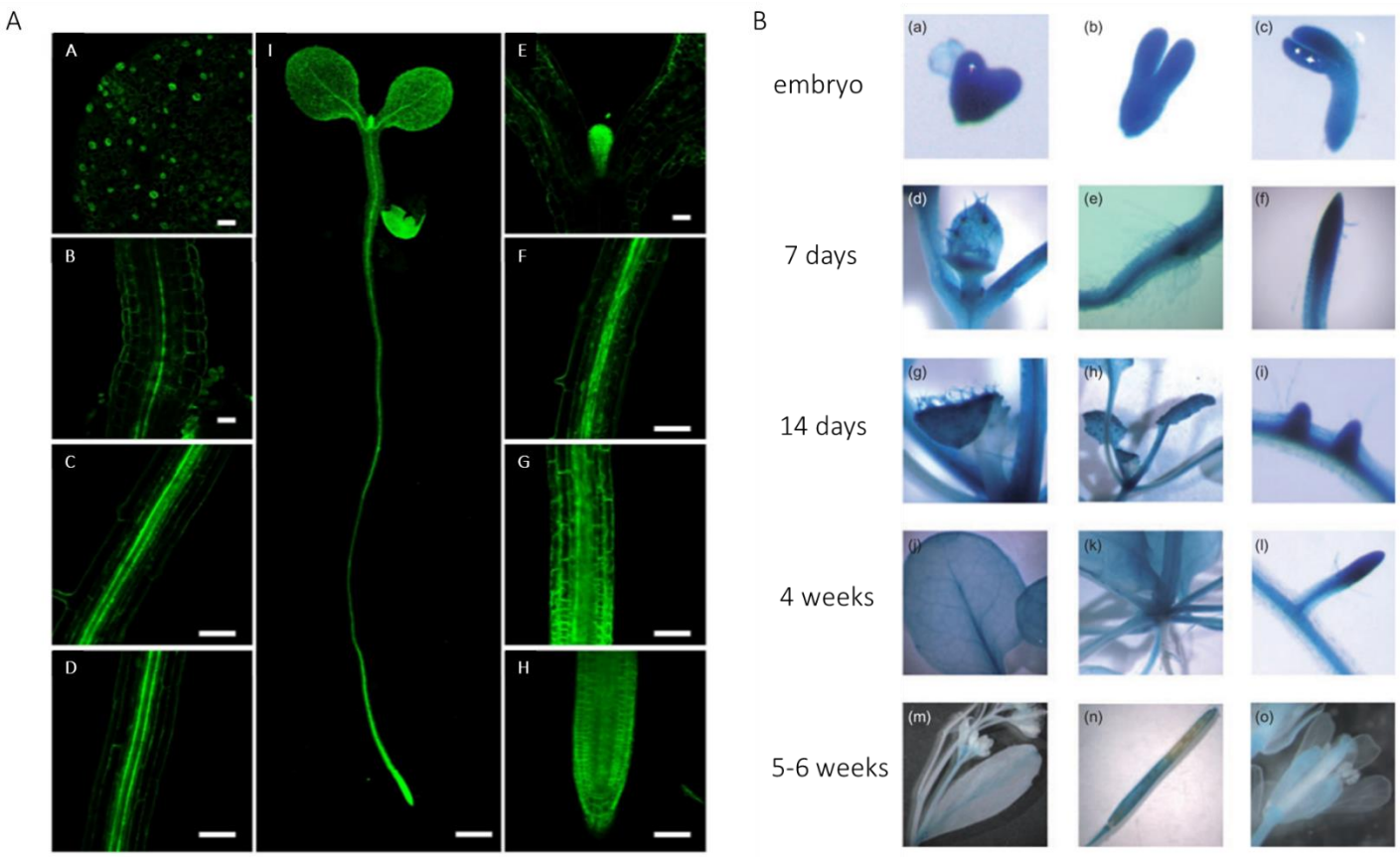

Fig. 4. Expression pattern of the translational fusion protein AtGLR3.3-eGFP and of the transcriptional reporter gene *pAtGLR3.7::uidA*. **A.** Confocal images of 7-day-old seedling defective in GLR3.3 expression complemented with the fusion protein AtGLR3.3-eGFP expressed under the AtGLR3.3 native promoter. AtGLR3.3-eGFP was expressed in guard cells (A), hypocotyl (B), cotyledons (E), stele tissues (C, D, F), epidermal and endodermal cells (G) and root tip cells (H). GLR3.3-eGFP was also expressed in cotyledon veins (I). Scale bars: 250µm for I, 40µm for C, D, F, G, H and 20µm for A, B, E. **B.** GUS staining of the transcriptional reporter *pAtGLR3.7::uidA* in embryo, 7 and 14 day-old seedlings, 4 and 5-6 week-old plants. In particular, the GLR3.7 promoter was active in root tip (f), root hairs (i), in vasculature tissues (f) of mature plants, in leaves, stem, floral abscission zone and sepals/petals of 5-6 week-old plants (m-o). Image edited from Roy *et al.* (Roy *et al.*, 2008)

II.4. Sub-cellular localization of AtGLR3.3 and AtGLR3.7

We moved further, and we defined the sub-cellular localization of AtGLR3.3 and AtGLR3.7. As regards AtGLR3.3 we assayed 7-day-old seedlings which stably expressed the translational fusion protein GLR3.3-eGFP (under the control of its native promoter). We firstly focused our analysis on the root

cells of the meristematic zone (Fig. 5A). In these tissues, AtGLR3.3-eGFP was mainly spotted at the endomembranes. In fact, the presence of nuclear envelopes, that in plant cells are in *continuum* with the endoplasmic reticulum (ER), suggested that AtGLR3.3 localized most likely at the ER and it has to be sorted by the secretory pathway to act as a plasma membrane channel (Fig. 5A, pictures J-M). This is consistent with a recent report by the Feijo laboratory which showed that AtGLR3.3 localizes at the sperm membranes and endomembranes, but not at the pollen tube plasma membrane. The Cornichon homolog proteins CNIH 1 and 4 eventually sort it to the plasma membrane (Wudick *et al.*, 2018b). Moreover, we also observed a clear polar localization of the fusion protein, with eGFP signal enriched at the apical and basal membranes perpendicular to the long axis of the primary root. This peculiar polar localization was particularly evident for AtGLR3.3 in epidermal cells and cortex (Fig. 5A, I, B, J). The same acquisition analysis confirmed a widespread localization to the endomembranes for AtGLR3.3 in root meristematic zone. Then, from root tissues analysis we moved to a single root cell analysis. In fact, outside of guard cells, AtGLR3.3 was also expressed in root hairs (Fig 5A and Supp. Mat. Fig. 2). Intriguingly, while AtGLR3.3 localized at the endomembranes of bulged and youngest root hairs (Fig. 5, K-N), the fusion protein clearly decorated the plasma membrane in longest root hairs (>80-100µm) (Fig. 5, O-P).

As reported above we failed to isolate a functional promoter for AtGLR3.7. So, in order to study the sub-cellular localization of this isoform we assayed 7-day-old Col-0 seedlings harbouring the fusion protein GLR3.7$_{cds}$-YFP under the control of an ubiquitously and constitutively active promoter (a double cauliflower mosaic virus promoter). Confocal analysis suggested that AtGLR3.7 localizes at the endomembranes in the root elongation zone even though we can not exclude an over-loaded issue due to the constitutively high expression of GLR3.7$_{cds}$-YFP (Fig. 5B, pictures A-C). Looking at single cells, similarly to AtGLR3.3, it is expressed in root hairs (Supp. Mat. Fig. 2) but differently from AtGLR3.3, AtGLR3.7 localized at the endomembranes in root hairs indipendently of the developmental stages (Fig. 5B, D-O). As a second approach, we investigated the sub-cellular localization of AtGLR3.7 when transiently expressed in *Nicotiana benthamiana* leaves and in Arabidopsis protoplasts isolated from mesophyll cells. The GLR3.7$_{cds}$-YFP fusion expressed in tobacco leaves localized at the endomembranes (nuclear envelope in continuity with ER membranes) and co-localized with the ER marker mCherry-HDEL (Fig. 5C). Similarly, we detected the fluorescence signal emitted from YFP at the endomembranes of Arabidopsis Col-0 mesophyll protoplasts expressing GLR3.7$_{cds}$-YFP, confirming our previous experiment in tobacco (Fig. 5D). Altogether, these results supported that these two GLRs mainly localize at the endomembranes. However, accordingly to cell

types and developmental stages, the two GLRs may be sorted to the plasma membrane (e.g. longer root hairs for AtGLR3.3).

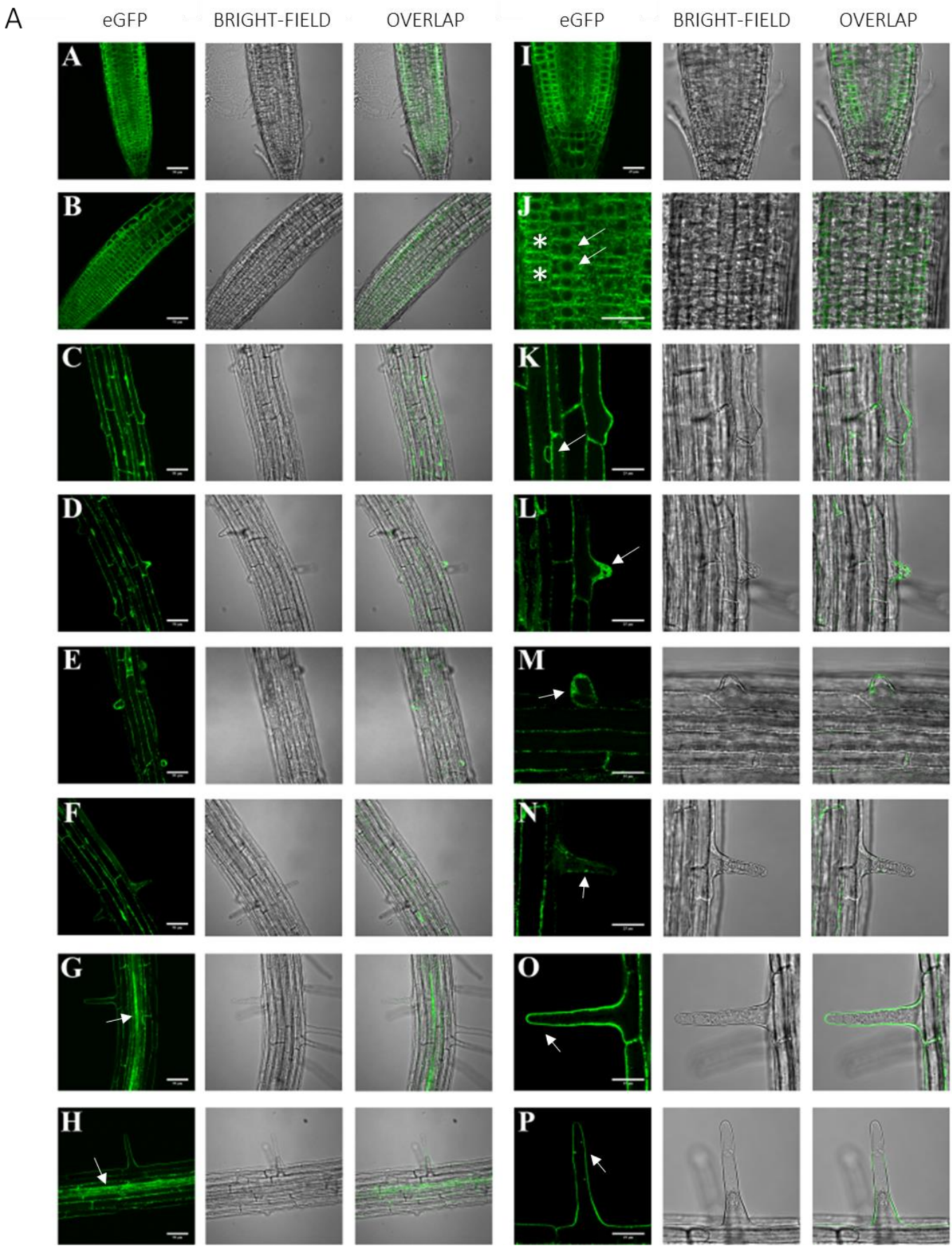
A
eGFP
BRIGHT-FIELD
OVERLAP
eGFP
BRIGHT-FIELD
OVERLAP
A
B
C
D
E
F
G
H
I
J
K
L
M
N
O
P

1189

1190

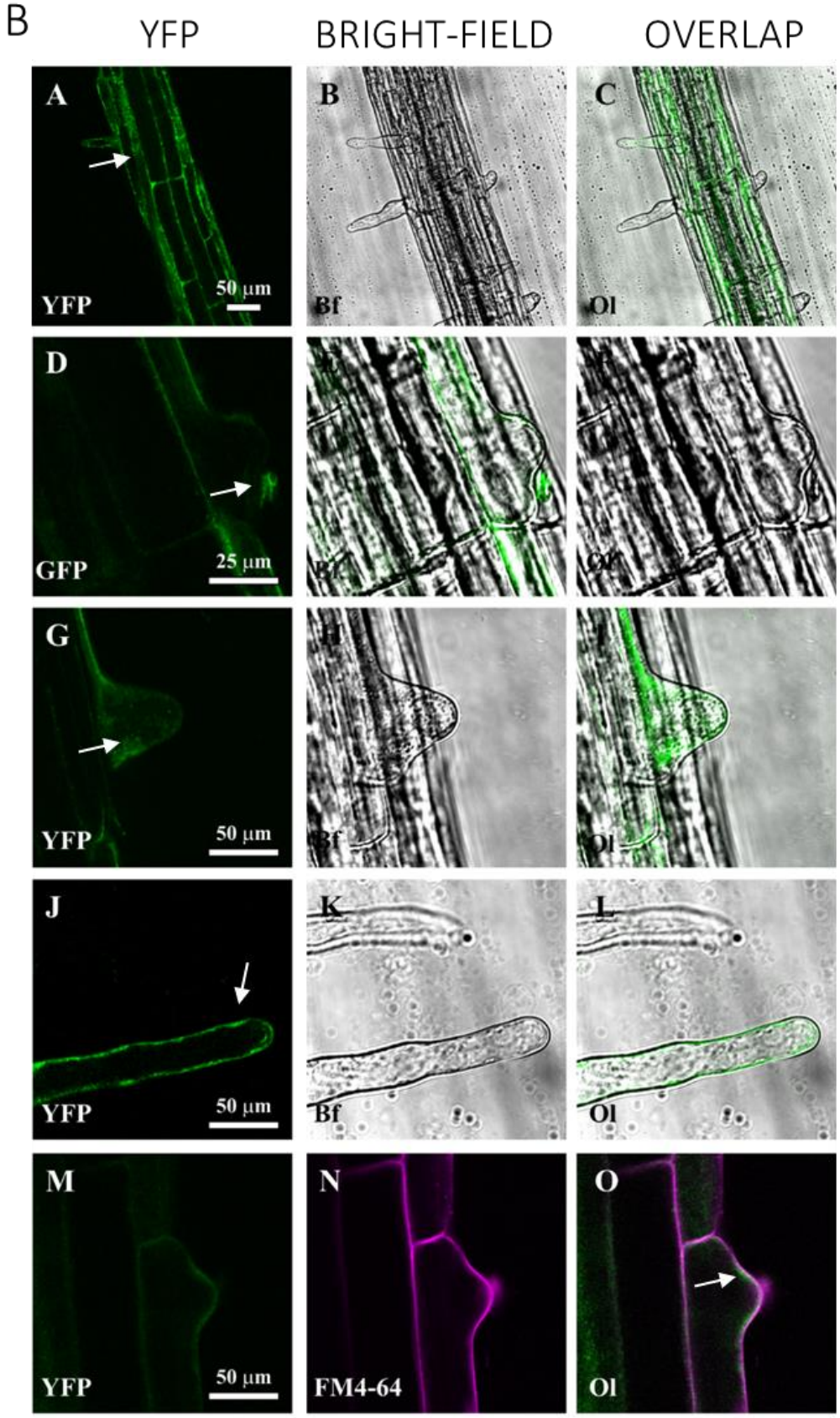
B
YFP
BRIGHT-FIELD
OVERLAP
A
B
C
YFP
50 µm
Bf
Ol
D
GFP
25 µm
G
YFP
50 µm
Bf
Ol
J
YFP
50 µm
K
L
Bf
Ol
M
N
O
YFP
50 µm
FM4-64
Ol

1191

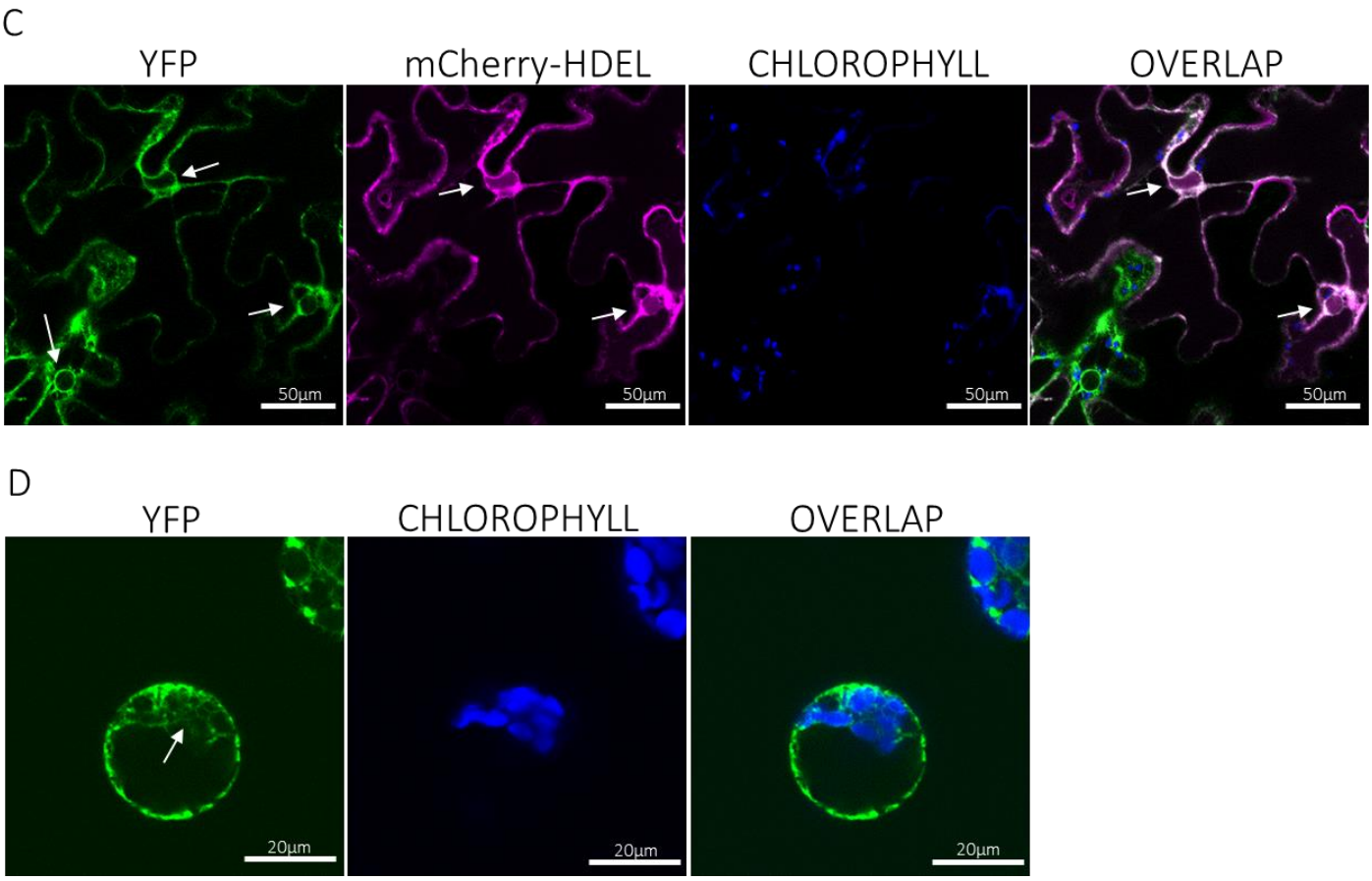

1192

1193 **Fig. 5. Sub-cellular localization study of AtGLR3.3 and AtGLR3.7.**

1194 **A.** A-H Low magnification acquisitions of primary root and root hairs of 7-day-old seedlings carrying
1195 pGLR3.3::GLR3.3-eGFP by means of confocal microscope. eGFP fluorescence was detected at the root
1196 meristematic zone (A-B) as well as in the lower and upper maturation zone (C-H). GLR3.3 localizes
1197 throughout the root body, with high abundance in the stele (G-H, arrows). I-P Higher magnification
1198 acquisitions. GLR3.3 localized at the endomembranes in cells of the root meristematic zone where it
1199 sorrounded the nuclear envelopes (J-K, arrows). In B and J GLR3.3 accumulation at the plasma
1200 membrane perpendicular to the y axis of the primary root is evident (white stars in J). GLR3.3 was
1201 also expressed in root hair cells (K-P). It accumulated at the endomembranes in young root hairs of
1202 the lower maturation zone (<80µm) (L-N, arrows), whereas it appeared at the plasma membrane in
1203 longer root hairs of the upper maturation zone (>80-100µm, arrows) (O-P). The three columns
1204 indicated eGFP fluorescence (first column, green), bright-field (second column, gray) and a composite
1205 image of eGFP channel and bright-field (third column). Scale bars: 50 µm (A-H), 25 µm (I-P). **B.**
1206 Confocal acquisition of Col-0 7-day old seedlings harbouring the fusion protein GLR3.7$_{cds}$-YFP whose
1207 expression was driven by a double 35S promoter. A-C GLR3.7$_{cds}$-YFP was observed at the
1208 endomembranes in the root elongation zone (arrow), as well as in root hairs at different

developmental stages (D-L). YFP (green) and FM4-64 (purple), a plasma membrane marker, fluorescences did not overlap (arrow) (M-O). **C.** GLR3.7$_{cds}$-YFP (green) expressed in *Nicotiana benthamiana* leaves localized at the ER (arrows indicated nuclear envelops) and co-localize with the ER marker mCherry-HDEL (purple). Chlorophyll in blue, scale bars: 50µm. **D.** GLR3.7$_{cds}$-YFP (green) localized at the endomembranes (arrow) in Arabidopsis mesophyll protoplast. Chlorophyll in blue, scale bars: 20µm. Images reported here are representative of >3 independent trials for each experimental set.

II.5. GLR-dependency of the amino acid-induced Ca^{2+} transients in the root meristematic zone of Arabidopsis

The observation that a primary Ca^{2+} increase induced by external AAs occured at the root meristematic zone which correlated with both AtGLR3.3 and AtGLR3.7 expressions, lead us to hypothesize that these channels could be involved in the amino acid-triggered cytosolic Ca^{2+} elevation. To test this hypothesis, we selected two independent *null-allele* for AtGLR3.3 (*glr3.3-1* and *glr3.3-2*) (Qi, Stephens and Spalding, 2006) and two independent insertional mutants for AtGLR3.7 (*glr3.7-1* (Michard *et al.*, 2011) and *glr3.7-2*). A third *non sense* mutant (*glr3.7-3*) in the *A. thaliana* accession C24 was also selected (Iwano *et al.*, 2015b). We firstly checked that all the *null-allele* lines were homozygous for the T-DNA insertions and we confirmed the *non-sense* mutation in the *glr3.7-3* by DNA sequencing (Suppl. Mat. Fig. 3B). We later confirmed the lack of AtGLR3.3 and AtGLR3.7 transcripts by quantitative RT-PCR (Suppl. Mat. Fig. 3C). To define the possible contribution of the AtGLR3.3 and AtGLR3.7 in the AA-induced Ca^{2+} transients in root meristematic cells, the isolated mutant lines were stably transformed with the Ca^{2+} sensor NES-YC3.6. We first checked if the lack of AtGLR3.3 could unbalance the resting cytosolic Ca^{2+} level. No differences of the resting cpVenus/CFP ratio were apparent in the mutant lines when compared with Col-0 (3.13±0.11 and for Col-0, 3.06±0.13 for *glr3.3-1*, 3.09±0.15 for *glr3.3-2*, as cpVenus/CFP ratio; n>5 for each line) (Fig. 6B, Supp. Mat. Table 1A). We moved further assaying the AAs-induced Ca^{2+} elevation in the two *null-alleles* for GLR3.3 side by side with Col-0. Interestingly, 1mM AAs treatments failed to trigger a cytosolic Ca^{2+} elevation on the two insertional mutants for GLR3.3, whereas a cytosolic Ca^{2+} increase was detected in Col-0 root meristematic cells (Fig. 6A, Supp. Mat. Table 2A). To confirm the functionality of the NES-YC3.6 sensor in the mutant lines we treated them with other stimuli known to induce a rise in cytosolic Ca^{2+} concentration. We chose adenosine 5'-triphosphate (ATP) as a stimulus, which can

function as a damage-associated molecular pattern molecule when released in the apoplast upon external stimuli (e.g. wounding). External ATP, eADP and other purine nucleotides are recognised by the L-type lectin receptor-like kinase DORN1 (DOESN'T RESPOND TO NUCLEOTIDE) that in turns triggers a rise in cytosolic Ca^{2+} concentration, Nitric Oxide and Reactive Oxygen Species production *in planta* (Costa *et al.*, 2013; Chen *et al.*, 2017). 100µm eATP application elicited a maximal increase in the normalized ΔR ($\Delta R_{max}/R_0$) as 0.75±0.09 in Col-0 root meristematic cells (Fig. 6A; Supp. Mat. Table 2A). In parallel, eATP induced a $\Delta R_{max}/R_0$ increase of 0.82±0.22 in *glr3.3-1* and 0.67±0.13 in *glr3.3-2*, respectively (*n*>5 for each line) (Fig. 6A; Supp. Mat. Table 2A). The maximum peaks triggered by eATP in the different backgrounds showed no statistical differences, hence demonstrating the proper functionality of the NES-YC3.6 sensor in the GLR3.3 *null-alleles*. Moreover, the fact that *loss-of-function* mutants for GLR3.3 failed in the AAs-triggered cytosolic Ca^{2+} increase but responded as Col-0 when exposed to eATP addition support the GLR3.3 specificity in the AAs perception and response.

We later assessed whether disruption of AtGLR3.7 could perturb the resting cytosolic Ca^{2+} concentration. As matter of fact, the cpVenus/CFP ratio remained unaltered in the three mutants for GLR3.7 when compared to controls (2.96±0.15 for Col-0 (1), 3.14±0.11 for Col-0 (2), 2.63±0.12 for C24 compared respectively to 3.17±0.15 for *glr3.7-1*, 2.96±0.14 for *glr3.7-2*, 2.68±0.07 for *glr3.7-3*) (*n*>5 for each line) (Fig. 7B; 8B, and 9B; Supp. Mat. Table 1A). We then monitored the responses to the AAs in the *loss-of-function* mutants for GLR3.7. Surprisingly, *glr3.7-1 loss-of-function* showed a higher cytosolic Ca^{2+} elevations compared to Col-0 (1) when transiently exposed to the 7 AAs (Fig. 7A, Supp. Mat. Table 2B). The exacerbation in the cytosolic Ca^{2+} increase upon AAs administration was then confirmed in *glr3.7-2* and *glr3.7-3* (in this latter genetic background we tested L-Glu and L-Cys, the two AAs that triggered the highest increase in cytosolic Ca^{2+} concentration) (Fig.8 and Fig. 9, respectively). Also for *glr3.7* mutant lines we checked for a proper functionality of the sensor. External ATP application triggered a comparable increase in the $\Delta R_{max}/R_0$ in the AtGLR3.7 *loss-of-function* mutants (0.63±0.1 for *glr3.7-1*, 0.77±0.17 for *glr3.7-2* and 0.40±0.04 for *glr3.7-3*) and controls (0.70±013 Col-0 (1), for 0.76±01 Col-0 (2) and 0.50±0.05 for C-24, respectively).

Altogether, the collected data are consistent with the hypothesis that AtGLR3.3 and AtGLR3.7 modulated the AAs-induced cytosolic Ca^{2+} elevation in the root cells of the meristematic zone. Disruption of the AtGLR3.3 leads to the failure of cytosolic Ca^{2+} increase upon AAs application and thus acting as a positive regulator of the response; AtGLR3.7, instead, negatively regulates the

cytosolic Ca^{2+} increase upon AAs exposition. A comprehensive scheme of maximal normalized ΔR ($\Delta R_{max}/R_0$) is shown in Fig. 10, while $\Delta R_{max}/R_0$ for *glr3.7-3* are shown in Fig. 9C.

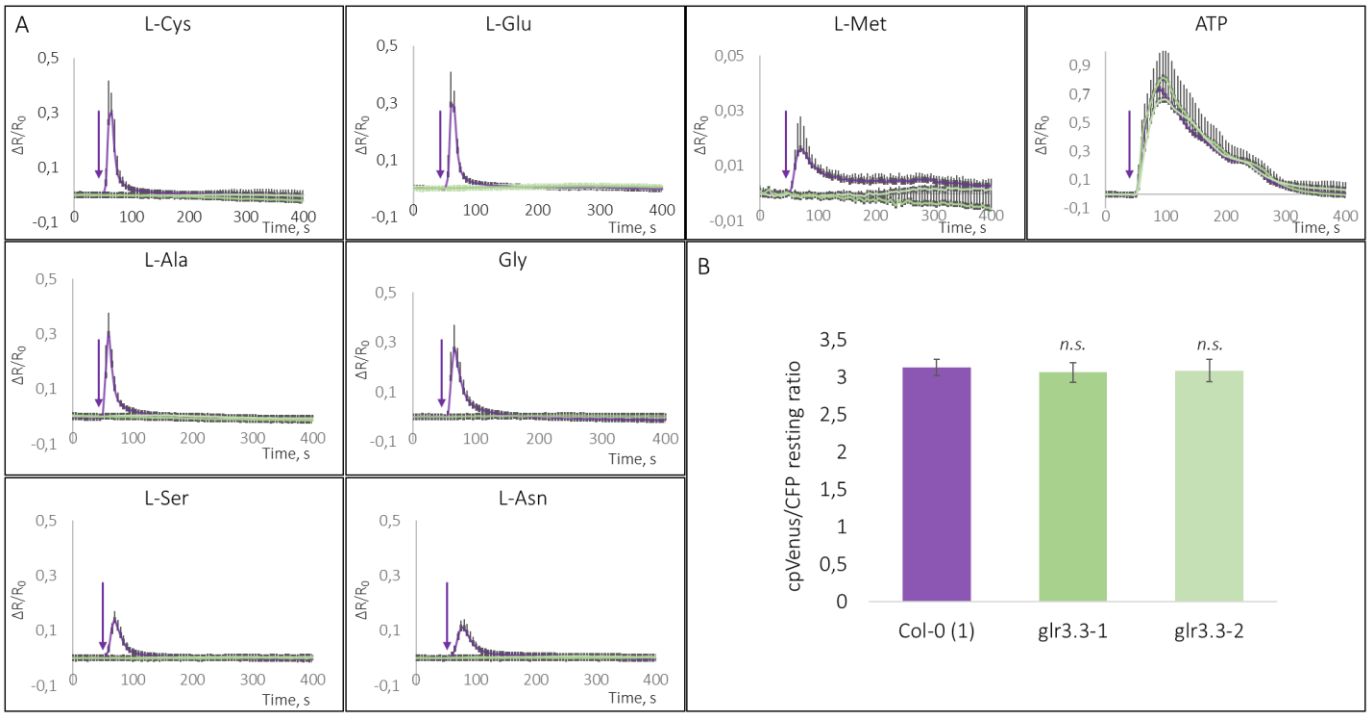

Fig. 6. Amino acids-evoked Ca^{2+} elevation in root cells of the meristematic zone in *glr3.3-1* and *glr3.3-2*. **A**. Trend of the normalized cpVenus/CFP ratios ($\Delta R/R_0$) recorded in Col-0 7-day-old seedlings expressing the FRET sensor NES-YC3.6 in parallel with the two *null-alleles* for GLR3.3. Samples were treated with different external amino acids at the final concentration of 1mM. Under a wide-field microscope, plantlets were constantly supefused with standard imaging solution and transiently exposed to the amino acid (dissolved in imaging solution) for 3min. Arrows indicated the time when seedlings faced 1mM AAs or 100µM ATP. **B**. Resting level of cpVenus/CFP ratios. Values are the average of 50s-time window before treatment application and are reported as average±SD. *n*>5; *n.s* non-statistical significant. **p*<0.5; ***p*<0.05; ****p*<0.005. Results were reported as average±SD. *p* values were calculated using Student's *t* test.

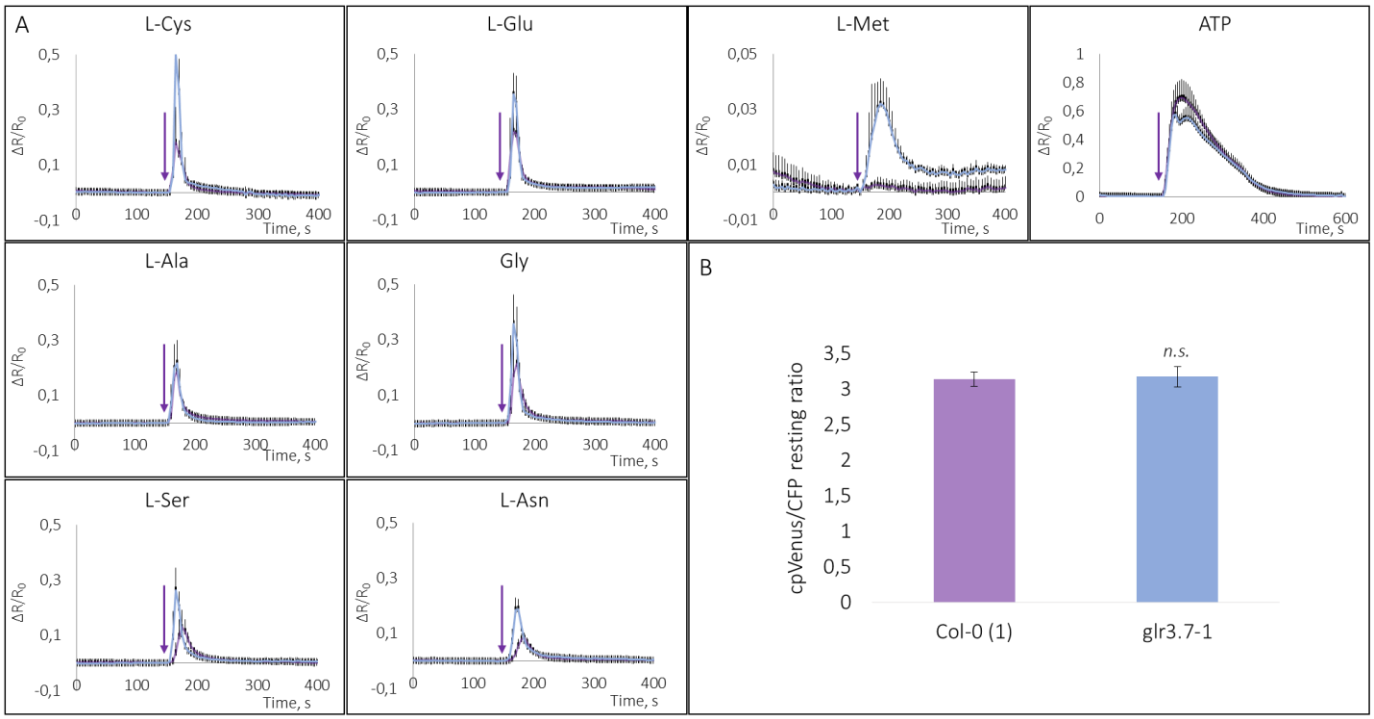

Fig. 7. Amino acids-evoked Ca^{2+} elevation in root cells of the meristematic zone in *glr3.7-1*.

A. Trend of the normalized cpVenus/CFP ratios ($\Delta R/R_0$) recorded in Col-0 7-day-old seedlings expressing the FRET sensor NES-YC3.6 in parallel with the *null-allele glr3.7-1*. Samples were treated with different external amino acids at the final concentration of 1mM. Under a wide-field microscope, plantlets were constantly supefused with standard imaging solution and transiently exposed to the amino acid (dissolved in imaging solution) for 3min. Arrows indicated the time when seedlings faced 1mM AAs or 100µM ATP. **B**. Resting level of cpVenus/CFP ratios. Values are the average of 50s-time window before treatment application and are reported as average±SD. *n*>5; *n.s* non-statistical significant. **p*<0.5; ***p*<0.05; ****p*<0.005. Results were reported as average±SD. *p* values were calculated using Student's *t* test.

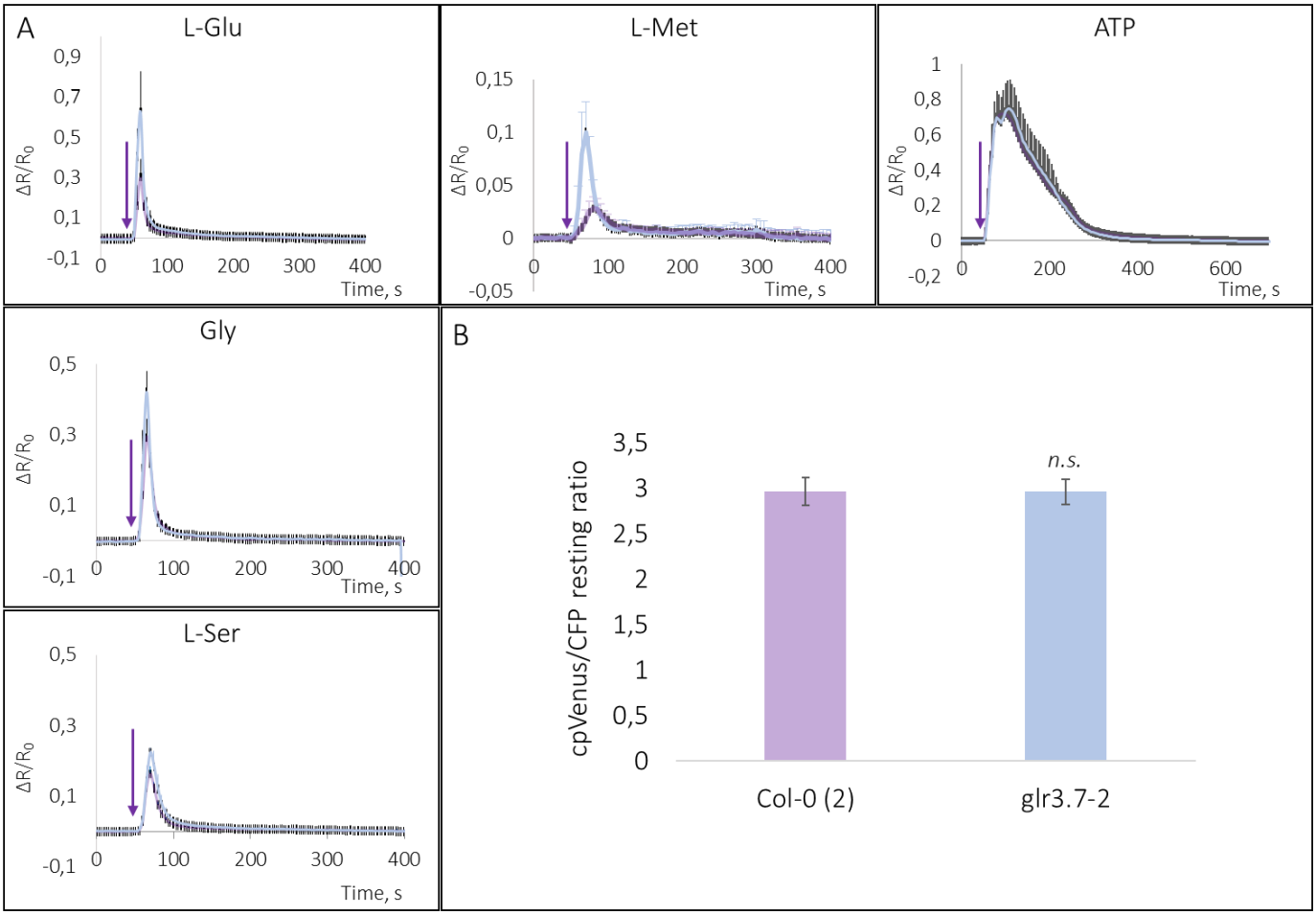

Fig. 8. Amino acids-evoked Ca^{2+} elevation in root cells of the meristematic zone in *glr3.7-2*.

A. Trend of the normalized cpVenus/CFP ratios ($\Delta R/R_0$) recorded in Col-0 7-day old seedlings expressing the FRET sensor NES-YC3.6 in parallel with the *null-allele glr3.7-2*. Samples were treated with different external amino acids at the final concentration of 1mM. Under a wide-field microscope, plantlets were constantly supefused with standard imaging solution and transiently exposed to the amino acid (dissolved in imaging solution) for 3min. Arrows indicated the time when seedlings faced 1mM AAs or 100µM ATP. **B**. Resting level of cpVenus/CFP ratios. Values are the average of 50s-time window before treatment application and are reported as average±SD. *n*>5; *n.s* non-statistical significant. **p*<0.5; ***p*<0.05; ****p*<0.005. Results were reported as average±SD. *p* values were calculated using Student's *t* test.

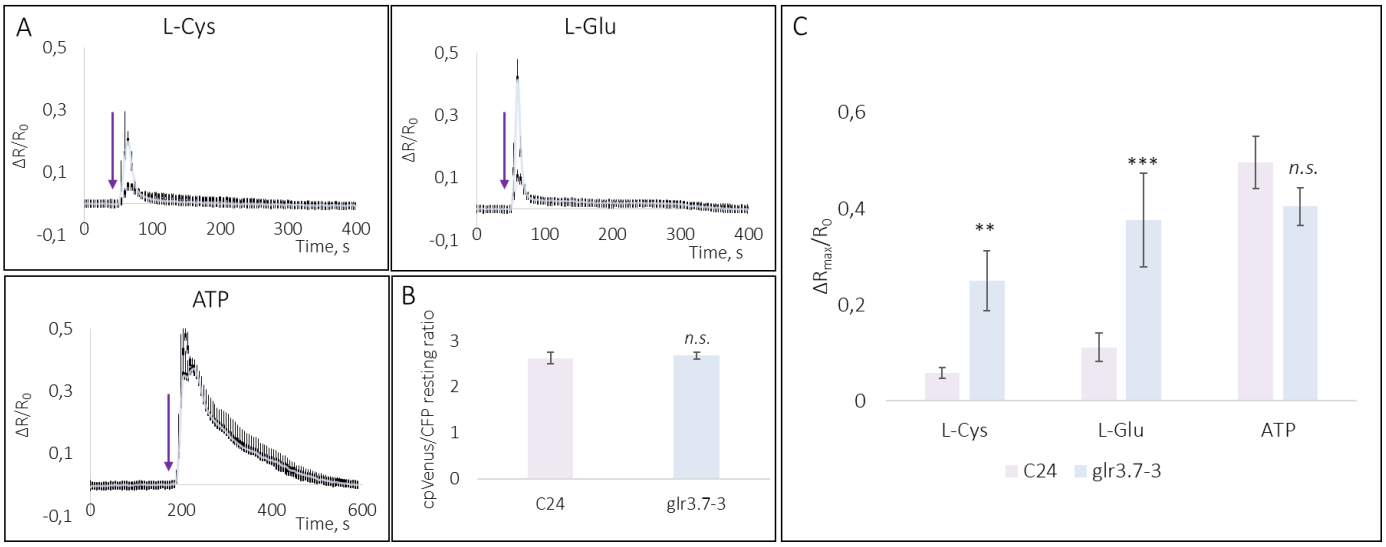

Fig. 9. Amino acids-evoked Ca^{2+} elevation in root cells of the meristematic zone in *glr3.7-3.*

A. Trend of the normalized cpVenus/CFP ratios ($\Delta R/R_0$) recorded in C24 7-day old seedlings expressing the FRET sensor NES-YC3.6 in parallel with the *nonsense* mutant *glr3.7-3*. Samples were treated with different external amino acids at the final concentration of 1mM. Under a wide-field microscope, plantlets were constantly supefused with standard imaging solution and transiently exposed to the amino acid (dissolved in imaging solution) for 3min. Arrows indicated the tiime when seedlings faced 1mM AAs or 100µM ATP. **B**. Resting level of cpVenus/CFP ratios. Values are the average of 50s-time window before treatment application and are reported as average±SD. **C.** Maximal normalized increase $\Delta R_{max}/R_0$ triggered by external AAs administration at 1mM final concentration in the *null-allele* for AtGLR3.7 compared to C24. *n*>5; *n.s* non-statistical significant. **p*<0.5; ***p*<0.05; ****p*<0.005. Results were reported as average±SD. *p* values were calculated using Student's *t* test.

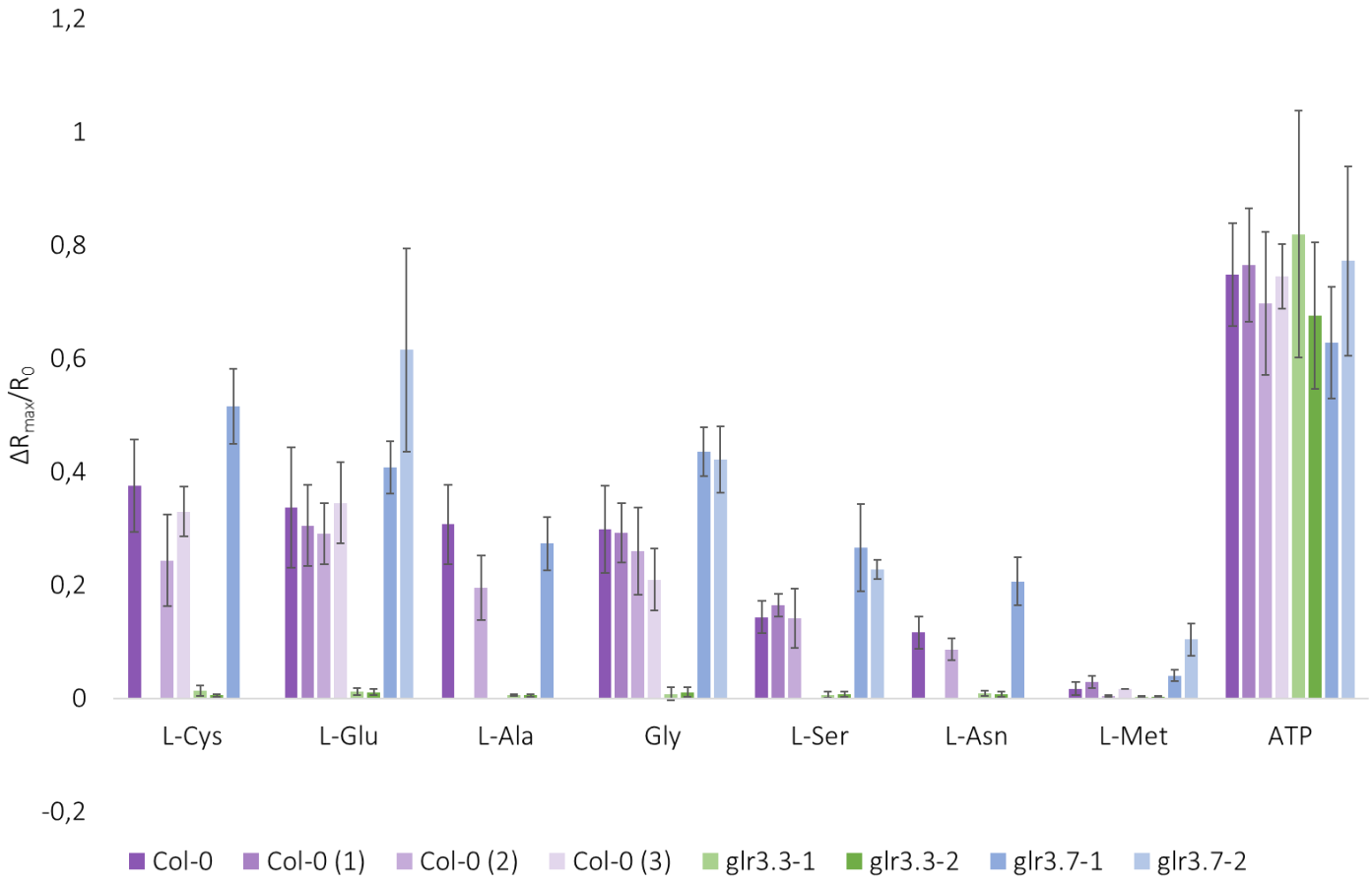

Fig. 10. Maximal increase in the normalized ratio $\Delta R_{max}/R_0$ elicited by external AAs administration in root tip cells of the meristematic zone.

Comprehensive scheme of the normalized ratio $\Delta R_{max}/R_0$ triggered by external AAs administration at 1mM final concentration in *null-alleles* for AtGLR3.3 and AtGLR3.7 in comparison with controls. $n>5$; *n.s* non-statistical significant. *$p<0.5$; **$p<0.05$; ***$p<0.005$. Results were reported as average±SD. *p* values were calculated using Student's *t* test.

II.6. Disruption of AtGLR3.3 unbalances cationic currents in single root cells

Our experiments performed at the root meristematic zone strongly suggested that AtGLR3.3 could act as a main scaffold necessary for the formation of a functional ion channel. In fact, when it is missing, no response to external AAs occured. AtGLR3.7, instead, seemed to play a role as a (negative) regulator more than be a channel *per se*. For this reason, we aimed at investigating the effect of disruption of AtGLR3.3, and not AtGLR3.7, on total currents of a single root cell. To this aim, we chose root hair cells. In fact, microarray data supported that AtGLR3.3 is consistently expressed in root hairs (Dinneny *et al.*, 2007; Winter *et al.*, 2007) (Supp. Mat. Fig. 2). Moreover, we reported a clear plasma

membrane localization for AtGLR3.3 in 80-150µm long root hairs (Fig 5A, O-P). To this purpose, in order to isolate apical membrane from long root hairs we applied UV laser micro-surgery at the root hair tip to selectively remove the cell wall. A fragmentation of the plasma membrane gave rise to a series of spheroplasts released from a single root hair upon plasmolysis-deplasmolysis treatment of 3-day old seedlings (Fig. 11). Whole-cell currents were recorded from apical (first) spheroplasts which resulted to be strongly dense cytoplasmic compared to the one isolated from longer root hairs or isolated at the end of the fragmentation event (the last ones) (Fig. 11, C). We drew up a protocol to measure inward and outward currents, with a holding potential of – 40mV (close to the resting potential of the spheroplasts in the patch-clamping solution) moving towards hyperpolarizing potentials (up to -195mV) by steps of 15mV. Similarly, we moved to depolarizing potentials, up to +75mV (Fig. 12A). Whole-cell recordings from apical Col-0 spheroplasts in a medium containing 10mM $CaCl_2$ showed slight inward-rectifying conductances at hyperpolarized voltage (<-105mV *circa*) and slight outward-rectifying currents at positive voltages (Fig. 12C, purple). The procedure applied to *glr3.3-1* root hairs proved that ablation of GLR3.3 did not alter the shape of the currents of the isolated spheroplasts when compared to Col-0 (Fig. 11C, green). The reversial potential of the inward current was -60mV *circa* for both Col-0 and *glr3.3-1*, which suggested the presence of K^+ (E_{K^+} = -56mV) and Cl^- (E_{Cl^-} = -88mV) currents. Moreover, larger currents were observed in spheroplasts both at hyperpolarizing and depolarizing potentials (one-way ANOVA *p*-value 0.0013 and 0.0202, respectively; *n*>4) in the *glr3.3-1* mutant compared to the Col-0 (Fig. 12C, green). For instance, at-165mV, Col-0 showed an averaged current of -30.65±7.68 pA while *glr3.3-1* showed -193.6±44.58pA. At +15mV, we recorded a whole current of 69.3±34 pA in Col-0 and 260.17±57.32 pA in *glr3.3-1* spheroplasts. Altogether these data suggested that the lack of AtGLR3.3 affects plasma membrane potential and potentially affects physiological process in root (hair) cells, thus playing a putative role in the regulation of ion movement across plasma membrane.

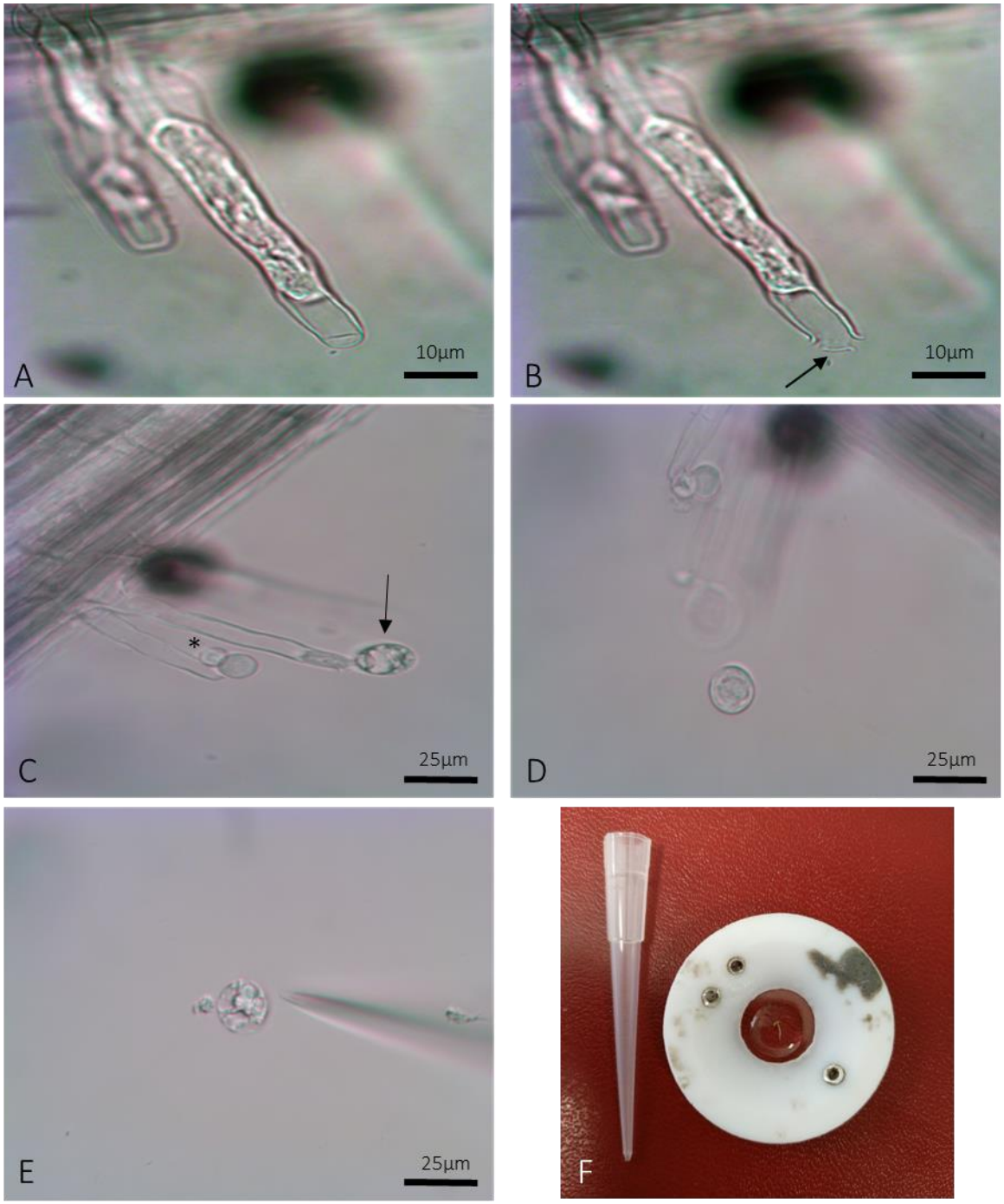

Fig. 11 *In situ* microsurgery and recovery of spheroplasts isolated from Col-0 root hairs. **A.** Root hair plasmolysis **B.** Cell wall laser dissected root hair **C-D.** Recovery of apical plasma membrane upon deplasmolysis. Arrow showed a dense cytoplasmic spheroplast, whereas star indicates a brighter spheroplast, released at the end of the fragmentation (most likely vacuolar) **E.** Isolated spheroplast before patch clamp recording. **F.** 3-day-old seedling used for spheroplasts isolation (compared to a p200 tip pipette). A-B: 40x magnification; C-D: 20x magnification. Arrow in B highlighted cell wall removal after UV laser dissection.

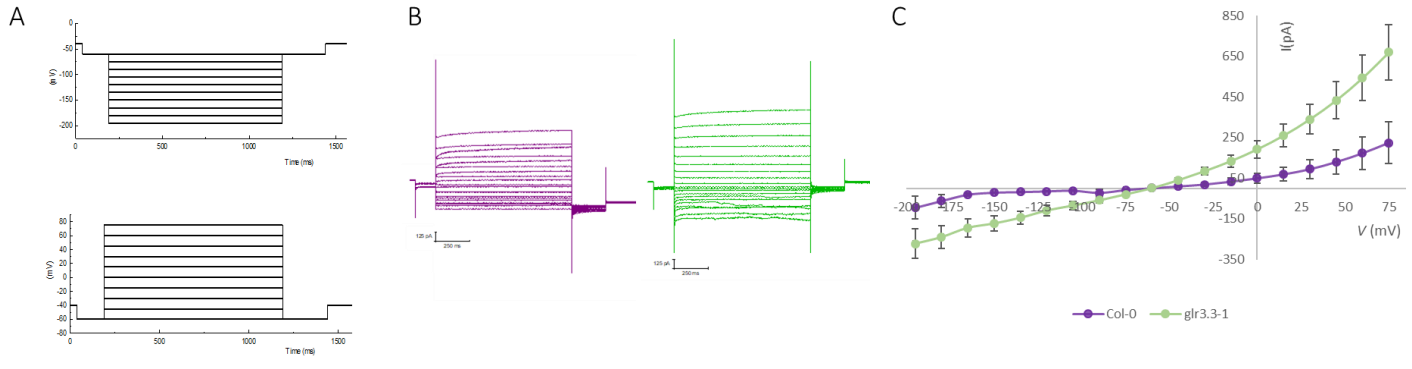

Fig. 12 Whole-cell currents isolated from Col-0 and *glr3.3-1* spheroplasts. A. Applied protocol showing hyperpolarizing or depolarizing steps of 1-s duration from a holding potential of -40mV., close to the resting potential of the spheroplasts in the patch-clamping solutions. **B.** Representetives currents recorded from Col-0 (purple) and *glr3.3-1* (green) spheroplasts at each clamped potential. **C.** Current–voltage relationship (*I–V* curve) reconstructed from averaged total whole-cell currents measured±SE. *n*>4; *p*-value=0,0202 One-way ANOVA for outward currents, Tukey HSD *p-value*= 0,0202345 - Tukey HSD inference *p*<0,05; *p*-value=0,0013 One-way ANOVA for inward currents, Tukey HSD *p*-value= 0,0012591 Tukey HSD inference *p*<0,01.

II.7. Flame application to the stem reveals fast electric and Ca^{2+} signals moving through an intricate stems connectome in Arabidopsis

In plants, long-distance-rapid systemic signalling has been reported (Mousavi *et al.*, 2013; Choi *et al.*, 2014; Evans *et al.*, 2016; Gilroy *et al.*, 2016; Nguyen *et al.*, 2018; Toyota *et al.*, 2018). The systemic signalling triggered by environmental cues such as wounding, salt stress, herbivore feeding involve local and distal changes of plasma membrane potential, progressive Ca^{2+} elevations and ROS signalling (Mittler *et al.*, 2011; Mousavi *et al.*, 2013; Evans *et al.*, 2016; Nguyen *et al.*, 2018; Toyota *et al.*, 2018). In plants, flaming is known to induce fast long-distance membrane depolarization (Vodeneev, Akinchits and Sukhov, 2015; Gilroy *et al.*, 2016). We set out the hypothesis that flame signalization among inflorescences might be dependent on the activity of GLRs and linked to transient cytosolic Ca^{2+} rises. To test this hypothesis, we designed a simple protocol which consisted of the application of flame to the primary stem of 5-week-old Col-0 NES-YC3.6 plants by means of a lighter (*c.* 10 cm from the primary inflorescence apexes) and monitored the level of cytosolic Ca^{2+} at the abscission zone (AZ), stem and sepal of the primary inflorescence (Fig. 13A and Fig. 14A). Remarkably,

stem flaming triggered a clear FRET response (with a maximal increase, reported as normalized ΔR ($\Delta R_{max}/R_0$), of 0.587 ±0.07) (Fig. 14E-F; *n*>3 for glr mutants, *n*=1 for *glr3.7-1*) primarily at the floral AZ and not at the stem (Fig. 14D). After the primary cytosolic Ca^{2+} increase occurring in the floral AZ we also observed a following increase of Ca^{2+} moving away from the AZ, forward to the sepals and backward to the stem, with an averaged speed propagation of 348 ±186µm/sec (AZ to sepals) and 40 ±8.5µm/sec (AZ to stem) (Fig. 15B-C). While the Ca^{2+} speed propagation from AZ to sepals is in accordance to the propagation rate of Ca^{2+} reported in Arabidopsis seedling root (396 ±28µm/sec) upon salt treatment (Choi *et al.*, 2014), both values (AZ to sepals/stem) were definitely slower compared to the one recently reported to occur between leaves by Toyota *et al.* (996 ±207µm/sec) (Toyota *et al.*, 2018). Interestingly, the same mechanism occurred when we flamed a lateral stem. In fact, a cytosolic Ca^{2+} elevation was observed at the lateral floral AZ (Fig. 13B and Fig. 16). From these experiments it appears clear that flaming a stem evokes a cytosolic Ca^{2+} increase primarily in systemic cells thus depending on another signal (not a Ca^{2+}-based signal) triggered by the flaming. Previous publications reported that a depolarization event occurred upon leaf wounding or chewing which anticipates an increase in the cytosolic Ca^{2+} concentration (Mousavi *et al.*, 2013; Nguyen *et al.*, 2018). By calculating the time required to observe a Ca^{2+} increase at the floral AZ from the flame application, we estimated that the flaming induced a signal moving towards the inflorescences apexes with an averaged speed of 12333 ±4481.4µm/sec (*n*=3; *glr3.7-1 n*=1) (Fig. 15A). This rate is consistent with the speed reported for the electrical signal called variation potentials (VP). VP relies on a long-term membrane depolarization generated by tissues deformation after flaming at the local damaged site, which is then probably propagated through the combination of a hydraulic wave and a transportation of a still unknown depolarizing chemical molecule (Vodeneev, Akinchits and Sukhov, 2015; Evans and Morris, 2017). Thus, we might suppose that we identified the floral AZ as the site where an electrical signal is converted to a cytosolic Ca^{2+} elevation. This observation leads us to consider the floral AZ as a HUB, where the electrical signal moving through the stem is transduced in a cytosolic Ca^{2+} rise which is then followed by a long-distance Ca^{2+} wave (Fig. 13C).

As the electrical signal moved throughout the stem, we predicted that the flame application on a lateral stem may induce a membrane depolarization which can propagate through the primary stem leading to a cytosolic Ca^{2+} rise at the primary floral AZ and then propagated backward to the primary stem again. To this aim, we designed a second experiment which consisted in the flaming application to the farest lateral stem (i.e. from the primary inflorescences apex) whilst monitoring the level of cytosolic Ca^{2+} at the abscission zone (AZ), stem and sepals of the primary inflorescence. Surprisingly,

upon fire application at a lateral stem we first detected a cytosolic Ca^{2+} increase at the primary stem level which preceded a cytosolic Ca^{2+} rise at the floral AZ (Fig. 13B – Fig 14D). Our observation suggested that the electrical signal generated at the lateral stem upon flaming was converted into a cytosolic Ca^{2+} increase before the electrical signal reached the primary inflorescence apex. We thus hypothesized that the node between the two stems (the primary and the lateral) could act as a HUB, i.e. it would transduce the electrical signal into a rise in cytosolic Ca^{2+} (Fig. 13B, C). Preliminary experiments suggested that the electrical signal generated at the lateral stem upon flaming moved to the node where it triggered the generation of a cytosolic Ca^{2+} rise which then propagated through the primary stem at *circa* >1000µm/sec (data not shown).

A cytosolic Ca^{2+} increase in the cells of the stem node has to be demonstrated, but our confocal FRET analyses show a cell populations site with apparently higher cytosolic Ca^{2+} levels at resting similarly to the floral AZ (Fig. 13C, ROIs), which might represent the cells that integrate the two signals (electrical and Ca^{2+}).

Preliminary experiments suggest that the flaming of a lateral stem did not induce a rise of cytosolic Ca^{2+} in the other lateral stems. Moreover, our experiments showed that flaming the primary stem did not trigger any change in the cytosolic Ca^{2+} at the floral AZ of lateral inflorescences (preliminary results schematically shown on Fig. 13B). Altogether, these observations may support the idea of the existence of an intricate stem connectome, with a single path of Ca^{2+} propagation. The electrical signal is triggered at the local injured site, propagated and decoded at the node. The cell populations at the node will convert the electrical stimulation in a Ca^{2+} signal which will be propagated throughout the primary stem (but not spreading to the lateral stems). The Ca^{2+} signal eventually arrived at the primary inflorescences apexes. This scenario would explain our observation of a primary Ca^{2+} increase at the stem preceding the elevation of cytosolic Ca^{2+} at the floral AZ upon lateral stem flaming.

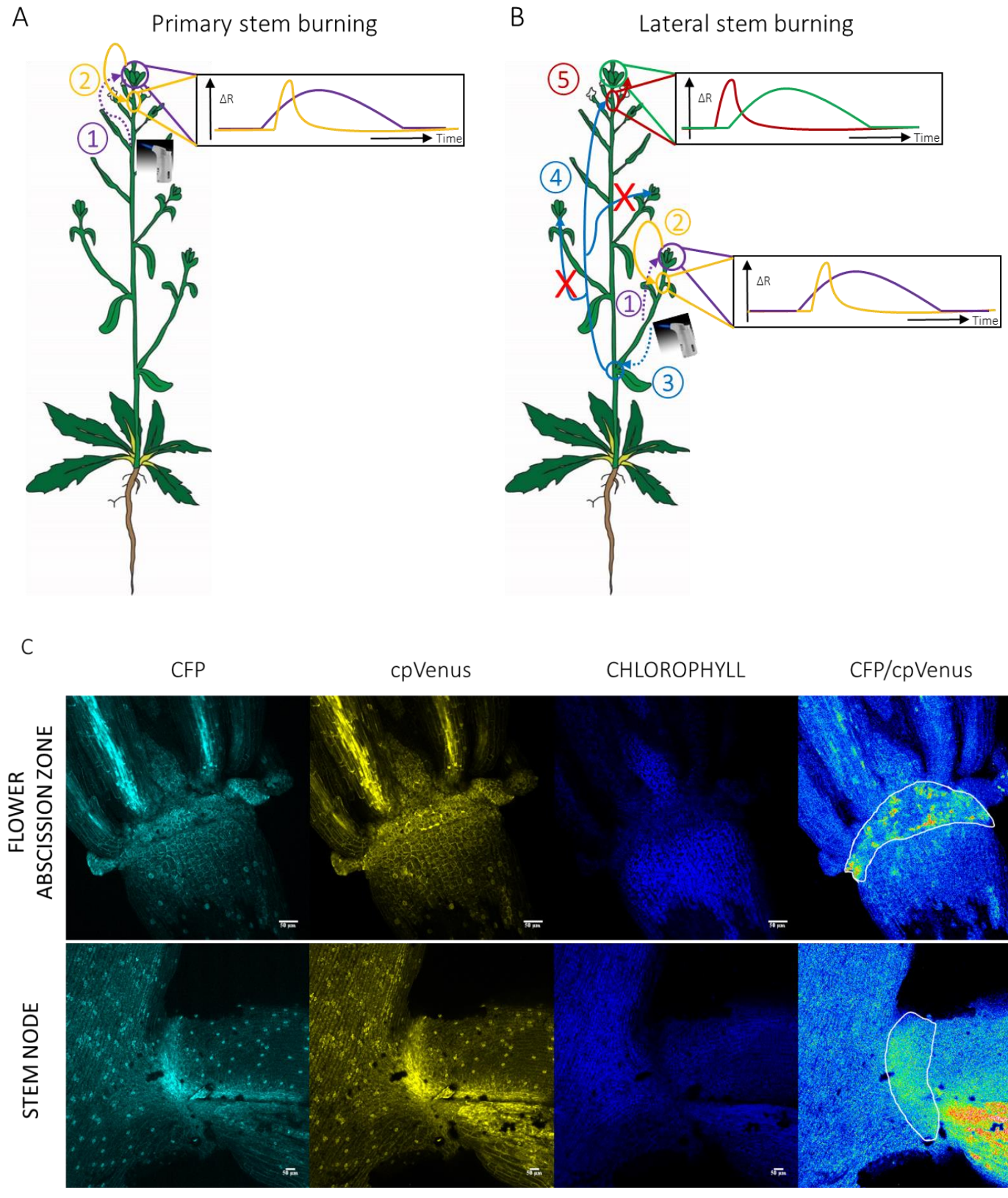

Fig. 13 Representation scheme of stem connectome and HUB acquisitions. A and B – 1-2. Upon stem flaming (primary or lateral) an electrical signal (purple dotted line) moved towards the inflorescence apex, throughout the stem (**1**). The floral AZ (HUB) transduced the electrical signal and triggered a cytosolic Ca^{2+} increase (purple line in the ΔR trend cartoons). The Ca^{2+} signal then propagated

backward (and forward) to the primary stem (orange line in the ΔR trend) (2). **B – 3-5.** Upon a lateral stem burning, an electrical signal moved backward towards the node (HUB). The node relayed the signal (3) and triggered a cytosolic Ca^{2+} increase that propagates shootward throught the primary stem, but no propagation occured in other lateral inflorescences (4). A Ca^{2+} increase occured primarly at the stem (red line in the ΔR trend cartoon) and then it propagated forward to the inflorescence apex (green line in the schematic ΔR trend cartoon) (5). **C.** Confocal images of flower abscission zone and stem node. Acquisitions of Col-0 NES-YC3.6 plants showing CFP (light blue), cpVenus (yellow), chlorophyll (blue) and FRET ratio cpVenus/CFP (in false colour). Notably, white ROIs in the FRET ratio images indicated the cell populations which putatively convert the electrical signal in cytosolic Ca^{2+} elevation (HUBs). Scale bars: 50µm; *n*=2 for each zone.

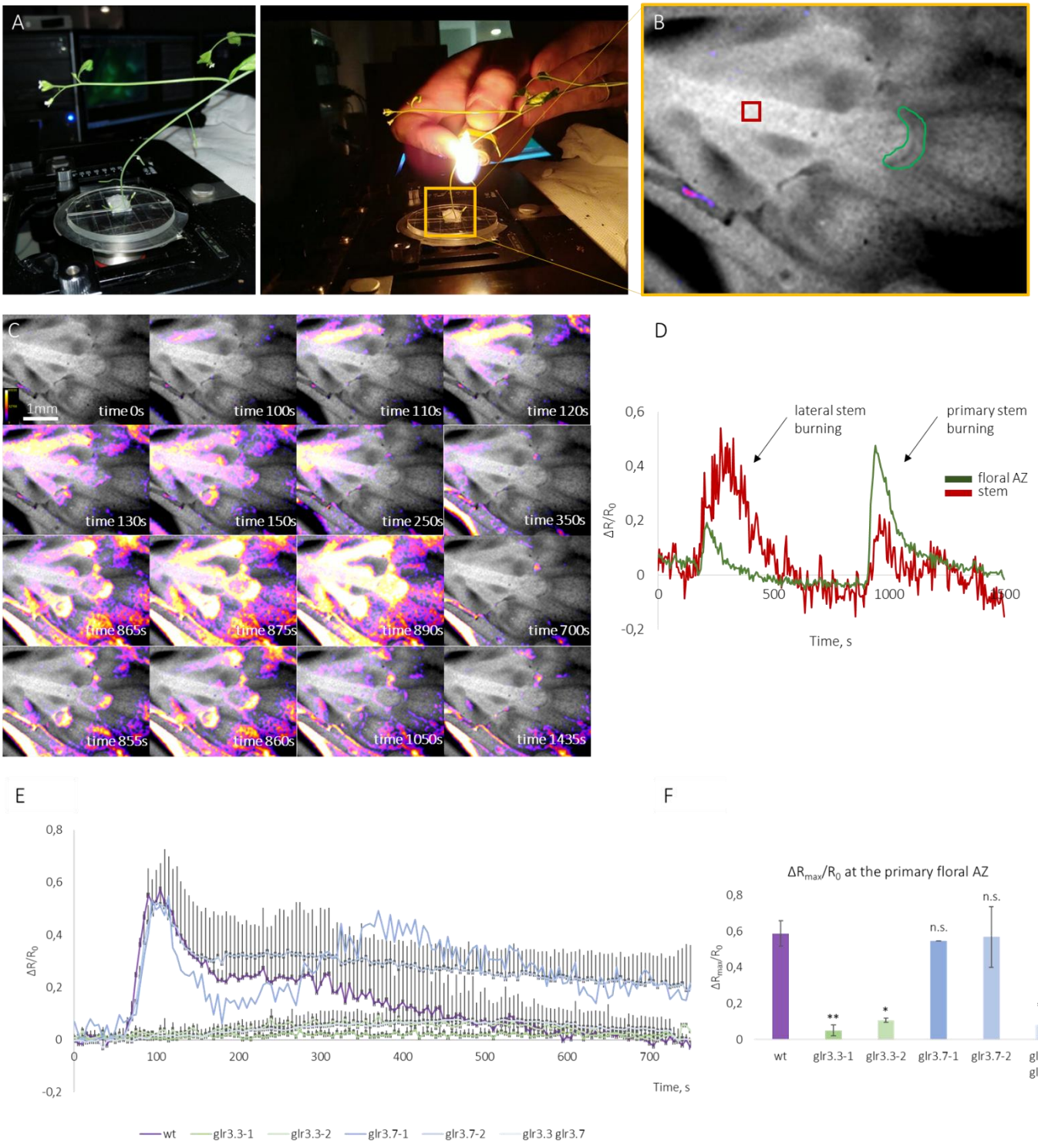

1466

1467 **Fig. 14 Cytosolic Ca^{2+} elevation at the primary floral AZ upon stem flaming. A.** Col-0 plant harbouring
1468 NES-YC3.6 sensor before (left) and during flaming challenge (right). A primary stem was burnt while
1469 monitoring primary inflorescences. **B.** Primary inflorescences apex of the plant reported in A showing
1470 two region of interests (ROIs) where the cytosolic Ca^{2+} rise was monitored (red square on primary
1471 stem, green circle on floral abscission zone). **C.** Time-lapse of Col-0 NES-YC3.6 primary inflorescences
1472 apex monitored for cytosolic Ca^{2+} increase upon stem burning (lateral and primary). From time 0s to

time 700s is reported a cytosolic Ca^{2+} increase at the primary floral AZ upon lateral stem flaming. From time 855s to the end a cytosolic Ca^{2+} increase at the primary floral AZ upon primary stem flaming is shown **D.** Representative trend of $\Delta R/R_0$ at the primary floral AZ upon stem flaming. The dynamics of cytosolic Ca^{2+} at the stem (purple ROI in B) and at the floral AZ is reported (green ROI in B). The first Ca^{2+} peak was triggered by flaming a lateral stem while the second Ca^{2+} peak was triggered by primary stem flaming. **E.** Normalized FRET ratio ($\Delta R/R_0$) monitored at the primary floral AZ of Col-0 and *glr* mutants challenged by flame at the primary stem. **F.** Normalized ratio $\Delta R_{max}/R_0$ monitored at the primary floral AZ for Col-0 and *glr* mutants challenged by flame at the primary stem. *n*=3; *glr3.7-1* *n*=1. *n.s* non-statistical significant. Results were reported as average±SD. **p*<0.5;***p*<0.05; ****p*<0.005. *p* values were calculated using Student's *t* test.

II.8. Cytosolic Ca^{2+} rises at the floral abscission zone are inversely switched by AtGLR3.3 and potentially by AtGLR3.7 upon stem flaming

We showed that stem flaming generates a cytosolic Ca^{2+} elevation at the floral AZ. Recent works have demonstrated that members of the family of the Glutamate Receptor-like channels are involved in the propagation of long-distance electric and Ca^{2+} signals in leaves (Mousavi *et al.*, 2013; Salvador-Recatalà, 2016; Nguyen *et al.*, 2018; Toyota *et al.*, 2018). Additionally, the investigation of the RNAseq data reported in Lee *et al.* (2018) revealed that AtGLR3.3 and AtGLR3.7 are both expressed at the floral AZ (Lee *et al.*, 2018). These indications lead us to investigate whether the ablation of AtGLR3.3 and AtGLR3.7 may affect the cytosolic Ca^{2+} rise at the floral AZ upon stem flaming. The primary stems of 5-week-old Arabidopsis knock out plants for the *AtGLR3.3* (*glr3.3-1* and *glr3.3-2*) were exposed to flaming. The rise in cytosolic Ca^{2+} at the primary floral AZ was severely affected by disruption of AtGLR3.3 as we calculated an elevation of cytosolic Ca^{2+} as high as 0.05 ±0.03 (as $\Delta R_{max}/R_0$) in *glr3.3-1* and 0.1 ±0.01 in *glr3.3-2* ($\Delta R_{max}/R_0$ of 0.587 ±0.07 in Col-0) (*n*=3; *glr3.7-1* *n*=1) (Fig. 14E-F). The following increase in Ca^{2+}, moving from AZ to sepals and from AZ to the primary stem, was impaired as well. In fact, the speed propagation was below the level of detection for *glr3.3-1* and corresponding to 30µm±53µm/sec for *glr3.3-2* (AZ to sepals) (Fig. 15B). Both alleles showed, if any, a Ca^{2+} increase below the sensitivity of the NES-YC3.6 sensor when measured from AZ to the stem (Fig. 15C). Similarly, we observed a sharp decrease in the speed of propagation of the electrical signal in *glr3.3* mutants when compared to Col-0 (2590 ±2500µm/sec in *glr3.3-2,* undetectable for *glr3.3-1*) (Fig. 15C). When we burnt a lateral stem, we detected an impairment of cytosolic Ca^{2+} increase in the

lateral floral AZ (0.02 ±0.01 for *glr3.3-1* and 0.05 ±0.02 for *glr3.3-2*) (Fig. 16B). As regards GLR3.7, while we did not measure any differences in the cytosolic Ca^{2+} maximum peak at the primary floral AZ upon primary stem burning (0.58 ±0.06 for Col-0, 0.54 for *glr3.7-1* and 0.56 ±0.17 for *glr3.7-2*, as $\Delta R_{max}/R_0$) (Fig. 14E-F), we detected an increased trend of the Ca^{2+} propagation speed (AZ to sepals/stem) in *glr3.7* mutants when a primary stem was burnt (348 ±186.18µm/sec for Col-0, 412.5 ±194.45µm/sec for *glr3.7-1* and 427.66 ±211.89µm/sec for *glr3.7-2*, AZ to sepals and 40 ±8.48µm/sec for Col-0, 91.66µm/sec for *glr3.7-1* and 75.66±35.55µm/sec for *glr3.7-2*, AZ to stem) (Fig. 15B-C). Apparently, our data show that the electrical signal speed propagation in *glr3.7* mutants is not altered when compared to Col-0 (Fig. 15A). The flaming of a lateral stem triggered a cytosolic Ca^{2+} increase at the lateral floral AZ as high as 0.926±0.45 in *glr3.7-2 (glr3.7-1* measurements are on going*)*, higher than Col-0 (0.299 ±0.07) (as $\Delta R_{max}/R_0$) (*n*=3; *glr3.7-1 n*=1).

In summary, disruption of *AtGLR3.3* gene impaired the cytosolic Ca^{2+} rise at the floral AZ. On the other hand, the lack of the AtGLR3.7 may lead to an exacerbation of the cytosolic Ca^{2+} elevation at lateral floral AZ upon lateral stem burning. The ablation of AtGLR3.3 impacted also the speed of the electrical signal leading to a sharp reduction of the speed propagation. These results were in agreement with the experiments performed in root meristematic cells, where the lack of AtGLR3.3 resulted in an impaired AAs-induced cytosolic Ca^{2+} rise and disruption of AtGLR3.7 lead to an exacerbation of the same phenomenon. However, further experiments are needed to confirm the data here shown.

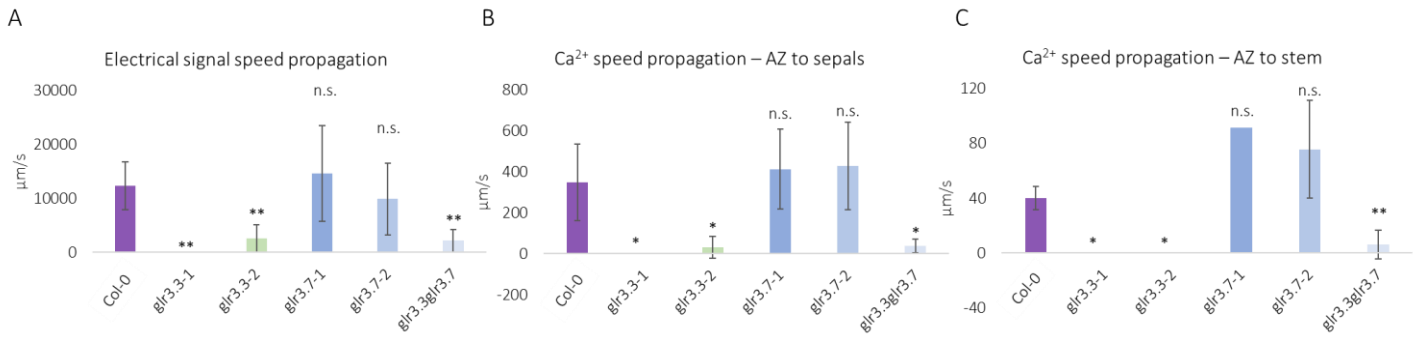

Fig. 15 Speed propagation rate along the primary stem and inflorescence apex upon primary stem flaming. A. Electrical signal speed propagation (VP) measured in Col-0 and *glr* mutants upon primary stem flaming. **B.** Ca^{2+} speed propagation measured from primary floral AZ to sepals in Col-0 and *glr* mutants upon primary stem flaming. **C.** Ca^{2+} speed propagation measured from primary floral AZ to stem in Col-0 and *glr* mutants upon primary stem flaming. *n*=3; *glr3.7-1 n*=1 at the stem. *n.s* non-statistical significant. Results were reported as average±SD. **p*<0.5;***p*<0.05; ****p*<0.005. *p* values were calculated using Student's *t* test.

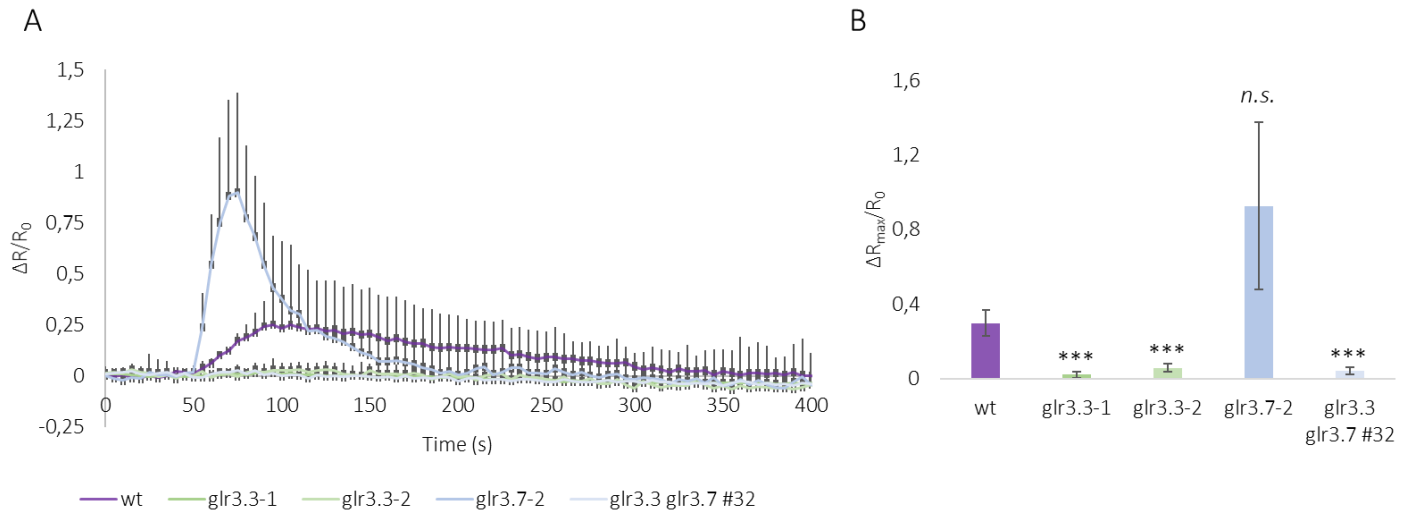

Fig. 16. Cytosolic Ca^{2+} dynamics at the lateral inflorescence apices upon lateral stem flaming in different genetic backgrounds. A. Trends of normalized ΔR increase ($\Delta R/R_0$) in lateral inflorescences apices upon lateral stem burning in Col-0, *glr3.3-1*, *glr3.3-2*, *glr3.7-2* and *glr3.3glr3.7* mutants. **B.** Maximal increase of normalized ΔR ($\Delta R_{max}/R_0$) in lateral inflorescences apices upon lateral stem flaming. $n>3$; *$p<0.5$; **$p<0.05$; ***$p<0.005$. p values were calculated using Student's t test.

II.9. Evidences for AtGLR3.3 and AtGLR3.7 co-localization and interaction in *Nicotiana benthamiana* leaves

Due to the antagonistic roles we reported for AtGLR3.3 and AtGLR3.7 in the regulation of Ca^{2+} fluxes upon AAs and flaming, we hypothesized that the two isoforms could interact in the formation of a heteromeric channel. We first checked if the two translational fusion proteins GLR3.3-eGFP and GLR3.7-mCherry localize in the same compartment. We transiently and independently transformed the two fusion proteins in *Nicotiana benthamiana* leaf cells and performed a microscope confocal analysis (Fig 17A). Both eGFP and mCherry alone decorated endomembranes that were reasonably endoplasmic reticulum (Fig 17) in accordance with the previously reported results (Fig. 4 and 5). We then co-transfected the two chimeric constructs in the same *N. benthamiana* leaf cells and acquired both eGFP and mCherry (Fig. 17B). The signals clearly overlapped thus suggesting a co-localization of GLR3.3-eGFP and GLR3.7-mCherry in tobacco leaves occurring mainly at the endomemrane levels (Fig. 17B). This latter observation let us to hypothesize that AtGLR3.3 and AtGLR3.7 may not only co-localize but also interact. We thus employed Fluorescence Lifetime Imaging Microscopy and Forster

Resonance Energy Transfer (FRET-FLIM) to detect whether the two translational fusion proteins interact. *Nicotiana benthamiana* leaves were again infiltrated with GLR3.3-eGFP alone or coupled with GLR3.7-mCherry. We therefore measured the exponential time decay of GFP photons in the two samples. We observed two different fluorescence lifetime (τ) for eGFP. We calculated an average τ of 2.55 ±0.0075ns for eGFP when expressed alone, whereas the average τ was 1.74 ±0.023ns when co-expressed with mCherry (*n*=2). This decrease in the time decay indicates that part of the GFP energy is donated to mCherry, a condition which only occurs if the distance between the two fluorophores is close to 5nm (Forster Radius) (Albertazzi *et al.*, 2009), which then suggest an interaction between the two fusion proteins. We then set the observed τ value for eGFP alone (i.e. 2.55ns) as threshold to calculate the overall FRET efficiency between donor (eGFP) and acceptor (mCherry) fluorescent proteins by using the SymphoTime64 software. All the τ values below this threshold will be accounted as a FRET event. We calculated a FRET percentage of -1.9% ±0.59 for eGFP when expressed alone, while the FRET efficiency increased to 46%±4.6 in presence of the acceptor mCherry (Fig. 17C). These experiments, albeit preliminary, suggested a possible interaction and formation of a heteromeric channel AtGLR3.3-AtGLR3.7, which will be further investigated.

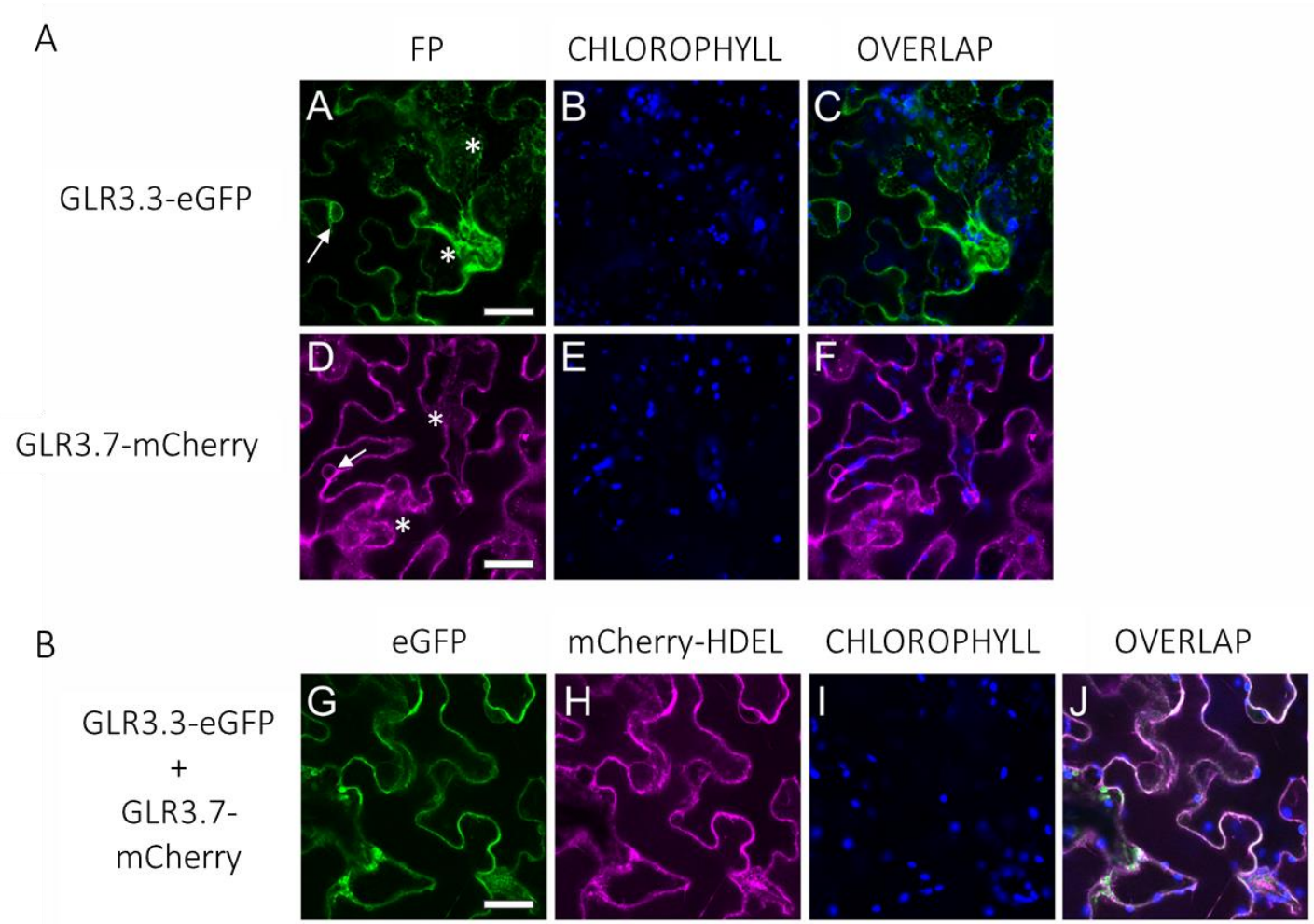
A
FP
CHLOROPHYLL
OVERLAP
GLR3.3-eGFP
GLR3.7-mCherry
A
B
C
D
E
F
B
eGFP
mCherry-HDEL
CHLOROPHYLL
OVERLAP
GLR3.3-eGFP
+
GLR3.7-
mCherry
G
H
I
J

1567

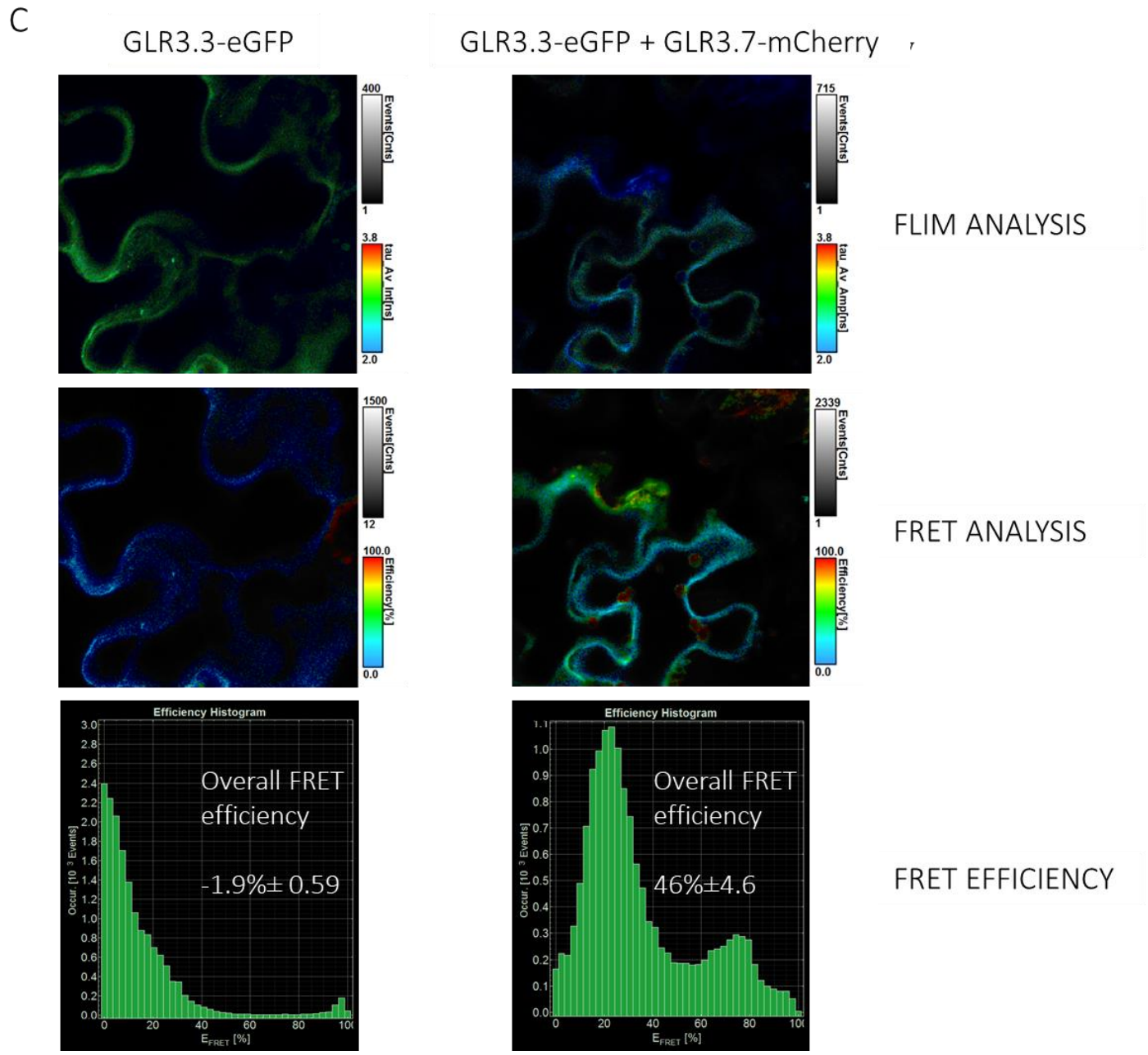

1568

1569 **Fig. 17. Co-localization study of translational fusion proteins in *Nicotiana benthamiana* leaves and FRET-**
1570 **FLIM measurement. A.** The fusion proteins GLR3.3-eGFP and GLR3.7-mCherry were independently
1571 expressed in tobacco leaf cells under the control of a single CaMV35 and UBQ10 promoter,
1572 respectively. Both GLR3.3-eGFP and GLR3.7-mCherry localised at the endomembranes. Indeed,
1573 nuclear envelopes (arrows) and ER membrane structures (stars) were decorated by the translational
1574 fusion proteins (A and D). Green and magenta for eGFP and mCherry, respectively; in blue
1575 chlorophyll. In the third column, merger of the two channels is shown. **B.** G-J. GLR3.3-eGFP and
1576 GLR3.7-mCherry co-localized at the endomembranes when co-transformed in *N. benthamiana*
1577 leaves. J showed the overlay between GFP and mCherry fluorescences. **C.** FRET-FLIM experiment.

Two different fluorescence lifetime τ for eGFP were calculated: a τ of 2.55 ±0.0075ns for eGFP when expressed alone in *N. benthamiana* leaves (left) and a τ as 1.74 ±0.023ns in presence of mCherry molecules (right). By setting the observed τ value for eGFP when expressed alone (i.e. 2.55ns as threshold to calculate the overall FRET efficiency, we calculated a FRET value of -1.9% ±0.59 for eGFP when expressed alone, while the FRET efficiency increased to 46%±4.6 in presence of the acceptor mCherry. Scale bar 25 µm. *n*=2.

II.10. Functional and genetic evidences for AtGLR3.3 and AtGLR3.7 interaction

Since the FRET-FLIM experiment suggested an interaction between AtGLR3.3 and AtGLR3.7, we pursued a genetic approach to further test this possibility. We therefore crossed the two homozygous T-DNA insertion lines *glr3.3-1* and *glr3.7-1* expressing the NES-YC3.6 in order to isolate a double knock-out line *glr3.3-1glr3.7-1* x NES-YC3.6. In the T_2 generation, we were able to isolate several double mutants showing homozygous T-DNA insertions in both genes and expressing the sensor. The reduction of the transcript levels for the two genes in the double mutant was then confirmed by quantitative RT-PCR (Suppl. Mat. Fig. 3A and C). We first checked if the simultaneous disruption of the two genes altered the cpVenus/CFP resting ratio comparing Col-0 and *glr3.3glr3.7* plants. We did not detect any significant statistical differences between Col-0 (3) and *glr3.3glr3.7* in the resting ratio, meaning that simultaneous ablation of the two isoforms did not alter the resting cytosolic Ca^{2+} level (*n*>4) (Fig. 18B; Suppl. Mat. Table 1). We then tested four out of seven AAs able to trigger a cytosolic Ca^{2+} rise in root meristematic cells. In accordance with our previous results in Col-0 Arabidopsis seedlings we detected a maximal increase of the normalized ratio ($\Delta R_{max}/R_0$) as 0.329±0.043 and 0.345±0.071 for L-Cysteine and L-Glutamate in Col-0 (3), respectively, whereas Glycine and L-Methionine triggered a $\Delta R_{max}/R_0$ as 0.209±0.055 and 0.017±0.0001 (Fig. 18A and C; Suppl. Mat. Table 2C). Interestingly, we failed to detect any change in the cpVenus/CFP ratio in the *glr3.3glr3.7* mutant when challenged with the same 4 AAs, while no differences were apparent in the eATP response in the two genetic backgrounds (0.74±0.06 for Col-0 (3) and 0.732±0.034 for *glr3.3glr3.7* as $\Delta R_{max}/R_0$) (*n*>4) (Fig. 18A and C; Suppl. Mat. Table 2C). Thus the simultaneous ablation of AtGLR3.3 and AtGLR3.7 completely abolished the exacerbation of the AA-evoked Ca^{2+} transients we observed in the *AtGLR3.7 loss-of-function* mutants. These results proved that the two isoforms are genetically linked in the response to the external AAs.

We then settled the question if the two channels can act in the same mechanism of Ca^{2+} regulation upon stem flaming. The primary stem of 5- to 6-week-old plants of both Col-0 and *glr3.3glr3.7* was flamed and the dynamics of cytosolic Ca^{2+} monitored at the primary floral AZ. As for the AAs response, fire application to the primary stem failed to trigger a cytosolic Ca^{2+} increase at the inflorescences apices of *glr3.3glr3.7* mutant (0.08±0.05 as $\Delta R_{max}/R_0$), while we detected a cytosolic Ca^{2+} increase of 0.58±0.07 in Col-0 (3) ($\Delta R_{max}/R_0$) (Fig. 14 E-F; Supp. Mat. Table 2D). This experiment strengthens the working hypothesis that AtGLR3.3 and AtGLR3.7 could assemble in the formation of a heterometic channel. Similarly, the concomitant ablation of the two GLRs impaired the electrical signal propagation through the stem upon primary stem flaming (12333 ±4481.4µm/sec for Col-0 and 2182 ±2090µm/sec for *glr3.3glr3.7*) (Fig. 15A). The propagation speed of Ca^{2+} from the primary floral AZ was also affected, both backward (stem) and forward (sepals) (348 ±186 µm/sec and 37 ±32 µm/sec (AZ to sepals) for Col-0 and *glr3.3glr3.7*, respectively; 40 ±8.48 µm/sec and 6.11 ±10 µm/sec (AZ to stem) for Col-0 and *glr3.3glr3.7*, respectively) (Fig. 15B-C). Flames application to the lateral stem failed to trigger a Ca^{2+} increase at the lateral floral AZ in *glr3.3glr3.7* ($n>3$) (Fig. 16A-B).

Altogether these experiments strongly suggested that two isoforms are genetically linked not only in the response to external AAs, but also in the generation/regulation of Ca^{2+} fluxes at the floral AZ upon stem flaming.

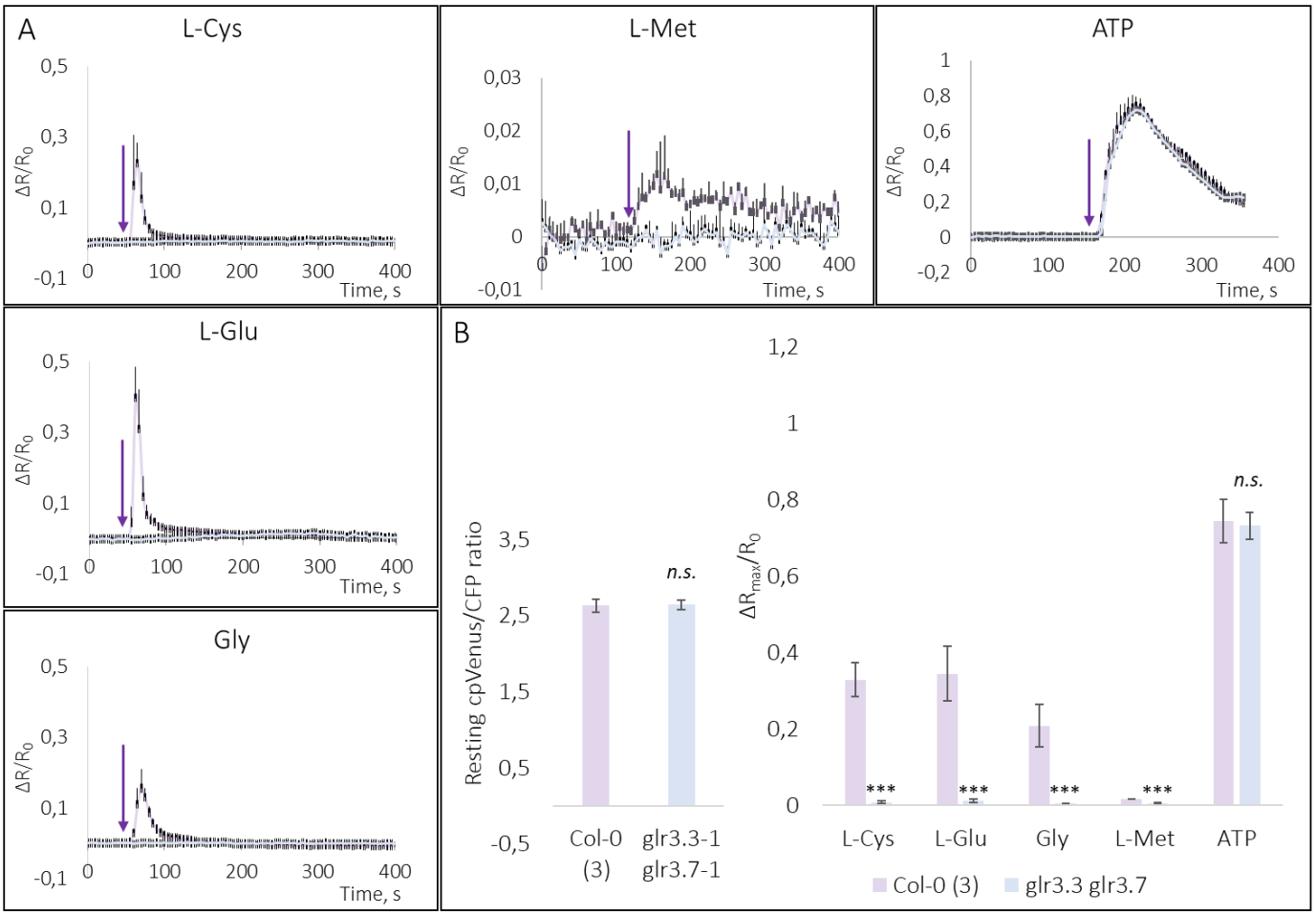

Fig. 18. A. Amino acids-evoked Ca^{2+} elevation in root cells of the meristematic zone in *glr3.3glr3.7.* A. Trend of the normalized cpVenus/CFP ratios ($\Delta R/R_0$) recorded in Col-0 7-day old seedlings expressing NES-YC3.6 in parallel with the *double null-allele* for *AtGLR3.3* and *AtGLR3.7*. Samples were treated with different external amino acids at the final concentration of 1mM. Under a wide-field microscope, plantlets were constantly supefused with standard imaging solution and transiently exposed to the amino acid (dissolved in imaging solution) for 3min. Arrows indicated the time when seedlings faced 1mM AAs or 100µM ATP, respectively. **B**. Resting level of cpVenus/CFP ratios. Values are the average of 50s-time window before treatment application and are reported as average±SD (left). Normalized maximal increase $\Delta R_{max}/R_0$ triggered by external AAs application at 1mM final concentration in Col-0 and *glr3.3glr3.7*. *n*>4; *n.s* non-statistical significant. **p*<0.5; ***p*<0.05; ****p*<0.005. Results are reported as average±SD. *p* values were calculated using Student's *t* test.

II.11. The ligand-binding pocket of AtGLR3.3 accommodates amino acidic ligands

We showed that AtGLR3.3 acts as a positive regulator of the amino acid sensing in root meristematic cells. Mutations that disrupt the reading frame of GLR3.3 lead to the impairment of the cytosolic Ca^{2+} elevation upon AAs application. This observation rises the fundamental question whether AtGLR3.3 can directly accommodate amino acids in its ligand binding pocket and whether this accommodation is responsible for the observed cytosolic Ca^{2+} increase. To answer this question, a colleague working in the laboratory where I carried out my PhD (Dr. Andrea Alfieri) prepared a construct recapitulating the GLR3.3 ligand-binding domain (LBD), consisting of the S1 and S2 segments joined by a short linker. The protein was expressed in *E. coli* and purified and its alo form was assayed for amino acid binding by means of the microscale thermophoresis technique, which is able to detect a change in the hydration shell of the biomolecule upon ligand-protein interaction. This technique revealed that the LBD of GLR3.3 is indeed able to bind the amino acids that triggered a cytosolic Ca^{2+} rise *in planta* (Fig. 19). Interestingly, by comparing K_d and $\Delta R_{max}/R_0$ (i.e. maximal ratio increase elicited by 1mM AAs treatment), we noticed a correlation between the lowest K_d (0.43 ±0.08µM) and the highest $\Delta R_{max}/R_0$ (0.374±0.082) for L-Cysteine. L-Glutamate, which triggers a cytosolic Ca^{2+} increase in root meristematic cells with the second highest $\Delta R_{max}/R_0$ (0.336±0.106) showed a K_d of 2.4 ±0.3µM, similar to L-Asn and L-Ser which were among the less effective amino acids to trigger a change in the ratio cpVenus/CFP. The case of the L-Methionine is peculiar, which showed the second lowest K_d (1.8 ±0.8 µM) but the lowest ability to trigger a cytosolic Ca^{2+} rise in root tip meristematic cells in Col-0 ($\Delta R_{max}/R_0$ = 0.016±0.011) (n>2) (Fig. 19). Following these exciting results, our colleague moved further and obtained crystals of the LBD which diffracted up to 2.0 Ångstrom resolution (Fig. 20A). The resulting electron density maps clearly showed the presence of a L-Glutamate molecule which is lodged in a cleft between the two lobes (Fig. 20B). This 'clamshell'-like conformation is shared with animal iGluRs. However, by comparing deposited structures of LBDs from different organisms (bacterial GluR0, rotifer AvGluR, rat iGluR), it is evident that L-Glutamate displays an unusual, unprecedented pose in the binding pocket of AtGLR3.3 (Fig. 20C). Moreover, in AtGLR3.3 two loops can be observed in lobe L1, lining the cleft between the two lobes, that appear to be specific to the plant lineage (shown in green in Fig. 20D).

LIGAND	K_d (µM)	$\Delta R_{max}/R_0$
L-Cys	0.43 ± 0.08	0.374 ±0.082
L-Met	1.8 ±0.8	0.016 ±0.011
L-Glu	2.4 ±0.3	0.336 ±0.106
L-Ala	2.4 ±0.9	0.307 ±0.07
L-Asn	2.5 ±0.3	0.116 ±0.029
L-Ser	2.7 ±0.8	0.143 ±0.028
Gly	5.5 ±1.6	0.298 ±0.077
D-Ser	22 ±6	0.003 ±0.002
L-Trp	no binding	0.006 ±0.004

Fig. 19. Comparison of dissociation constants and maximal ratio increase for different amino acidic ligands of GLR3.3 LBD. Dissociation constant K_d (µM) is reported for several AAs observed by means of the microscale thermophoresis technique. In parallel, the average maximal ratio increase $\Delta R_{max}/R_0$ elicited by 1mM AAs treatment in root meristematic cells in Col-0 seedlings is reported.

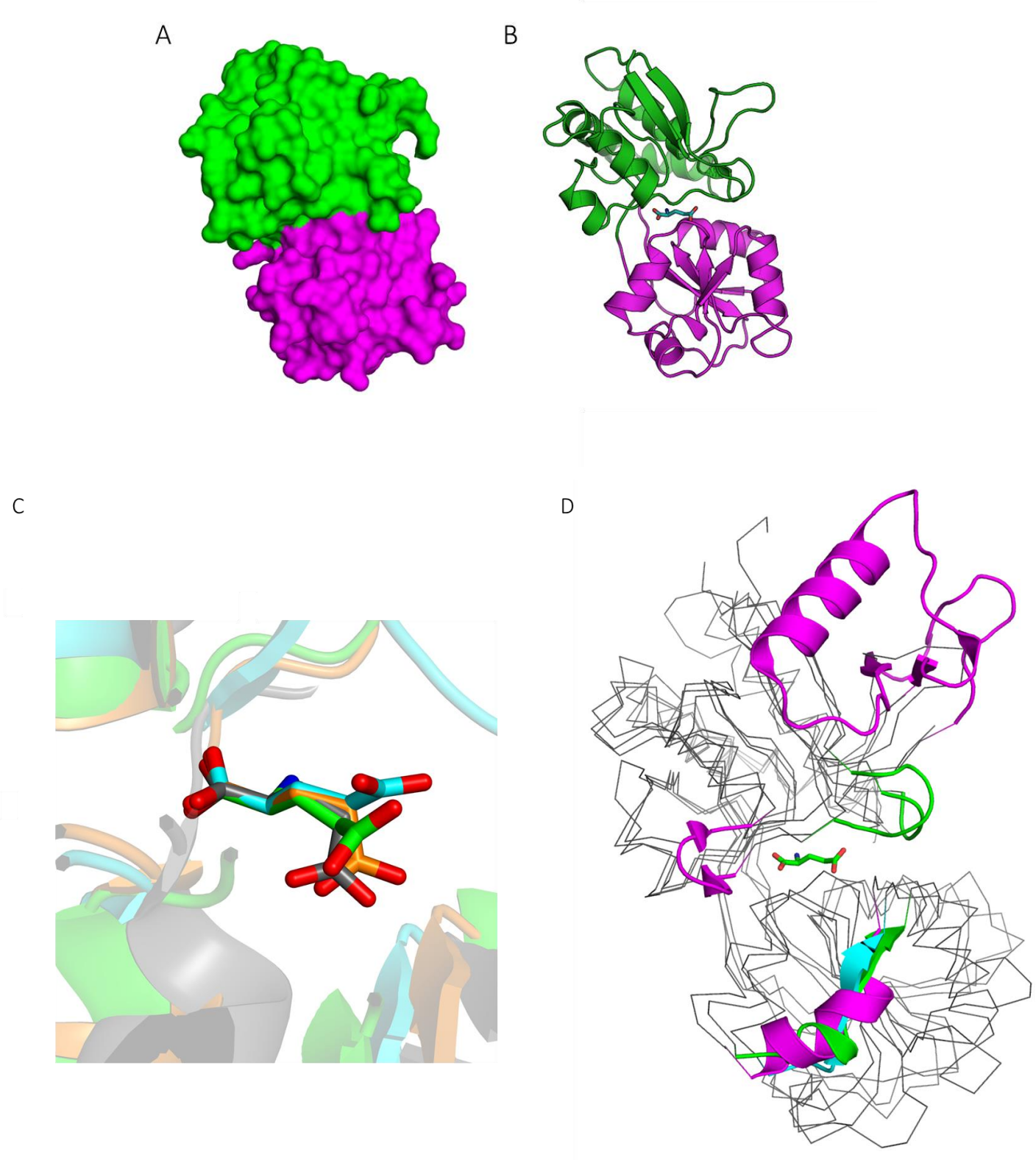

Fig. 20. The ligand binding domain structure of AtGLR3.3. A. Surface view of the AtGLR3.3 ligand-binding domain. L1 and L2 lobes are shown in green and magenta, respectively. **B.** Structure of the L1 and L2 lobes of AtGLR3.3 LBD represented as ribbon diagram. L-Glutamate accommodated into

the clamshell conformation of the LBD shown as stick model. **C.** Comparison of the binding pose of the Glutamate molecule in AtGLR3.3 LBD (green sticks), rat AMPA sub-type RnGluA2 (grey, PDB ID 1ftj), rotifer AvGluR (orange, PDB ID 4io2) and cyanobacterium GluR0 (cyan, PDB ID 1ii5). Superposition of the amino-Cα-carboxy part of the Glutamate molecule allows comparison of the different arrangement of the side chain in different proteins. Oxygen atoms in red, nitrogen atoms in blue **D.** Cα traces of LBDs of AtGLR3.3 (green), rat NMDA iGluR (magenta, PDB ID 2rc7) and cyanobacterium GluR0 (cyan, PDB ID 1ii5). Only regions which significantly differ are shown in colours. L-Glutamate of AtGLR3.3 is shown in stick representation. Note the two loops of AtGLR3.3 which protrude towards the binding pocket and the large insertion in the NMDA receptor L1.

II.12. Heterologous expression of AtGLR3.3 shows evidences for Na^+ transport

As animal iGluRs are non-selective cation channels with permeability to Ca^{2+}, Na^+ and K^+ (Traynelis *et al.*, 2014), a colleague (Dr. Maria Cristina Bonza) employed a functional complementation assay in yeast to investigate the ionic permeability of AtGLR3.3 and AtGLR3.7.

The G19 mutant strain of *S. cerevisiae,* lacking Na^+-ATPases, is salt hypersensitive and hence can not grow in media with high NaCl concentration. Thus, this strain was employed as heterologous expression system to assay the ability of AtGLR3.3 and AtGLR3.7 to transport Na^+. G19 cells expressing the four tested expression constructs (pYES2 empty vector EV; pYES2+AtGLR3.3, pYES2+AtGLR3.7; pYES2+OsHKT2;1) grew in a similar way on non-selective synthetic complete medium (SC-URA without NaCl) (Fig. 21A). The addition of 150mM NaCl evoked severe growth inhibition of cells that expressed OsHKT2;1, a rice Na^+/K^+ co-transporter used as control (Horie *et al.*, 2007). We observed a similar severe phenotype for G19 cells expressing AtGLR3.3, but not the AtGLR3.7 which acted similarly to the cells carrying the EV (negative control) (Fig. 21A). These results showed that G19 cells transformed with AtGLR3.3 have a higher sensitivity toward Na^+, which suggests a higher Na^+ influx and therefore accumulation. On the other hand, G19 cells expressing AtGLR3.7 did not show any altered growth parameter, suggesting that this isoform alone did not mediate Na^+ transport inside the cell.

In order to test if the two GLRs could mediate also K^+ uptake, the *S. cerevisiae* mutant strain CY162, which is defective in the two-major yeast high affinity K^+ transporters (*Δtrk1,2*) was employed (Lichtenberg, Heyer and Höfer, 1999). CY162 strain fails to grow in media which contains less than 2mM KCl, unless it expresses heterologous proteins which allow the transport of K^+ inside the cell. In

our case CY162 cells which expressed OsHKT2;4, a rice Na^+/K^+ co-transporter (Horie *et al.*, 2011), grew normally both in selective and non-selective media (Fig. 21B, positive control). However, the expression of AtGLR3.3 or AtGLR3.7 was not able to allow the yeast growth in the KCl-depleted medium (0.1mM).

Altogether, these results suggested that, in our experimental conditions, AtGLR3.3 could mediate Na^+ but not K^+ influx, while we did not detect any ability for AtGLR3.7 to carry Na^+ or K^+.

Future experiments by using yeast strains defective in Ca^{2+} transport will be performed to evaluate whether AtGLR3.3 and AtGLR3.7 are permeable to Ca^{2+}. Moreover, simultaneous expression of the two isoforms (GLR3.3 and GLR3.7) in yeast defective strains may add a new level of knowledge about the formation of a possible heteromeric channel and its ionic conductivity.

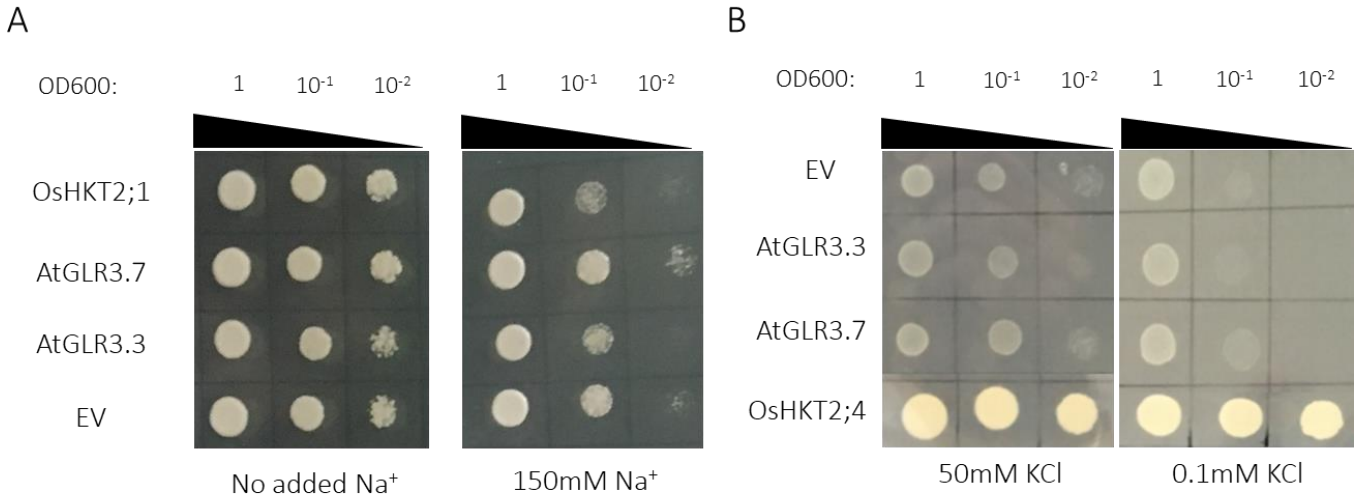

Fig. 21. Heterologous expression of AtGLR3.3 and AtGLR3.7 in yeast mutant strains. A. Serial dilutions of the Na^+ hypersensitive G19 strain transformed with OsHKT2;1, AtGLR3.7, AtGLR3.3 or EV grew at 30°C for 72h in non-selective (no added Na^+) and selective conditions (150mM Na^+). **B.** Serial dilutions of the K^+ sensitive CY162 strain transformed with OsHKT2;4, AtGLR3.7, AtGLR3.3 or EV grew at 30°C for 72h in non-selective (50mM KCl) and selective conditions (0.1mM KCl). *n*>2.

Chapter III. Conclusions and future perspectives

Environmental cues have to be perceived by specific receptors which will give rise to a series of cascade events eventually resulting in acclimation to the new external conditions. A transient rise in the cytosolic Ca^{2+} concentration is one of the first events that occurs upon the perception of an external stimulus. We here reported that seven L-proteinogenic amino acids trigger an elevation of cytosolic Ca^{2+} concentration in the root tip cells of the model plant *Arabidopsis thaliana*. *In vivo* 4D live imaging acquisitions revealed that the primary response to amino acids, in terms of cytosolic Ca^{2+} elevation, occurred at the lateral root cap of the root meristematic zone. We aimed at investigating the molecular determinants involved in the perception of external amino acids. Our investigation focused on the Glutamate Receptor-like family and in particular on two genes belonging to the Clade III, AtGLR3.3 and AtGLR3.7 (herein called as AtGLR3.x). Interestingly, in our hands, both AtGLR3.3 and AtGLR3.7 proteins mainly localised at the endomembranes and not at the plasma membrane. This was consistent with Wudick *et al.* (2018) and Nguyen *et al.* (2018) reports (Nguyen *et al.*, 2018; Wudick *et al.*, 2018b) where AtGLR3.3 mainly localized at the endomembranes. This suggests that AtGLR3.x may be subjected to a complex trafficking regulation and that only a low amount of protein (possibly under the detection limit of fluorescent light microscopy) can effectively reach the plasma membrane.

We evaluated the contribution of AtGLR3.3 and AtGLR3.7 to the perception of amino acids by disrupting AtGLR3.x genes. Amino acids application failed to trigger any cytosolic Ca^{2+} increase in the *loss-of-function* alleles for AtGLR3.3, while mutations of the AtGLR3.7 lead to an exacerbation of the Ca^{2+} transient upon amino acid stimulation. In parallel, we also proved that AtGLR3.x are involved in long-distance Ca^{2+} wave generation. Indeed, we found out a similar behaviour for AtGLR3.x mutants when subjected to stem flaming. In fact, we detected an impairment of cytosolic Ca^{2+} increase at the inflorescence apex upon stem flaming in *glr3.3* mutants, whereas a putative exacerbated rise of the Ca^{2+} transient was detected on *glr3.7 loss-of-function* mutants. Due to the antagonistic role played by AtGLR3.x, we assayed the possibility they might form a heteromeric channel. We observed a decrease in the fluorescence lifetime τ for eGFP in a FLIM experiment when AtGLR3.3-eGFP and AtGLR3.7-mCherry were co-expressed in Nicotiana leaf cells, which suggested a distance of <5nm and hence, an interaction between them. Moreover, we calculated an overall FRET efficiency of 46%, which suggested that in almost half of the case the formation of an AtGLR3.3-AtGLR3.7 channel may exist *in planta*. Albeit preliminary, the evidence of an heterometic AtGLR3.x channel by FRET-FLIM

measurement was confirmed by genetics. Indeed, the double mutant *glr3.3glr3.7* reverted the exacerbation of the cytosolic Ca^{2+} rise upon amino acids treatment that we observed in *glr3.7* single mutants, mimicking *glr3.3 loss-of-functions* (no response). Similarly, the cytosolic Ca^{2+} elevation at the floral abscission zone was impaired in the *glr3.3glr3.7* as in *glr3.3* mutants. These experiments strongly suggested that AtGLR3.3-AtGLR3.7 are genetically linked. However, simultaneous expression in a heterologous system (yeast, COS or HEK cells) would be necessary to prove the formation of a functional heteromeric channel. Altogether, these results suggested that AtGLR3.x inversely regulate local and long-distance Ca^{2+} signalling. In particular, AtGLR3.3 would act as a scaffold protein whose loss resulted in a *null* response, whereas AtGLR3.7 might play a negative regulation on the channel. More so, the fact that in yeast cells AtGLR3.7 does not seem to function as homomeric channel, whereas the AtGLR3.3 does, leads us to speculate that the AtGLR3.7 is a regulatory subunit not able to form a channel *per se*. At the present time we can hypothesize that this negative regulation, on AtGLR3.3 activity, exerted by AtGLR3.7 may be played at different levels: e.g. gating, export or folding of the heteromeric channel.

The flame experiments, which suggested a prominent role for AtGLR3.x, give rise to a fundamental question: is the amino acid binding necessary for the AtGLR3.x-mediated cytosolic Ca^{2+} increase at the floral abscission zone upon stem flaming?

We first investigated whether AtGLR3.3 ligand binding pocket could accommodate external amino acids. Our colleague showed that AtGLR3.3 LBD could bind amino acids, with different affinities. The two amino acids with the lowest K_d (i.e. the highest affinity) were L-Cysteine and L-Methionine. Intriguingly, L-Cysteine, and not L-Glutamate (as for iGluRs), showed the lowest K_d *in vitro* and the maximal increase in $\Delta R_{max}/R_0$ *in planta* when applied exougenously. An apparent discrepancy was found out for L-Methionine. In fact, while L-Methionine showed a higher affinity (K_d = 1.8±0.8 µM) compared to L-Glu (K_d = 2.4±0.3 µM), it triggered a low increase in the $\Delta R_{max}/R_0$ (0.016±0.011 as $\Delta R_{max}/R_0$) in root meristematic cells. Intriguingly, both L-Cysteine and L-Methionine contain a sulfur group in their side chain which could act as important antioxidants and contribute to the stability of the LBD structure upon binding.

Crystals of the AtGLR3.3 LBD were obtained with a L-Glutamate molecule lodged in the binding pocket. The AtGLR3.3 LBD showed a clamshell-like conformation that is shared with animal iGluRs. However, important differences were found out by comparing binding pockets from different organisms (bacterial GluR0, rotifer AvGluR, rat iGluR). In fact, L-Glutamate displayed a different

position in the binding pocket of AtGLR3.3. Moreover, AtGLR3.3 LBD showed a loop, specific for plant GLRs, nearby the accommodation pocket; however, AtGLR3.3 LBD misses a huge loop specific for NMDA receptors, which probably originated after the division of animal and plant Glutamate Receptors. To the best of our knowledge, this represented the first report of a plant GLR structure. Point mutations of key residues essential for ligand coordination are ongoing (Fig. 22). The mutants which will show lower affinity or no binding for amino acids will be then reintroduced in *glr3.3* mutant and tested for amino acid-induced cytosolic Ca^{2+} elevation at the root meristematic zone (here used as a tool to show that the mutations drammatically affect Ca^{2+} dynamics upon amino acids treatment) and then subjected to flaming. These experiments will give us an answer to the question whether amino acids release by damaged tissues are involved in stem-inflorescences apex communication upon flaming. A fascinating hypothesis is, in fact, that at the damaged site, amino acids are released and they could act as depolarizing factors acting through the AtGLR3.x and be at the basis of the variation potential propagation. Recently, it has been shown that leaf wounding leads to local leaking of Glutamate, up to 50mM. In our hypothesis, Glutamate or other amino acids could locally activate GLR3.x and trigger the initiation of electrical signal propagating through the plants, possibly *via* xylem (Nguyen *et al.*, 2018) (GLR3.3 is highly expressed in the vasculature). This would explain the impairment of the *glr3.3* mutants to induce a cytosolic Ca^{2+} elevation at the flower abscission zone upon stem flaming.

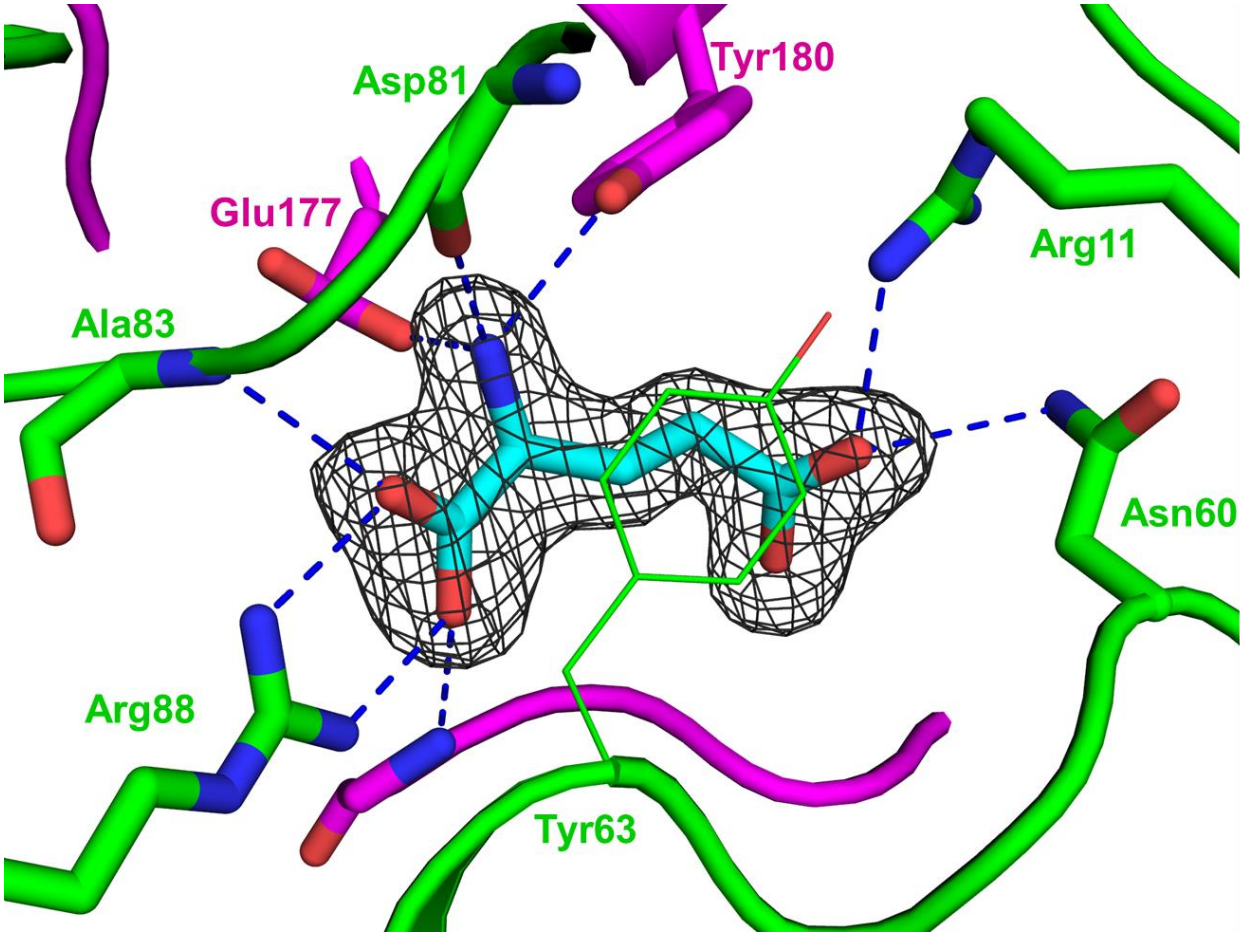

Fig. 22 Magnification of AtGLR3.3 ligand binding domain. Electron density map visualized at 2 Ångstrom for L-Glutamate (light blue, shown as stick model) in the binding pocket. Residues essential for L-Glutamate coordination into the LBD are shown as sticks (except for Tyr63 lateral chain, showed as lines for better visualization). Hydrogen bonds are shown in dashed blue lines. Nitrogen and oxygen atoms are shown in blue and red, respectively. Carbon atoms are shown in green if belonging to S1, and in magenta if belonging to S2, respectively (credit to Dr. Andrea Alfieri).

Chapter IV: Materials and methodologies

IV.1. Plant material and growth conditions

Arabidopsis thaliana plants used in this study were of the Columbia-0 ecotype (Col-0) and C24. Plants were grown on 16/8 h cycles of light (70µm m^{-2} s^{-1}) at 22°C and 75% Relative Humidity. Seeds of *Arabidopsis* were surface sterilized by vapor-phase sterilization (100ml of 15% (v/v) sodium hypoclorite with 3ml 37% (v/v) hydrochloric acid for 5h) and plated in sterile conditions (using a sterile toothpick to plate the seeds individually) on half strength Murashige and Skoog medium (Murashige and Skoog, 1962) (Duchefa, Netherlands) supplemented with 0.1% (w/v) sucrose, 0.05% (w/v) MES, pH 5.8 and solidified with 0.8% (w/v) of plant agar (Duchefa, Netherlands). After stratification at 4°C in the dark for 3 days, seeds were transferred to the growth chamber with 16/8 h cycles of light (70µm m^{-2} s^{-1}) at 22°C. Plates were kept vertically. Seedlings used for the analyses were 6-7-day old, whose corresponds an average root length of about 3cm.

IV.2. Bacterial strains

Plasmid amplification was performed in the DH5α *Escherichia coli*. The *Agrobacterium tumefaciens* strain used for plant transformation was GV3101/pMP90.

IV.3. Genetic material

DNA amplification of GLRs coding sequences (CDS) were carried out by PCR using Phusion® High-Fidelity DNA Polymerase (New England Biolabs NEB). Colony PCR and orientation/insertion screening were performed by PCR using GoTaq® DNA Polymerase (Promega).

Digestions were performed in a final volume of 60µl, using 1-5units/enzyme per 1µg DNA and generally performed for 2h 30 minutes at 37°C. ApaI digestion was performed at 25°C O/N. Ligations were performed in a final volume of 20µl, using 1:3 molar ratio vector/insert, performed at 15°C O/N. 1-3 units/T4 DNA ligase was used.

Sanger sequencing methodology analyses was used to confirm the integrity and the right orientation of all constructs. The sequence of all primers used in this work is reported in Appendix Table 1.

IV.4. Polymerase chain reaction (PCR) conditions

PCR Go-Taq® standard protocol: <10 ng/25µl DNA, 0.5µl 10mM dNTPs mix, 5µl 5X Green Go-Taq Reaction Buffer (Promega), 0.1µl 5U/µl Go-Taq® G2 DNA Polymerase (Promega), 0.5µl 10µM forward and reverse primers, bi-distilled H_2O to final volume of 25µl.

PCR Phusion® standard protocol: <10ng DNA, 10µl 5X Phusion® HF Reaction Buffer (NEB), 1µl dNTPs 10 mM mix, 1.5µl 10µM forward (F) and reverse (R) primers, 1µl 2U/µl Phusion-HF® DNA polymerase (NEB), 1.5µl 100% DMSO (NEB), bi-distilled H_2O to final volume of 50µl.

IV.5. Mutants isolation

T-DNA insertion alleles of Col-0 ecotype were isolated from the T-DNA SALK collection. Two independent T-DNA insertion alleles were isolated for both AtGLR3.3 (*glr3.3-1* and *glr3.3-2*) (Qi, Stephens and Spalding, 2006) and AtGLR3.7 (*glr3.7-1* (Michard *et al.*, 2011) and *glr3.7-2*). *glr3.7-2* insertional mutant was kindly provided by Dr. Julia Davies, Cambridge University, UK). A third independent allele was isolated for AtGLR3.7 in the C24 accession, harbouring a non sense mutation at position 765 (Triptophan to TGA) (Iwano *et al.*, 2015b). The double mutant *glr3.7glr3.3* was obtained by crossing *glr3.3-1* and *glr3.7-1* plants (Fig. 1).

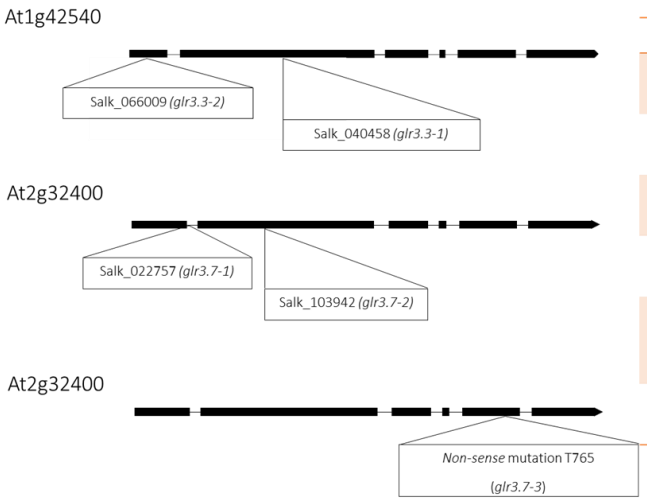

Locus	Genotype	SALK line	T-DNA insertion	Ecotype
At1g42540	*glr3.3-1*	Salk_040458	Second exon	Col-0
At1g42540	*glr3.3-2*	Salk_066009	First exon	Col-0
At2g32400	*glr3.7-1*	Salk_022757	First intron	Col-0
At2g32400	*glr3.7-2*	Salk_103942	Second exon	Col-0
At2g32400	*glr3.7-3*	-	Non sense mutation of T765	C24
At1g42540 At2g32400	*glr3.3-1* *glr3.7-1*	Salk_040458 Salk_022757	Second exon First intron	Col-0

Figure 1 – Schematic representation and table showing T-DNA integration in *AtGLR3.3* and *AtGLR3.7* loci (left) with their corresponding SALK lines and ecotype (right).

IV.6. Plasmid DNA extraction

E. coli competent DH5α strain cells were transformed with the constructs of interest and plated for selection on solid Luria & Bertani (LB) growth medium (10g/l Bacto-Tryptone, 5g/l Bacto-yeast extract, 5g/l NaCl, distilled H_2O to 1l volume, 20g/l Agar) containing the specific selective antibiotic

and incubated for 12-16 hours at 37°C. Resulting colonies were inoculated in 5ml liquid LB growth medium with the specific selective antibiotic and shaken (280 revolutions per minute) at 37°C O/N.

Plasmid DNA alkaline extractions were performed using the Promega Wizard® Plus SV Minipreps DNA purification Sytem kit. Midiprep preparations were performed in the same way, starting from 200ml O/N cell culture using the Macherey-Nagel® NucleoSpin Plasmid kit.

IV.7. Genomic DNA extraction

A small leaf from a wild type *Arabidopsis thaliana* plant was placed in 2ml Eppendorf tube and rapidly frozen in liquid nitrogen. Sample was mashed into tiny bits using a plastic applicator in presence of freshly prepared 500µl Extraction Buffer (100mM Tris pH 8.5, 50mM EDTA, 500mM NaCl). 35µl SDS 20% (w/v) were added after leaf smashing in order to solubilize proteins and lipids. The sample was incubated 5 minutes at 65°C and treated with 130µl 5M potassium acetate (KOAc) which decreased mixture alkalinity and kept 5 minutes at 0°C. The sample was then centrifugated for 10 minutes at 10000 x g at room temperature and the supernatant transferred to a new tube where 640µl Isopropyl alcohol and 60 µl 3M sodium acetate (NaOAc) were added. Samples were then incubated 30minutes at -20°C to enhance DNA aggregation and centrifugated for 10minutes at 15000 x g to precipitate the DNA in a pellet. Washing the pellet with 300µl ethanol 70% (v/v) was performed to eliminate SDS and salts and enhance the DNA precipitation after a successive centrifugation step (5 minutes, 15000 x g). Pellet was later re-suspended in 40µl bi-distilled H_2O and heated at 65°C for 10 minutes. Supernatant was collected after 5minutes centrifugation at full speed.

IV.8. DH5α *E. coli* competent cells transformation

Constructs of interest were introduced in DH5α *E. coli* competent cells by freeze-thaw method. About 150ng DNA was added to 50µl DH5α *E. coli* competent cells and then incubated in ice for 30 minutes. Cells were incubated at 42°C for 45s and immediately chilled at 0°C for at least 2minutes. 500µl LB growth medium was added to the cells allowing them to recover and maintained at 37°C for 1h. Transformed cells were plated on agar LB containing the selective antibiotic and incubated at 37°C for 24h. Depending on the plasmid, the antibiotic concentration was as follow: 50mg/l ampicillin, 50mg/l kanamycin, spectinomycin 50 mg/l.

IV.9. *Agrobacterium tumefaciens* transformation

Constructs of interest were introduced in *A. tumefaciens* GV3101/pMP90 strain by freeze-thaw method. About 1µg of plasmid DNA was added to 100µl competent cells then frozen in liquid

nitrogen. Cells were thawed by incubating the test tubes in a 37°C water bath for 5min. The bacterial culture was later incubated at 28°C for 2-4h with gentle shaking in 1ml yeast extract peptone YEP medium (10g/l bacto-tryptone, 10g/l yeast extract, and 5g/l NaCl, pH 7.0). This time allows the bacteria to express the antibiotic resistance genes. After 1min centrifugation in an Eppendorf Centrifuge (4 min at 5000 x g), the supernatant solution was discarded and cells re-suspended in 0.1ml YEP medium. Cells were then spread out on a yeast extract peptone agar plate containing the appropriate antibiotic selection and incubated at 28°C (for 2-3 days, until transformed colonies appeared). The antibiotic concentration was as follow: 50 mg/l gentamycin, 50mg/l rifampicin, 50 mg/l kanamycin and 50 mg/l tetracycline.

IV.10. Transgenic plants

The *A. tumefaciens* GV3101/pMP90 strain, transformed with the construct of interest, was used to generate transgenic plants by the floral dip method (Clough and Bent, 1998). Developing floral tissues were dipped into a solution containing *Agrobacterium tumefaciens* harbouring the construct of interest. Transformed *A. tumefaciens* cultures were incubated O/N in 250ml YEP growth medium with the selective antibiotic and centrifuged for 15min at 7000 x g at 10°C. Supernatant was discarded and the pellet was re-suspended in a 500ml solution containing sucrose 5% (w/v) and 0.05% (v/v) of the surfactant Silwett L-77 which enhances bacteria penetration into relatively inaccessible plant tissues. Flowering plants were kept upside-down into pot containing the infiltration solution and dipped 10s for three times spaced out by 10s pause. Transformed plants were kept in the dark at 22°C for 24h before being transferred to the normal growth conditions.

IV.11. Mutants genotyping

Two couples of PCR primers have been employed for the genotyping of *glr3.7-1* mutant plants. The first one (Lb1.3/AC355) was used to assure T-DNA insertion on *AtGLR3.7*; the second one (AC355/AC356) to confirm the lack of the wild type *AtGLR3.7* gene. Indeed, PCR amplification with AC355/AC356 primer was prevented by the presence of the T-DNA on the *GLR3.7* locus. The same strategy was followed to validate *glr3.7-2* mutant using the couples of primers Lb1.3/AC452 and AC451/AC452. Non sense mutation on *glr3.7-3* was validated by amplifying 641bp (AC404-0S858) DNA fragment using as a template genomic DNA extracted from C24 (negative control) and *glr3.7-3* leaves. Sanger sequencing reaction was employed to track the point mutation on At*GLR3.7*.

The couple of primers AC400/AC401 annealed on wt *AtGLR3.3*, while Lb1.3/AC401 have been employed for T-DNA isolation on *glr3.3-1* and *glr3.3-2* by PCR. The homozygous insertion of the two T-DNA fragments in the double mutant *glr3.3glr3.7* was evaluated by using Lb1.3/AC355 and Lb1.3/AC401.

IV.12. Quantitative Reverse Transcription Polymerase Chain Reaction (qRT-PCR)

Quantitative Reverse Transcription Polymerase Chain Reaction (qRT-PCR) experiments were performed on 7-day-old seedlings grown in standard conditions (see 'Plant material and growth conditions'). Seedlings were pooled in 2ml tubes containing two steel balls. Tubes were rapidly frozen in liquid nitrogen and seedlings ground using a tissue-lyser (Retsch). For each genotype, 10-20 seedlings were used as starting material. Total RNA was isolated using the Nucleospin RNA Plant Kit (Macherey-Nagel®). To remove gDNA contamination from RNA samples, deoxyribonuclease (rDNase) was applied onto the silica membrane (on column rDNase). DNA digestion was performed for 15min. The RNA bound to the resin was washed with 75% (v/v) ethanol, dried and finally resuspended in bi-distilled H_2O. RNA was quantified using a NanoPhotometer Pearl (Implen). 1µg of total RNA was retro-transcribed using SuperScript II Reverse Transcriptase (Invitrogen®). 1µl Oligo-dT (500µg/ml) was used to selectively retro-transcribe messenger RNAs in a final volume of 5µl. In order to open the dsRNA structures eventually present, RNA mixes were pre-heated at 70°C for 5 minutes. Reverse-transcription (RT) PCR was performed in a final volume of 20µl and the reaction components were as follow: RNA mix 5µl, 1µl of 5X RT-PCR Buffer, 1µl of 25mM $MgCl_2$, 2µl of (10mM each dNTP) dNTPs and bi-distilled H_20 to volume. The reaction temperature was shifted from initial 25°C to a final 42°C allowing RT. RT reaction was inactivated turning up to 70°C for 15min. The obtained cDNAs were subjected to 5-fold dilution. Quantification of gene expression was carried out in a final volume of 10µl using a Mastercycler Realplex2 (Eppendorf®). Real-time qRT-PCR reactions were carried out using 5µl of 2X Maxima SYBR Green qPCR Master Mix (containing dNTPs, Go-Taq Thermo Scientific and SYBR Green), 0.7µl of each primer (10µM working solution), 1µl of cDNA template and bi-distilled H_2O to volume.

Primers used to quantify the messenger RNA amounts of *GLR3.7*, *GLR3.3* and *TUBULIN4* (*TUB4*) are listed in Appendix Table 1. The expression levels of *GLR3.7* and *GLR3.3* monitored by qRT-PCR were normalized based on the control gene TUB4. Primers were designed to amplify a small fragment of the 3' region of the CDSs.

To test primers efficiency, a standard curve on serial diluted Col-0 gDNA was performed. Melting curve assured highly specific amplification product. The $2^{-\Delta\Delta CT}$ method was used to calculate the relative changes in gene expression determined by the Real-Time qRT-PCR measurements.

Please note that the quantification of *GLR3.7* expression level by Real Time qRT-PCR in *glr3.7-1* mutant confirmed RT published data (Michard *et al.*, 2011) according to which *glr3.7-1* is not a completely knock-out mutant.

IV.13. Constructs for GLR3.x sub-cellular localization and FRET-FLIM experiments

The GLR3.7 coding sequence (CDS) was amplified by PCR with primers AC332/AC333 (see Appendix Table1) from complementary DNA retro transcribed from RNA extracted from *Arabidopsis thaliana* Col-0 seedlings (kindly provided by Dr. Vittoria Brambilla, University of Milan, Italy). GLR3.7 CDS harboring NcoI sites at both 5'- and 3' was digested with NcoI (NEB) and ligated into the pGREEN 00029 2xp35S::YFP (Valerio *et al.*, 2011) previously digested with NcoI and dephosphorylated (Antartic phosphatase, NEB) to prevent self-ligation. *Loss-of-function* plants for AtGLR3.3 and plants complemented with pGLR3.3::GLR3.3-GFP have been assayed for *AtGLR3.3* expression and localization (kindly provided by Prof. Edgar Spalding, University of Wisconsin-Madison, USA) (Vincill *et al.*, 2013). The two couples of primer Lb1.3-AC 401 and AC400-AC401 were used to detect the presence of the T-DNA insertion and construct complementation, respectively. AC509-AC510 allowed to amplify an amplicon by PCR confirming that the construct harbours a GFP nucleotide sequence.

For FRET-FLIM analysis, the two constructs B7FWG2,0 p35S::GLR3.3cDNA-eGFP and pGPTVII pUBQ10::GLR3.7-mCherry were used. A LR reaction (Gateway, ThermoFisher) was employed to swap *AtGLR3.3* cDNA from a pDONR201-GLR3.3 vector (kindly provided by Prof. Josè Feijo, University of Maryland, USA) (Wudick *et al.*, 2018b) to the destination vector B7FWG2,0 p35S::EGFP (kindly provided by Prof. Paolo Pesaresi, University of Milan, Italy). Constructs were validated by PCR reactions and restriction enzymes digestions. Prof. Joerg Kudla (University of Munster, Germany) kindly provided pGPTVII pUBQ10::GLR3.7-mCherry construct which was checked by PCR reaction (for primers used to validate the constructs see Appendix Table).

IV.14. Transient expression in *Nicotiana benthamiana* leaves

Plants were cultivated for 5–6 weeks in a greenhouse under a 12h light/12-h dark cycle with 60% atmospheric humidity at 20°C. Leaf infiltration was performed using *A. tumefaciens* GV3101/pMP90 strain carrying the specified constructs together with the p19K-enhanced expression system (Waadt

and Kudla, 2008) resuspended to a final OD_{600} of 0.1-0.2 in the infiltration buffer (150µM acetosyringone, 10mM MES, 10mM $MgCl_2$, pH 5.6 KOH) (p2x35S::GLR3.7-YFP OD_{600} = 0.2, mCherry-HDEL OD_{600} = 0.3, p35S::GLR3.3-eGFP OD_{600} = 0.25, pUBQ10::GLR3.7-mCherry OD_{600} = 0.2, p19K $0D_{600}$ = 0.3). Acetosyringone (3,5-dimethoxy-4-hidroxy acetophenone) was used in to enhance *A. tumefaciens* transformation efficiency (0.15mM final concentration) (Waadt and Kudla, 2008). After leaves infiltration, plants were kept (3–5 days) under conditions as described above.

IV.15. *Arabidopsis thaliana* protoplast isolation and transformation

For GLR3.7 sub-cellular localization studies, leaves from 4 week old *Arabidopsis thaliana* Col-0 plants (Yoo, Cho and Sheen, 2007) were collected and cut in 0.5-1mm strips with fresh razor blades without wounding and put into multiwell cell culture in presence of the following enzymatic plasmolysis mix: 20mM KCl, 10mM $CaCl_2$, 0.4M D-Mannitol, 20mM MES, 1.25% R10 Cellulase (w/v) and 0.3% R10 Macerozyme (w/v), 0.1% Bovine Serum Albumin BSA (w/v). Enzymes were pre-heated at 55°C for 10 minutes. $CaCl_2$ and BSA were added to the mix after the 55°C incubation. Enzymatic mix was filtered (0.45µm pore size membrane disc filter) and added to the cut leaves. 10min vacuum favored enzymes entering into the leaves through the cuticle. Digestion was continued in the dark for about 3h without shaking. Following enzyme incubation, protoplasts were separated from the cell debris filtering the incubation mixture through a nylon sieve of 50µm pore size (*A. thaliana* mesophyll protoplasts have 20-30µm average dimensions). Protoplasts were spun at 100 x g for 6min in a round-bottomed tube in presence of 50mM $CaCl_2$ which helps protoplasts pelleting. Protoplasts were washed once in cold W5 washing solution (154mM NaCl, 125mM $CaCl_2$, 5mM KCl, 2mM MES) to wash and make protoplasts competent to DNA transformation), centrifuged 100 x g for 6min and resuspended in the same solution. After incubation on ice for 30min, protoplasts were resuspended in 600µl MMg (0.4M D-Mannitol, 15mM $MgCl_2$, 4mM MES pH 5.7) and centrifuged for 1min at 100 x g. The PolyEthylene Glycol PEG-mediated- protoplasts transformation procedure was as follow: 5-10µg DNA (~10µl) and 100µl MMg protoplasts resuspended solution were mixed in 2ml microfuge tube and incubated at room temperature for 20min in presence of an equal amount of PEG solution (40% v/v, 4g PEG4000, 0.364g D-Mannitol, 1ml $CaCl_2$ (1M) and 5.5ml distilled H_20). To remove PEG, the protoplasts suspension was diluted by adding a 4-fold volume of W5. Supernatant was carefully removed after 3min centrifugation at 100 x g and the transformed protoplasts were re-suspended in 1ml W5 solution, transferred into a 6-well plate and maintained in the growth chamber (23°C) in the dark. Protoplasts were microscopically analyzed 16-24h after transformation.

IV.16. Spheroplasts isolation for patch clamp measurements

For patch clamp experiments, protoplasts were isolated from 3-day-old Col-0 and *glr3.3-1* seedlings grown on half strength Murashige and Skoog media (Murashige and Skoog, 1962) (Sigma basal medium) supplemented with 0.1% (w/v) sucrose, 0.05% (w/v) MES, pH 5.8 and solidified with 0.8% (w/v) of plant agar (Duchefa, Netherlands). Seeds were surface sterilized by means of a solution of dichlor (Bayrochlor) (150g dissolved in 40ml Ethanol 50%) (w/v). 1ml dichlor solution was added at 1.5ml Eppendorf containing few seeds and mixed for 20 minutes. Under sterile conditions, seeds were washed three times with EtOH 100% (v/v) and left under the hood overnight to let the ethanol evaporate. With the help of a toothpick, seeds were one by one transferred to MS sterile plate. After stratification at 4°C in the dark for 24-48h, seeds were transferred to the growth chamber with 16/8 h cycles of light at 22°C. Plates were kept vertically. Root hair membranes recovery was assessed by means of laser microsurgery. Seedlings were gently transferred into the chamber for patch clamp measurement in presence of 40µl *circa* plasmolysis solution (350mM D-Mannitol, 5mM $CaCl_2$, 0.01% calcofluor) (w/v). Calcofluor enhanced laser dissection effectiveness. 5min treatment was enough to let the plasma membrane shriking. UV laser cell wall microdissection was performed at the tip of the hairs by means of a Nitrogen-based laser. The release of a series of protoplasts was achieved by adding a drop of deplasmolysis solution (200mM D-Mannitol, 2.5mM $CaCl_2$) (w/v). The osmolarity was then reduced to 275mOsM. By gently shaking the chamber a series of spheroplasts were released. The removal of the seedling from the chamber was achieved with the help of sharp tweezer. Few seconds were sufficient to let the spheroplasts lie at the bottom of the chamber. Deplasmolysis solution was then diluted with large amount of patch clamp external solution. Due to the formation of a new cell wall, seal formation became difficult to achieve. For this reason, new spheroplasts were isolated in a cycle of 25-35 minutes.

IV.17. Patch clamp solutions and recordings

The bath (external) solution was composed of 10mM $CaCl_2$, 10mM KCl, 10mM MES, 2mM CsCl, 225mM D-Sorbitol pH 5,8 TRIS while the pipette (internal) solution comprised 100mM K-Gluconate, 4mM $CaCl_2$, 10mM CsCl, 10mM EGTA, 2mM Mg^{2+}-ATP, 10mM Hepes, 60mM D-Sorbitol, pH 7,5 TRIS. Data were sampled at 1 kHz and filtered at 200 Hz. The voltage-clamp protocol consisted of a series of depolarizing and/or hyperpolarizing steps of 1s duration starting from a holding potential of -40mV, where was not detected any significant current activity (-40mV was close to the resting potential of spheroplasts in the bath solution). From the holding potential, 10mV depolarizing and/or

hyperpolarizing steps were applied and the two protocols separately recorded. Current-voltage relationships (I-V curves) were calculated averaging total whole-cell currents measured from each voltage clamp step. Measurements were performed after at least 10min from Gigaseal achievement, in order to equilibrate the pipette solution with the spheroplast's cytoplasm. Pipette resistence ranged from 7 to 12 MΩ.

IV.18. Time-lapse Ca^{2+} imaging analyses and confocal microscopy analyses

For Ca^{2+} imaging analysis of *Arabidopsis thaliana* plants harbouring the NES-YC3.6 Ca^{2+} Cameleon biosensor, we used an inverted fluorescence Nikon microscope (Ti-E; http://www.nikon.com/) with a CFI ×4 NA (numerical aperture) 0.13 dry objective for the Arabidopsis inflorescences or a ×20 NA 0.75 for seedling roots. Excitation light was produced by a fluorescent lamp (Prior Lumen 200 PRO; Prior Scientific; http://www.prior.com) at 440 nm (436/20 nm) set to 50% for inflorescences and 20% for seedlings. Images were collected with a Hamamatsu Dual CCD camera (ORCA-D2; http://www.hamamatsu.com/). For Cameleon analysis, the FRET cyan fluorescent protein (CFP)/YFP optical block A11400-03 (emission 1, 483/32 nm for CFP; emission 2, 542/27 nm for FRET) with a dichroic 510 nm mirror (Hamamatsu) was used for the simultaneous CFP and cpVenus acquisitions. Exposure times changed accordingly (200ms-500ms) to the expression level of the biosensor in the different genetic backgrounds under investigation. The camera binning was 2x2 for seedlings and 4x4 for inflorescences. Images were acquired every 2-5 s. Filters and the dichroic mirror were purchased from Chroma Technology (http://www.chroma.com/). NIS-Elements (Nikon; http://www.nis-elements.com/) was used as a platform to control microscope, illuminator, camera, and post-acquisition analyses. Regarding time-course experiments, fluorescence intensity was determined over regions of interest (ROIs), which correspond to the root tip zone or inflorescence apex. cpVenus and CFP emissions of the analyzed ROIs were used for the ratio (R) calculation (cpVenus/CFP) and normalized to the initial ratio (R_0) and plotted versus time ($\Delta R/R_0$). Background subtraction was performed in each channel before FRET ratio calculation by selecting a ROI outside the sample (Bonza *et al.*, 2013).

Confocal microscopy analyses were performed using a SP2 (Leica, Germany, http://www.leica-microsystems.com) or a Nikon Eclipse Ti2 microscope laser scanning confocal imaging systems for FRET acquisitions. For YFP, excitation was at 514 nm and emission between 525/540 nm. For FM4-64 and mCherry detection, excitation was at 561 nm and emission between 575/625 nm. Post-acquisition images analyses were performed with the ImageJ bundle software

(http://rsb.info.nih.gov/ij/). Confocal laser scanning microscopy FRET acquisitions were performed using a Nikon Eclipse Ti2 microscope, equipped with a Nikon A1R+ laser scanning device (Nikon, http://www.nikon.com/products/microscope-solutions/lineup/confocal/a1/index.htm). Cameleon was excited with a 445 nm diode laser. CFP and cpVenus emissions were collected at 460-500 nm and 520-550 nm, respectively.

IV.19. Light Sheet Fluorescence Microscopy for FRET measurements

Light Sheet Fluorescence Microscopy used in this work consist of a home-made built system equipped with two objectives, one for excitation and one for acquisition, which stand into an imaging chamber where the sample is placed. The specimen is illuminated with a static light sheet (2.6µm thin) provided by a laser for CFP excitation (452nm). A 20X water immersion objective placed orthogonally to the excitation axis was used for detection. A white LED illuminator allowed focusing the sample without exciting it. The detection path is splitted into two spectral channels with a dichroic filter at 505nm and two band-pass filters of 480nm and 535nm for CFP and cpVenus detection, respectively. The dection of the two channels was allowed by a sCMOS Camera (Andor Neo 5.5, http://www.andor.com). The software used to control the instrument was Labview (home-made).

IV.20. Sample preparation for Light Sheet Fluorescence Microscopy (LSFM) acquisitions

The samples consist of 5- to 7-day-old transgenic Arabidopsis seedlings expressing the cytosolic localized Cameleon YC3.6 (NES-YC3.6) (Nagai *et al.*, 2004; Krebs *et al.*, 2012). Seeds were surface sterilized by vapor-phase sterilization (see Plant material) and placed, with a toothpick, in plate filled with half strength Murashige and Skoog medium (Murashige and Skoog, 1962) (MS, including Vitamins, Duchefa) supplemented with 0.1% (w/v) sucrose, 2.34mM MES with a final pH of the media to 5.8 with 0.5M KOH and solidified with 0.8% (w/v) of plant agar (Duchefa, The Netherlands). Seeds were stratified at 4°C for 48h and transferred to the growth chamber (see Plant material) in a horizontal position for 36h for seeds germination. After having checked for seed's germination and fluorescence, seeds were transferred to the top of the LSFM tubes. These consist of a 3cm long Fluorinated Ethylene Propylenle (FEP) tubes assembled with 10µl pipette tip. FEP tubes, before sterilization, were washed with NaOH (1M and 0.5M) and 70% Ethanol (v/v) and rinsed 5 times with distilled water (Romano-Armada, 2019). FEP tubes were filled with half strength MS medium gelified with 0.5% Phytagel™ (Sigma) (w/v) and sealed at the top with a plug of half strength MS plant agar 0.8% (w/v) to prevent evaporation of Phytagel-gelified media. FEP tubes were then transferred to a transparent plastic box filled with sterile half strength MS solution for hydroponic culture (no sucrose)

and placed in a growth chamber under 16/8 h cycles of white light at 22°C. The hydroponic system allows the seedling roots to grow, following the positive gravitropism, first into the MS gelified medium and subsequently directly in hydroponic solution (Fig. 2). Once the root comes out the hole of the tube (800µm *circa* for amino acids treatment), the specimen is transferred to the LSFM-FRET setup into the imaging chamber filled with the desired solution. For the amino acid-induced Ca^{2+} elevation analyses a 10mM MES, 5mM KCl, 10mM $CaCl_2$, adjusted to pH 5.8 with Tris-Base solution was employed. Amino acids were dissolved in the same imaging solution and added by gently pipetting. This procedure prevents any kind of damages or major stress to the root and maintains the seedling in a vertical position. Indeed, the LSFM guarantees a high spatial and temporal resolution and thanks to a dedicated specimen mounting protocol allows the Arabidopsis seedlings to be kept in an upright position, in controlled, close-to physiological conditions throughout the entire analysis (Costa *et al.*, 2013; Candeo *et al.*, 2017).

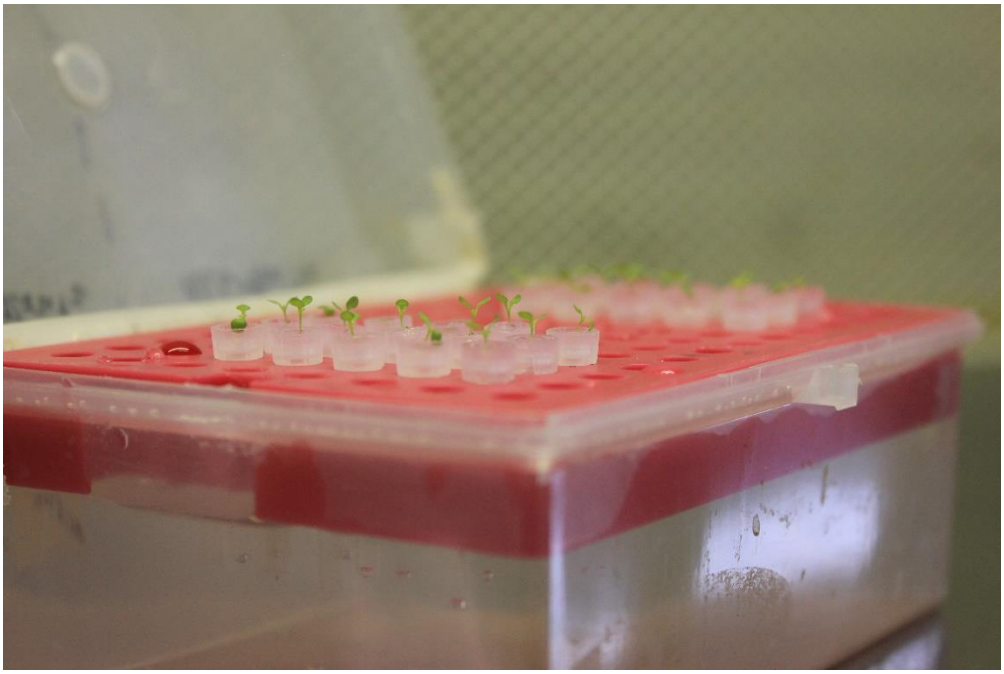

Fig. 2. Hydroponic system used for Light Sheet Fluorescence Microscopy sample preparation (Romano-Armada *et al.*, 2019).

IV.21. FRET-FLIM analysis

Tobacco transformed leaves expressing the GLR3.3-eGFP alone or together with GLR3.7-mCherry were used for frequency-domain FLIM measurements. FLIM analysis was performed by means of a Nikon Eclipse Ti2 microscope laser scanning confocal imaging system equipped with a single-photon counting device which allowed picosecond time resolution (PicoQuant, www.picoquant.com). eGFP

was excited with a 485 nm modulated diode laser (LDH Series Picosecond Pulsed Diode Laser Heads) and the corresponding emission was detected with a FLIM-compatible photomultiplier tube from 495 to 530 nm by time-correlated single-photon counting using a Picoharp 300 module (PicoQuant). Each time-correlated single-photon counting histogram was reconvoluted with a corresponding instrument response function and fitted against a monoexponential decay function to unravel the GFP fluorescence lifetime of each cell with SymPhoTime 64 software.

IV.22. Imaging solution

For root tip Ca^{2+} dynamic analyses a 10mM MES, 5mM KCl, 10mM $CaCl_2$, pH 5.8 adjusted with Tris-Base solution was employed and denoted as standard imaging solution (Gilroy, 1991; Bonza *et al.*, 2013; Costa *et al.*, 2013; Corso *et al.*, 2018; Storti *et al.*, 2018).

IV.23. Amino acids-induced cytosolic root tip Ca^{2+} transient measurements

For amino acid-induced cytosolic root tip Ca^{2+} transient measurements, the powder (Formedium) of each tested amino acid (L-Glutamate, L-Asparagine, L-Cysteine, L-Alanine, L-Serine, Glycine, L-Methionine) was dissolved in bi-distilled H_20 water to obtain a 100mM stock solution, and then diluted to the final 1mM concentration in standard imaging solution. In an imaging experiment, amino acid application was highly standardised in the following way: seedlings were placed in an open top chamber overlaid with a piece of cotton and allowed to recover for 5 minutes, by a continuous perfusion with imaging solution, before starting the images recording. Each specimen was then imaged for 2min before the amino acid treatment that was pulsed for three minutes and then removed. The specimens were then again continuously supefused with the imaging solution and the images acquisition continued for other 5min (total 10min per experiment). For each amino acid treatment, at least 5 independent experiments were performed for each genotype.

Regarding control experiments, spatio-temporal dynamics of the cytosolic Ca^{2+} concentration rise were analyzed treating seedlings with external ATP (eATP) and NAA. The final concentration for eATP was 0.1mM. The stock ATP solution was diluted in a Tris buffer (pH 7.4) in order to prevent any pH change of the imaging solution. ATP was used as magnesium salt. At least 4 measurements were performed per genotype. NAA stock solution (10.74mM) was diluted up to 10µM final concentration.

IV.24. Time-course data analyses

Cytosolic Ca^{2+} concentration reported by the ratiometric FRET sensor NES-YC3.6 was evaluated as following. A small region of interest (ROI) identified on tissues of interest (root meristematic zone,

stem, node, abscission zone and sepals) was used to calculate the ratio between cpVenus and CFP emissions (see Fig. 1A, for ROIs). Background was subtracted from cpVenus and CFP fluorescences before ratio calculation, evaluated on a ROI drawn outside the sample of interest. FRET Ratio calculation was perfomed using the Open Source Fiji software (https://fiji.sc/). FRET ratio is calculated as (cpVenus- cpVenus background)/(CFP-CFP background). The higher the FRET efficiency (higher ratio), the higher the increase in cytosolic Ca^{2+} concentration. Ratio was then normalized to the pre-stimulus ratio value (R_0; $\Delta R/R_0$) and plotted versus time. Per each set of experiments (e.g. different genotypes and/or treatment), the highest normalized ratio values were averaged and plotted as histograms $\Delta R_{max}/R_0 \pm SD$.

Ca^{2+} analysis on 4D measurements (*x, y, z, t*) acquired by LSFM was calculated as following. By means of the Fiji software, z stacks were opened as virtual stacks (cpVenus and CFP emissions) and properties edited according to the measurement (for instance, Fig. 2B pixel width 0.367, voxel depth 3µm, frame interval 5s). Stacks images were then converted to hyperstack and halved in size. For both emissions (cpVenus and CFP) background was subtracted before ratio calculation that was performed after the two emissions were split. The ratio was then converted from 32bit to 16bit and the 'Fire' false color from Look Up Table (LUT) menu was used for FRET increase representation. Lastly, cpVenus and Ratio channels were merged. A reslice of the merged image was performed for cross section analyses. Ratio values collected from ROIs were normalized to the pre-stimulus value (R_0¸($\Delta R/R_0$) and plotted versus time.

IV.25. Electrical signal and Ca^{2+} wave speed determination

For electrical signal speed rate detection upon stem burning, an indirect calculation was performed. We monitored the window of time spent from the fire application to the stem until the appeareance of the change in the FRET ratio in the abscission zone. This value was subsequently divided by the distance between the local damage site and the abscission zone. Results were reported as the average speed propagation rate ±SD.

For the speed of Ca^{2+} signal propagation upon stem burning through both the sepals and stem (back and forward), two different ROIs were drawn mapping on the abscission zone and on the stem/sepal. The occurance of the first change in the FRET ratio in both ROIs was monitored and calculated the delay occurring in the two events. Afterwards, this time window was divided over the distance between ROI1 and ROI2. Results were reported as the average speed propagation rate ±SD.

2188

Chapter V: Supplementary Materials

Pre-AAs treament	Resting cpVenus/CFP ratio ΔR									
Col-0	*glr3.3-1*	*glr3.3-2*	Col-0 (1)	*glr3.7-1*	Col-0 (2)	*glr3.7-2*	C24	*glr3.7-3*	Col-0 (3)	*glr3.3glr3.7*
3.126 ±0.106	3.06 ±0.13	3.086 ±0.146	2.964 ±0.157	3.17 ±0.147	3.136 ±0.105	2.96 ±0.148	2.625 ±0.125	2.678 ±0.076	2.629 ±0.085	2.64 ±0.065

Table 1. Resting level of cpVenus/CFP ratio monitored in different lines before amino acids treatment. Values are the average of 50s-time window before treatment application and are reported as average±SD. *n*>5

A

		$\Delta R_{max}/R_0$		
concentration	stimulus	Col-0	*glr3.3-1*	*glr3.3-2*
1mM	L-Cysteine	0.374 ±0.082	0.013 ±0.009	0.005 ±0.002
1mM	L-Glutamate	0.309 ±0.072	0.011 ±0.006	0.01 ±0.005
1mM	L-Alanine	0.307 ±0.07	0.005 ±0.002	0.005 ±0.002
1mM	Glycine	0.262 ±0.035	0.008 ±0.01	0.01 ±0.008
1mM	L-Serine	0.143 ±0.028	0.006 ±0.005	0.007 ±0.005
1mM	L-Asparagine	0.115 ±0.029	0.009 ±0.005	0.007 ±0.004
1mM	L-Methionine	0.017 ±0.011	0.003 ±0.0007	0.002 ±0.001
1mM	L-Triptophan	0.006 ±0.004	N.A.	N.A.
1mM	D-Serine	0.003 ±0.002	N.A.	N.A.
10mM	D-Serine	0.006 ±0.005	N.A.	N.A.
0.1mM	eATP	0.747 ±0.09	0.82 ±0.22	0.67 ±0.13
10nM	NAA	N.A.	N.A.	N.A.

B

		$\Delta R_{max}/R_0$					
concentration	stimulus	Col-0 (1)	*glr3.7-1*	Col-0 (2)	*glr3.7-2*	C24	*glr3.7-3*
1mM	L-Cysteine	0.243 ±0.08	0.515 ±0.066	N.A.	N.A.	0.058 ±0.011	0.249 ±0.062
1mM	L-Glutamate	0.29 ±0.054	0.407 ±0.046	0.305 ±0.072	0.615 ±0.179	0.111 ±0.03	0.376 ±0.098
1mM	L-Alanine	0.194 ±0.057	0.273 ±0.047	N.A.	N.A.	N.A.	N.A.
1mM	Glycine	0.259 ±0.077	0.435 ±0.043	0.292 ±0.052	0.421 ±0.058	N.A.	N.A.
1mM	L-Serine	0.141 ±0.052	0.266 ±0.077	0.163 ±0.02	0.227 ±0.02	N.A.	N.A.
1mM	L-Asparagine	0.086 ±0.019	0.206 ±0.041	N.A.	N.A.	N.A.	N.A.
1mM	L-Methionine	0.004 ±0.002	0.039 ±0.009	0.029 ±0.01	0.104 ±0.029	N.A.	N.A.
0.1mM	eATP	0.697 ±0.126	0.628 ±0.099	0.76 ±0.1	0.772 ±0.17	0.496 ±0.053	0.404 ±0.039
10nM	NAA	0.129 ±0.005	0.118 ±0.018	N.A.	N.A.	N.A.	N.A.

C

		$\Delta R_{max}/R_0$	
concentration	stimulus	Col-0 (3)	*glr3.3glr3.7*
1mM	L-Cysteine	0.329 ±0.043	0.009 ±0.003
1mM	L-Glutamate	0.345 ±0.071	0.012 ±0.004
1mM	L-Alanine	N.A.	N.A.
1mM	Glycine	0.209 ±0.055	0.006 ±0.0008
1mM	L-Serine	N.A.	N.A.
1mM	L-Asparagine	N.A.	N.A.
1mM	L-Methionine	0.017 ±0.0001	0.006 ±0.001
0.1mM	eATP	0.74 ±0.06	0.732 ±0.034
10nM	NAA	N.A.	N.A.

Table 2. Maximal increase of the normalized ratio $\Delta R_{max}/R_0$ elicited by external amino acids administration, ATP, NAA in Col-0, C24, *glr3.3-1* and *glr3.3-2, glr3.7-1, glr3.7-2, glr3.7-3, glr3.3glr3.7*. Each amino acid was applied at 1mM final concentration, with the exception of D-Ser which was also tested at 10mM final concentration. ATP and NAA were applied at 100µM and 10µM final concentration, respectively. Root meristematic cells zone was analyzed as region of interest for amino acids, ATP and NAA treatment. Values are the average of >5 experiments per each treatment. Results are shown as average±SD.

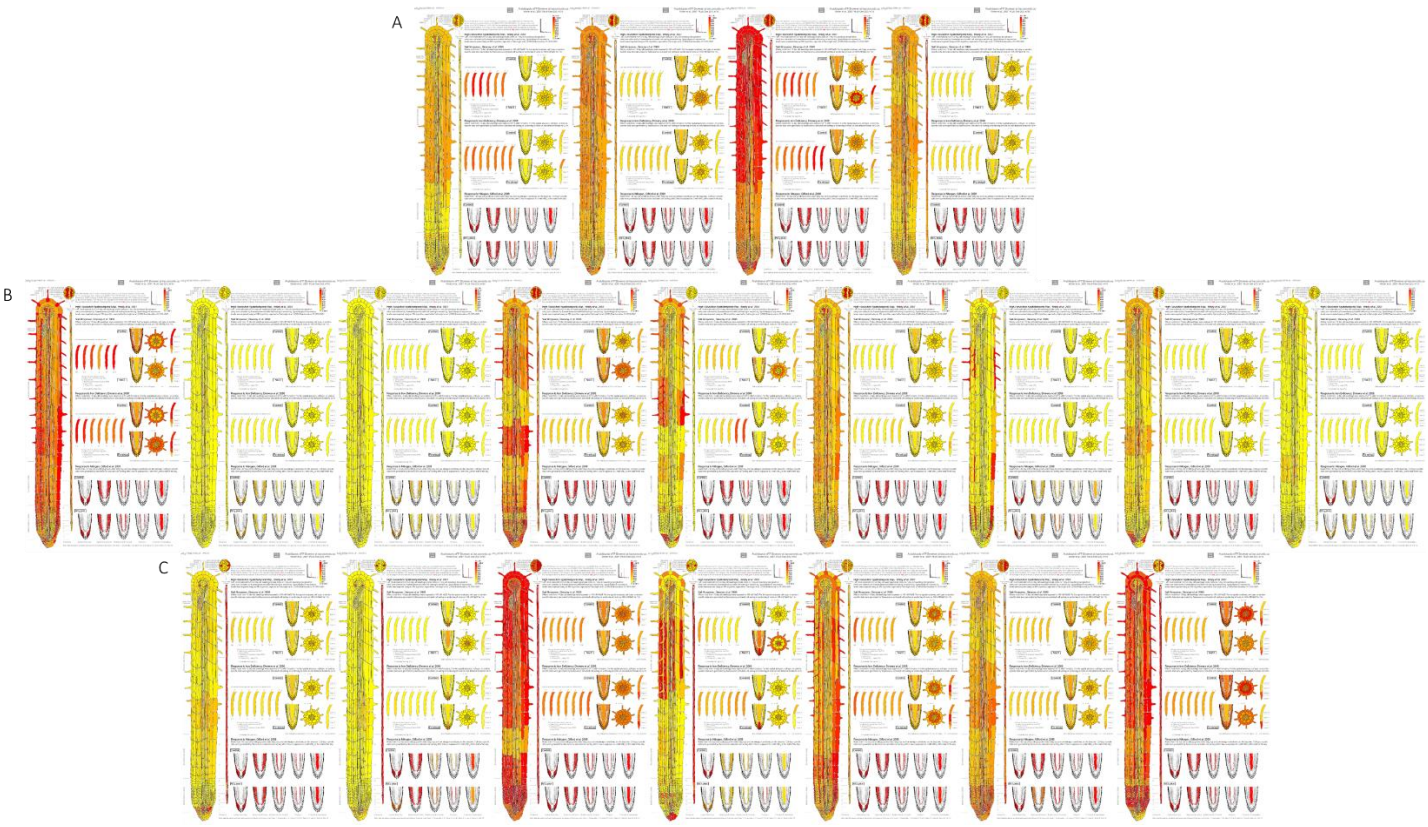

2202

2203 **Fig. 1 GLRs expression in root of *Arabidopsis thaliana*. A.** Clade I (from AtGLR1.1 to AtGLR1.4) **B.** Clade
2204 II (from GLR2.1 to AtGLR2.9). **C.** Clade III (from AtGLR3.1 to AtGLR3.7). Data isolated from eFP
2205 browser. Values are reported as absolute expression with a threshold set at 100.

2206

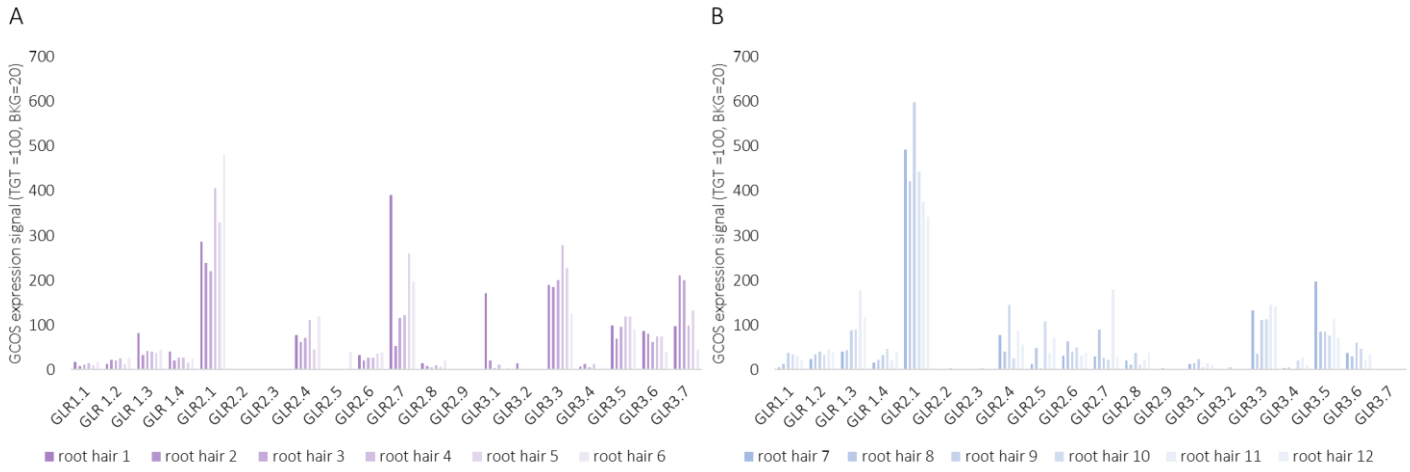

2207

2208 **Fig. 2. GLRs expression in root hairs of *Arabidopsis thaliana* A.** Absolute expression of GLRs in young
2209 root hairs (root hair 1 younger than root hair 6) from 6-7-day-old seedlings. Values were collected
2210 from eFP browser (Dinneny *et al.*, 2007; Winter *et al.*, 2007). *n*>2, reported as Gene-Chip Operating
2211 Signal expression signal (target intensity TGT=100 and background BKG=20). **B.** Absolute expression

of GLRs in old root hairs from 6-7-day-old seedlings (root hair 7 younger than root hair 12). Values were collected from eFP browser(Dinneny *et al.*, 2007; Winter *et al.*, 2007). *n*>2, reported as Gene-Chip Operating Signal expression signal (target intensity TGT=100 and background BKG=20).

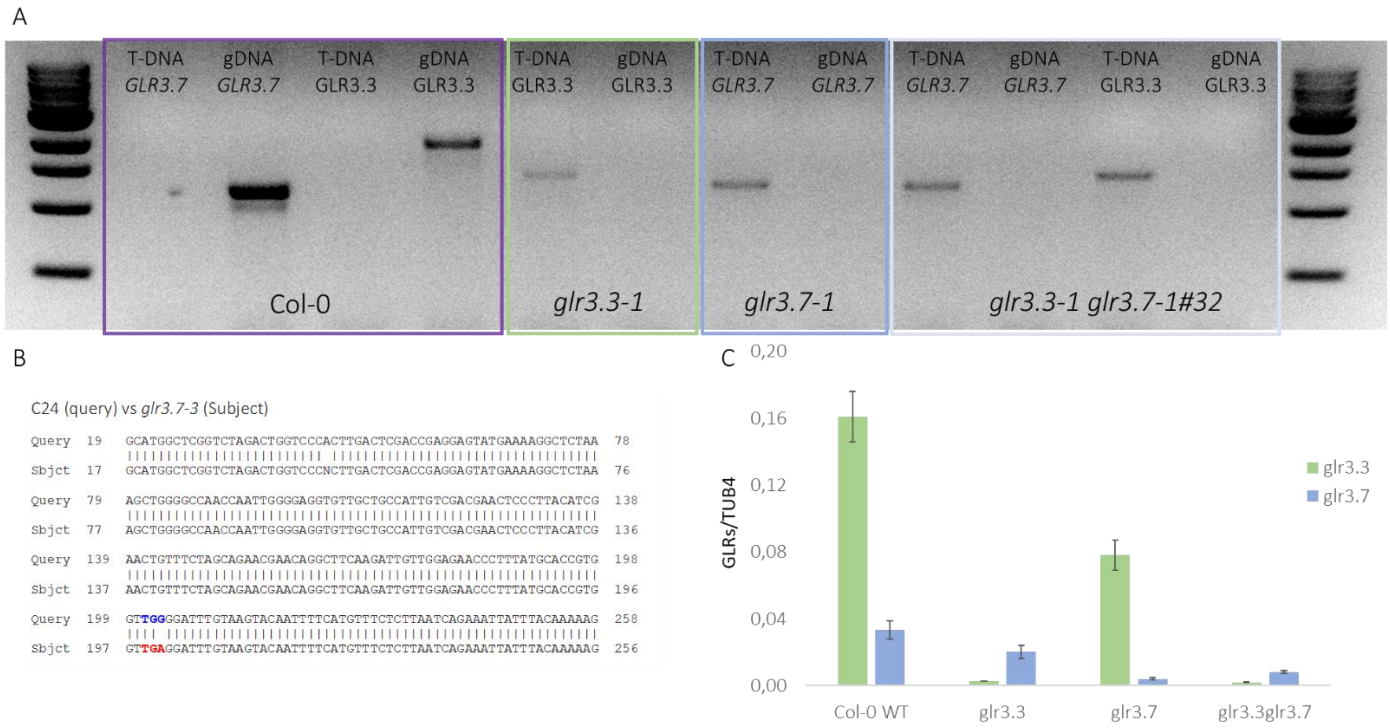

Fig. 3. GLRs expression level.

A. Electrophoresis gel showing PCR results using as template gDNA isolated from Col-0, *null-allele* lines *glr3.3-1* and *glr3.7-1* and double knock-out *glr3.3-1glr3.7-1* line#32. Col-0 expressed wild-type form of the genes, whereas *null-allele* lines resulted homozygote for the T-DNA insertions. **B.** Genomic DNA sequencing of the *nonsense* mutation in the *glr3.7-3*. Codon TGG encoding for Trp765 (2295bp) in C24 (blue) was reverted in a premature stop codon (TGA) in *glr3.7-3* (red) **C.** Relative expression (GLRs/TUB4) of GLRs in Col-0, *glr3.3-1*, *glr3.7-1* and *glr3.3-1glr3.7-1 #32* using as template cDNA isolated from RNA retro-transcribed from the above-mentioned 7-day old seedlings.

Chapter VI: References

Albertazzi, L. *et al.* (2009) 'Quantitative FRET analysis with the E0GFP-mCherry fluorescent protein pair', *Photochemistry and Photobiology*, 85(1), pp. 287–297. doi: 10.1111/j.1751-1097.2008.00435.x.

Alexandre, J. and Lassalles, J. P. (1990) 'Effect of d-myo-Inositol 1,4,5-Trisphosphate on the Electrical Properties of the Red Beet Vacuole Membrane.', *Plant physiology*, 93(2), pp. 837–40. doi: 10.1104/PP.93.2.837.

Ali, R. *et al.* (2007) 'Death Don't Have No Mercy and Neither Does Calcium: Arabidopsis CYCLIC NUCLEOTIDE GATED CHANNEL2 and Innate Immunity', *the Plant Cell Online*, 19(3), pp. 1081–1095. doi: 10.1105/tpc.106.045096.

Baughman, J. M. *et al.* (2011) 'Integrative genomics identifies MCU as an essential component of the mitochondrial calcium uniporter', *Nature*. Nature Publishing Group, 476(7360), pp. 341–345. doi: 10.1038/nature10234.

Behera, S. *et al.* (2015) 'Analyses of Ca^{2+} dynamics using a ubiquitin-10 promoter-driven Yellow Cameleon 3.6 indicator reveal reliable transgene expression and differences in cytoplasmic Ca^{2+}responses in Arabidopsis and rice (Oryza sativa) roots', *New Phytologist*, 206(2), pp. 751–760. doi: 10.1111/nph.13250.

Behera, S. *et al.* (no date) 'Cellular Ca^{2+} signals generate defined pH signatures in plants'.

Bonza, M. C. *et al.* (2013) 'Analyses of Ca^{2+} Accumulation and Dynamics in the Endoplasmic Reticulum of Arabidopsis Root Cells Using a Genetically Encoded Cameleon Sensor', *Plant Physiology*, 163(3), pp. 1230–1241. doi: 10.1104/pp.113.226050.

De Bortoli, S. *et al.* (2016) 'Evolutionary insight into the ionotropic glutamate receptor superfamily of photosynthetic organisms', *Biophysical Chemistry*. Elsevier B.V., 218, pp. 14–26. doi: 10.1016/j.bpc.2016.07.004.

Bose, J. *et al.* (2011) 'Calcium Efflux Systems in Stress Signaling and Adaptation in Plants', *Frontiers in Plant Science*, 2(December), pp. 1–17. doi: 10.3389/fpls.2011.00085.

Boursiac, Y. *et al.* (2010) 'Disruption of the Vacuolar Calcium-ATPases in Arabidopsis Results in the Activation of a Salicylic Acid-Dependent Programmed Cell Death Pathway', *Plant Physiology*, 154(3),

pp. 1158–1171. doi: 10.1104/pp.110.159038.

Brandizzi, F., Fricker, M. and Hawes, C. (2002) 'A greener world: The revolution in plant bioimaging', *Nature Reviews Molecular Cell Biology*, 3(7), pp. 520–530. doi: 10.1038/nrm861.

Candeo, A. *et al.* (2017) 'Light Sheet Fluorescence Microscopy Quantifies Calcium Oscillations in Root Hairs of Arabidopsis thaliana', *Plant and Cell Physiology*, 58(7), pp. 1161–1172. doi: 10.1093/pcp/pcx045.

Carpaneto, A. and Gradogna, A. (2018) 'Modulation of calcium and potassium permeation in plant TPC channels', *Biophysical Chemistry*. Elsevier, 236(March), pp. 1–7. doi: 10.1016/j.bpc.2018.02.006

Charpentier, M. (2018) 'Calcium signals in the plant nucleus: origin and function', *Journal of Experimental Botany*, 69(17), pp. 4165–4173. doi: 10.1093/jxb/ery160.

Charpentier, M. *et al.* (2016) 'FRET-based genetically encoded sensors allow high-resolution live cell imaging of Ca^{2+} dynamics', *Plant Journal*. Elsevier Ltd, 8(1), pp. 181–192. doi: 10.1126/science.aae0109.

Chen, B. and Roche, K. W. (2010) 'Receptors Via Protein Kinase B / Akt Phosphorylation of NR2C', 62(4), pp. 471–478. doi: 10.1016/j.neuron.2009.04.015.Growth.

Chen, D. *et al.* (2017) 'Extracellular ATP elicits DORN1-mediated RBOHD phosphorylation to regulate stomatal aperture', *Nature Communications*. Springer US, 8(1). doi: 10.1038/s41467-017-02340-3.

Chiu, J. *et al.* (1999) 'Molecular evolution of glutamate receptors: A primitive signaling mechanism that existed before plants and animals diverged', *Molecular Biology and Evolution*, 16(6), pp. 826–838. doi: 10.1093/oxfordjournals.molbev.a026167.

Cho, D. *et al.* (2009) 'De-regulated expression of the plant glutamate receptor homolog AtGLR3.1 impairs long-term Ca^{2+}-programmed stomatal closure', *Plant Journal*, 58(3), pp. 437–449. doi: 10.1111/j.1365-313X.2009.03789.x.

Cho, D. *et al.* (2012) 'Vacuolar CAX1 and CAX3 Influence Auxin Transport in Guard Cells via Regulation of Apoplastic pH', *Plant Physiology*, 160(3), pp. 1293–1302. doi: 10.1104/pp.112.201442.

Choi, W.-G. *et al.* (2014) 'Salt stress-induced Ca^{2+} waves are associated with rapid, long-distance root-to-shoot signaling in plants', *Proceedings of the National Academy of Sciences*, 111(17), pp.

6497–6502. doi: 10.1073/pnas.1319955111.

Choi, W. G. *et al.* (2017) 'Orchestrating rapid long-distance signaling in plants with Ca^{2+}+, ROS and electrical signals', *Plant Journal*, 90(4), pp. 698–707. doi: 10.1111/tpj.13492.

Chung, C., Wu, W. H. and Chen, B. S. (2015) 'Identification of novel 14-3-3 residues that are critical for isoform-specific interaction with GluN2C to regulate N-methyl-D-aspartate (NMDA) receptor trafficking', *Journal of Biological Chemistry*, 290(38), pp. 23188–23200. doi: 10.1074/jbc.M115.648436.

Clough, S. J. and Bent, A. F. (1998) 'Floral dip: A simplified method for Agrobacterium-mediated transformation of *Arabidopsis thaliana*.', *Plant Journal*, 16(6), pp. 735–743. doi: 10.1046/j.1365-313X.1998.00343.x.

Corso, M. *et al.* (2018a) 'Endoplasmic reticulum-localized CCX2 is required for osmotolerance by regulating ER and cytosolic Ca $^{2+}$ dynamics in *Arabidopsis*', *Proceedings of the National Academy of Sciences*, 115(15), pp. 3966–3971. doi: 10.1073/pnas.1720422115.

Corso, M. *et al.* (2018b) 'Endoplasmic reticulum-localized CCX2 is required for osmotolerance by regulating ER and cytosolic Ca^{2+} dynamics in *Arabidopsis*', *Proceedings of the National Academy of Sciences*, 115(15), pp. 3966–3971. doi: 10.1073/pnas.1720422115.

Costa, A. *et al.* (2010) 'H_2O_2 in plant peroxisomes: An in vivo analysis uncovers a Ca^{2+}-dependent scavenging system', *Plant Journal*, 62(5), pp. 760–772. doi: 10.1111/j.1365-313X.2010.04190.x.

Costa, A. *et al.* (2013) 'Calcium Dynamics in Root Cells of Arabidopsis thaliana Visualized with Selective Plane Illumination Microscopy', *PLoS ONE*, 8(10). doi: 10.1371/journal.pone.0075646.

Costa, A. *et al.* (2017) 'Ca^{2+}-dependent phosphoregulation of the plasma membrane Ca^{2+}+-ATPase ACA8 modulates stimulus-induced calcium signatures', *Journal of Experimental Botany*, 68(12), pp. 3215–3230. doi: 10.1093/jxb/erx162.

Costa, A. and Kudla, J. (2015) 'Colorful insights: Advances in imaging drive novel breakthroughs in Ca^{2+} signaling', *Molecular Plant*, 8(3), pp. 352–355. doi: 10.1016/j.molp.2014.11.020.

Costa, A., Navazio, L. and Szabo, I. (2018) 'The contribution of organelles to plant intracellular calcium signalling', *Journal of Experimental Botany*, 69(17), pp. 4175–4193. doi: 10.1093/jxb/ery185.

Cucu, B. *et al.* (2017) 'Vesicle fusion and fission in plants and yeast', *Cell Calcium*, 67(August), pp. 40–45. doi: 10.1016/j.ceca.2017.08.007.

Davies, J. (2014) 'Annexin-Mediated Calcium Signalling in Plants', *Plants*, 3(1), pp. 128–140. doi: 10.3390/plants3010128.

DeFalco, T. A., Bender, K. W. and Snedden, W. A. (2010) 'Breaking the code: Ca^{2+} sensors in plant signalling', *Biochemical Journal*, 425(1), pp. 27–40. doi: 10.1042/BJ20091147.

DeFalco, T. A., Moeder, W. and Yoshioka, K. (2016) 'Opening the Gates: Insights into Cyclic Nucleotide-Gated Channel-Mediated Signaling', *Trends in Plant Science*. Elsevier Ltd, 21(11), pp. 903–906. doi: 10.1016/j.tplants.2016.08.011.

Demidchik, V. *et al.* (2003) 'Is ATP a Signaling Agent in Plants?', *Plant Physiology*, 133(2), pp. 456–461. doi: 10.1104/pp.103.024091.

Dennison, K. L. and Spalding, E. P. (2000) 'Glutamate-Gated Calcium Fluxes in Arabidopsis', *Plant Physiology*, 124(4), pp. 1511–1514. doi: 10.1104/pp.124.4.1511.

Dinneny, J. R. *et al.* (2007) 'Dominant Expression Patterns', *Cell*, (24), pp. 801–806.

Dodd, A. N., Kudla, J. and Sanders, D. (2010) 'The Language of Calcium Signaling', *Annual Review of Plant Biology*, 61(1), pp. 593–620. doi: 10.1146/annurev-arplant-070109-104628.

Drago, I. *et al.* (2008) 'Calcium dynamics in the peroxisomal lumen of living cells', *Journal of Biological Chemistry*, 283(21), pp. 14384–14390. doi: 10.1074/jbc.M800600200.

Dubos, C. *et al.* (2003) 'A role for glycine in the gating of plant NMDA-like receptors', pp. 800–810. doi: 10.1046/j.1365-313X.2003.01849.x.

Dziubinska, H. *et al.* (2003) 'Variation and action potentials evoked by thermal stimuli accompany enhancement of ethylene emission in distant non-stimulated leaves of *Vicia faba* minor seedlings', *Journal of Plant Physiology*, 160(10), pp. 1203–1210. doi: 10.1078/0176-1617-00914.

Dziubińska, H., Trębacz, K. and Zawadzki, T. (2001) 'Transmission route for action potentials and variation potentials in *Helianthus annuus L.*', *Journal of Plant Physiology*, 158(9), pp. 1167–1172. doi: 10.1078/S0176-1617(04)70143-1.

Edel, K. H. *et al.* (2017) 'The Evolution of Calcium-Based Signalling in Plants', *Current Biology*, 27(13), pp. R667–R679. doi: 10.1016/j.cub.2017.05.020.

2337 Evans, M. J. *et al.* (2016) 'A ROS-Assisted Calcium Wave Dependent on the AtRBOHD NADPH
2338 Oxidase and TPC1 Cation Channel Propagates the Systemic Response to Salt Stress', *Plant*
2339 *Physiology*, 171(3), pp. 1771–1784. doi: 10.1104/pp.16.00215.

2340 Evans, M. J. and Morris, R. J. (2017) 'Chemical agents transported by xylem mass flow propagate
2341 variation potentials', *Plant Journal*, 91(6), pp. 1029–1037. doi: 10.1111/tpj.13624.

2342 Evans, N. H., McAinsh, M. R. and Hetherington, A. M. (2001) 'Calcium oscillations in higher plants',
2343 *Curr. Opin. Plant Biol.*, 4(5), pp. 415–420. doi: 10.1016/S1369-5266(00)00194-1.

2344 Feijó, J. A. and Wudick, M. M. (2018) 'Calcium is life', *Journal of Experimental Botany*, 69(17), pp.
2345 4147–4150. doi: 10.1093/jxb/ery279.

2346 Felle, H. H. and Zimmermann, M. R. (2007) 'Systemic signalling in barley through action potentials',
2347 *Planta*, 226(1), pp. 203–214. doi: 10.1007/s00425-006-0458-y.

2348 Felle, H. (1989) 'Ca^{2+} -Selective Microelectrodes and Their Application to Plant Cells and Tissues ',
2349 *Plant Physiology*, pp. 1239–1242.

2350 Ferro, M. *et al.* (2010) 'AT_CHLORO, a Comprehensive Chloroplast Proteome Database with
2351 Subplastidial Localization and Curated Information on Envelope Proteins', *Molecular & Cellular*
2352 *Proteomics*, 9(6), pp. 1063–1084. doi: 10.1074/mcp.M900325-MCP200.

2353 Filek, M. and Kościelniak, J. (1997) 'The effect of wounding the roots by high temperature on the
2354 respiration rate of the shoot and propagation of electric signal in horse bean seedlings (*Vicia faba L.*
2355 *minor*)', *Plant Science*, 123(1–2), pp. 39–46..

2356 Fisahn, J. *et al.* (2004) 'Analysis of the Transient Increase in Cytosolic Ca^{2+} during the Action
2357 Potential of Higher Plants with High Temporal Resolution: Requirement of Ca^{2+} Transients for
2358 Induction of Jasmonic Acid Biosynthesis and PINII Gene Expression', *Plant Physiology*, 45(4), pp.
2359 456–459.

2360 Julien, J. and Frachisse, M. (1992) 'Involvement of the proton pump and proton conductance
2361 change in the wave of depolarization induced by wounding in *Bidens pilosa*' Can. J. Bot.

2362 Frank, J. *et al.* (2018) 'Chloroplast-localized BICAT proteins shape stromal calcium signals and are
2363 required for efficient photosynthesis', *New Phytologist*. doi: 10.1111/nph.15407.

2364 Frei dit Frey, N. *et al.* (2012) 'Plasma Membrane Calcium ATPases Are Important Components of

2365 Receptor-Mediated Signaling in Plant Immune Responses and Development', *Plant Physiology*,
2366 159(2), pp. 798–809. doi: 10.1104/pp.111.192575.

2367 Fromm, J. and Bauer, T. (1994) 'Action potentials in maize sieve tubes change phloem
2368 translocation', *Journal of Experimental Botany*, 45(273), pp. 463–469. doi: 10.1093/jxb/45.4.463.

2369 Fu, Y.-L. *et al.* (2013) 'Arabidopsis Histone Methylase CAU1/PRMT5/SKB1 Acts as an Epigenetic
2370 Suppressor of the Calcium Signaling Gene CAS to Mediate Stomatal Closure in Response to
2371 Extracellular Calcium', *The Plant Cell*, 25(8), pp. 2878–2891. doi: 10.1105/tpc.113.113886.

2372 Gao, D. *et al.* (2004) 'Self-reporting Arabidopsis expressing pH and [Ca^{2+}] indicators unveil ion
2373 dynamics in the cytoplasm and in the apoplast under abiotic stress', *Plant Physiol.*, 134(3), pp. 898–
2374 908. doi: 10.1104/pp.103.032508.

2375 Geisler, M. *et al.* (2000) 'Molecular aspects of higher plant P-type Ca^{2+}+-ATPases', *Biochimica et*
2376 *Biophysica Acta - Biomembranes*, 1465(1–2), pp. 52–78. doi: 10.1016/S0005-2736(00)00131-0.

2377 Gilroy, S. (1991) 'Role of Calcium in Signal Transduction of Commelina Guard Cells', *the Plant Cell*
2378 *Online*, 3(4), pp. 333–344. doi: 10.1105/tpc.3.4.333.

2379 Gilroy, S. *et al.* (2016) 'ROS, Calcium, and Electric Signals: Key Mediators of Rapid Systemic Signaling
2380 in Plants', *Plant Physiology*. Rice, 171(3), pp. 1606–1615. doi: 10.1104/pp.16.00434.

2381 Grams, T. E. E. *et al.* (2009) 'Heat-induced electrical signals affect cytoplasmic and apoplastic pH as
2382 well as photosynthesis during propagation through the maize leaf', *Plant, Cell and Environment*,
2383 32(4), pp. 319–326. doi: 10.1111/j.1365-3040.2008.01922.x.

2384 Guo, J. *et al.* (2016) 'Structure of the voltage-gated two-pore channel TPC1 from Arabidopsis
2385 thaliana', *Nature*. Nature Publishing Group, 531(7593), pp. 196–201. doi: 10.1038/nature16446.

2386 Hamilton, E. S., Schlegel, A. M. and Haswell, E. S. (2015) 'United in Diversity: Mechanosensitive Ion
2387 Channels in Plants', *Annual Review of Plant Biology*, 66(1), pp. 113–137. doi: 10.1146/annurev-
2388 arplant-043014-114700.

2389 Haswell, E. S. and Meyerowitz, E. M. (2006) 'MscS-like proteins control plastid size and shape in
2390 Arabidopsis thaliana', *Current Biology*, 16(1), pp. 1–11. doi: 10.1016/j.cub.2005.11.044.

2391 He, X.-Y. *et al.* (2016) 'GluA1 signal peptide determines the spatial assembly of heteromeric AMPA
2392 receptors', *Proceedings of the National Academy of Sciences*, 113(38), pp. E5645–E5654. doi:

10.1073/pnas.1524358113.

Hedrich, R. *et al.* (2018) 'Structure and Function of TPC1 Vacuole SV Channel Gains Shape', *Molecular Plant*. pp. 764–775. doi: 10.1016/j.molp.2018.03.017.

Hochmal, A. Karin. *et al.* (2015) 'Calcium-dependent regulation of photosynthesis', *Biochimica et biophysica acta*. Elsevier B.V., 1847(9), pp. 993–1003. doi: 10.1016/j.bbabio.2015.02.010.

Horie, T. *et al.* (2007) 'Rice OsHKT2;1 transporter mediates large Na+influx component into K+-starved roots for growth', *EMBO Journal*, 26(12), pp. 3003–3014. doi: 10.1038/sj.emboj.7601732.

Horie, T. *et al.* (2011) 'K^+ Transport by the OsHKT2;4 Transporter from Rice with Atypical Na+ Transport Properties and Competition in Permeation of K^+ over Mg^{2+} and Ca^{2+} Ions', *Plant Physiology*, 156(3), pp. 1493–1507. doi: 10.1104/pp.110.168047.

Huang, L. (1994) 'Correction: Characterization of a Gene Encoding a Ca^{2+}-ATPase-Like Protein in the Plastid Envelope', *Proceedings of the National Academy of Sciences*, 91(20), p. 9664c–9664. doi: 10.1073/pnas.91.20.9664c.

Iwano, M. *et al.* (2009) 'Fine-Tuning of the Cytoplasmic Ca^{2+} Concentration Is Essential for Pollen Tube Growth', *Plant Physiology*, 150(3), pp. 1322–1334. doi: 10.1104/pp.109.139329.

Iwano, M. *et al.* (2015a) 'Calcium signalling mediates self-incompatibility response in the Brassicaceae', *Nature Plants*. Nature Publishing Group, 1(9), pp. 1–8. doi: 10.1038/nplants.2015.128.

Iwano, M. *et al.* (2015b) 'Calcium signalling mediates self-incompatibility response in the Brassicaceae', *Nature Plants*, 1, pp. 1–20. doi: 10.1038/nplants.2015.128.

JC, C. *et al.* (2002) 'Phylogenetic and expression analysis of the glutamate-receptor-like gene family in Arabidopsis thaliana', 19 I : 7(September), pp. 1066–1082.

Jin, H. *et al.* (2009) 'A plant-specific calreticulin is a key retention factor for a defective brassinosteroid receptor in the endoplasmic reticulum.', *Proceedings of the National Academy of Sciences of the United States of America*, 106(32), pp. 13612–13617. doi: 10.1073/pnas.0906144106.

Kang, J., Mehta, S. and Turano, F. J. (2004) 'Regulates Abscisic Acid Biosynthesis and Signaling to Control Development and Water Loss', 45(10), pp. 1380–1389.

Kang, J. and Turano, F. J. (2003) 'The putative glutamate receptor 1.1 (AtGLR1.1) functions as a regulator of carbon and nitrogen metabolism in Arabidopsis thaliana', *Proceedings of the National Academy of Sciences*, 100(11), pp. 6872–6877. doi: 10.1073/pnas.1030961100.

Katicheva, L. *et al.* (2014) 'Ionic nature of burn-induced variation potential in wheat leaves', *Plant and Cell Physiology*, 55(8), pp. 1511–1519. doi: 10.1093/pcp/pcu082.

Keinath, N. F. *et al.* (2015) 'Live Cell Imaging with R-GECO1 Sheds Light on flg22- and Chitin-Induced Transient $[Ca^{2+}]_{cyt}$ Patterns in Arabidopsis', *Molecular Plant*, 8(8), pp. 1188–1200. doi: 10.1016/j.molp.2015.05.006.

Kelner, A. *et al.* (2018) 'Dual Color Sensors for Simultaneous Analysis of Calcium Signal Dynamics in the Nuclear and Cytoplasmic Compartments of Plant Cells', *Frontiers in Plant Science*, 9(February), pp. 1–14. doi: 10.3389/fpls.2018.00245.

Kiep, V. *et al.* (2015) 'Systemic cytosolic Ca^{2+} elevation is activated upon wounding and herbivory in Arabidopsis', *New Phytologist*, 207(4), pp. 996–1004. doi: 10.1111/nph.13493.

Klüsener, B. *et al.* (1995) 'Gadolinium-sensitive, voltage-dependent calcium release channels in the endoplasmic reticulum of a higher plant mechanoreceptor organ.', *The EMBO journal*, 14(12), pp. 2708–14.

Knight, H. (1996) 'Cold Calcium Signaling in Arabidopsis Involves Two Cellular Pools and a Change in Calcium Signature after Acclimation', *the Plant Cell Online*, 8(3), pp. 489–503. doi: 10.1105/tpc.8.3.489.

Knight, M. R. *et al.* (1991) 'Transgenic plant aequorin reports the effects of touch and cold-shock and elicitors on cytoplasmic calcium', *Nature*, pp. 524–526. doi: 10.1038/352524a0.

Kong, D. *et al.* (2015) 'Arabidopsis Glutamate Receptor Homolog3.5 Modulates Cytosolic Ca^{2+} Level to Counteract Effect of Abscisic Acid in Seed Germination', *Plant Physiology*, 167(4), pp. 1630–1642. doi: 10.1104/pp.114.251298.

Kong, D. *et al.* (2016) 'L-Met Activates Arabidopsis GLR Ca^{2+} Channels Upstream of ROS Production and Regulates Stomatal Movement', *Cell Reports*. ElsevierCompany., 17(10), pp. 2553–2561. doi: 10.1016/j.celrep.2016.11.015.

Krebs, M. *et al.* (2012) 'FRET-based genetically encoded sensors allow high-resolution live cell

imaging of Ca^{2+} dynamics', *Plant Journal*, 69(1), pp. 181–192. doi: 10.1111/j.1365-313X.2011.04780.x.

Krüger, F. and Schumacher, K. (2018) 'Pumping up the volume – vacuole biogenesis in *Arabidopsis thaliana*', *Seminars in Cell and Developmental Biology*. Elsevier Ltd, 80, pp. 106–112. doi: 10.1016/j.semcdb.2017.07.008.

Kudla, J. *et al.* (2018) 'Advances and current challenges in calcium signaling', *New Phytologist*, 218(2), pp. 414–431. doi: 10.1111/nph.14966.

Kwaaitaal, M. *et al.* (2011) 'Ionotropic glutamate receptor (iGluR)-like channels mediate MAMP-induced calcium influx in *Arabidopsis thaliana*', *Biochemical Journal*, 440(3), pp. 355–373. doi: 10.1042/BJ20111112.

Kwak, J. M., Nguyen, V. and Schroeder, J. I. (2006) 'The Role of Reactive Oxygen Species in Hormonal Responses', *Plant Physiology*, 141(June), pp. 323–329. doi: 10.1104/pp.106.079004.ROS.

Lam, H.-M. *et al.* (1998) 'Glutamate-receptor genes in plants.', *Nature*, 396(November), pp. 125–126. doi: 10.1038/24066.

Lamotte, O. *et al.* (2004) 'Analysis of nitric oxide signaling functions in tobacco cells challenged by the elicitor cryptogein.', *Plant physiology*, 135(1), pp. 516–29. doi: 10.1104/pp.104.038968.

Lee, S. M. *et al.* (2007) 'Identification of a calmodulin-regulated autoinhibited Ca^{2+}-ATPase (ACA11) that is localized to vacuole membranes in Arabidopsis', *FEBS Letters*, 581(21), pp. 3943–3949. doi: 10.1016/j.febslet.2007.07.023.

Lee, Y. *et al.* (2018) 'A Lignin Molecular Brace Controls Precision Processing of Cell Walls Critical for Surface Integrity in Arabidopsis', *Cell*. Elsevier Inc., 173(6), p. 1468–1480.e9. doi: 10.1016/j.cell.2018.03.060.

Lemtiri-Chlieh, F. *et al.* (2003) 'Inositol hexakisphosphate mobilizes an endomembrane store of calcium in guard cells', *Proceedings of the National Academy of Sciences*, 100(17), pp. 10091–10095. doi: 10.1073/pnas.1133289100.

Lenzoni, G., Liu, J. and Knight, M. R. (2018) 'Predicting plant immunity gene expression by identifying the decoding mechanism of calcium signatures', *New Phytologist*, 217(4), pp. 1598–1609. doi: 10.1111/nph.14924.

Li, F. *et al.* (2013) 'Glutamate Receptor-Like Channel3.3 Is Involved in Mediating Glutathione-Triggered Cytosolic Calcium Transients, Transcriptional Changes, and Innate Immunity Responses in Arabidopsis', *Plant Physiology*, 162(3), pp. 1497–1509. doi: 10.1104/pp.113.217208.

Li, J. *et al.* (2006) 'A rice glutamate receptor-like gene is critical for the division and survival of individual cells in the root apical meristem.', *The Plant cell*, 18(2), pp. 340–9. doi: 10.1105/tpc.105.037713.

Lichtenberg, H., Heyer, M. and Höfer, M. (1999) 'Tpr1, a Schizosaccharomyces pombe protein involved in potassium transport', *FEBS Letters*, 457(3), pp. 363–368. doi: 10.1016/S0014-5793(99)01068-6.

Loro, G. *et al.* (2012) 'Targeting of Cameleons to various subcellular compartments reveals a strict cytoplasmic/mitochondrial Ca^{2+} handling relationship in plant cells', *Plant Journal*, 71(1), pp. 1–13. doi: 10.1111/j.1365-313X.2012.04968.x.

Loro, G. *et al.* (2016) 'Chloroplast-specific in vivo Ca^{2+} imaging using Yellow Cameleon fluorescent protein sensors reveals organelle-autonomous Ca^{2+} signatures in the stroma', *Plant Physiology*, p. pp.00652.2016. doi: 10.1104/pp.16.00652.

Mahmood, T., Ashraf, M. and Shahbaz, M. (2009) 'Does exogenous application of glycinebetaine as a pre-sowing seed treatment improve growth and regulate some key physiological attributes in wheat plants grown under water deficit conditions?', *Pakistan Journal of Botany*, 41(3), pp. 1291–1302. doi: 10.1105/tpc.109.072769.

Malone, M. (1992) 'Kinetics of wound-induced hydraulic signals and variation potentials in wheat seedlings', *Planta*, 187(4), pp. 505–510. doi: 10.1007/BF00199969.

Malone, M. (1996) Rapid, Long-distance Signal Transmission in Higher Plants, *Advances in Botanical Research*. Elsevier Masson SAS. doi: 10.1016/S0065-2296(08)60058-0.

Malone, M. (1994) 'Wound-induced hydraulic signals and stimulus transmission in *Mimosa pudica* L', *New Phytologist*, 128(1), pp. 49–56. doi: 10.1111/j.1469-8137.1994.tb03985.x.

Mancuso, S. (1999) 'Hydraulic and electrical transmission of wound-induced signals in *Vitis vinifera*', *Australian Journal of Plant Physiology*, 26(1), pp. 55–61. doi: 10.1071/PP98098.

Manzoor, H. *et al.* (2013) 'Involvement of the glutamate receptor AtGLR3.3 in plant defense

2505 signaling and resistance to *Hyaloperonospora arabidopsidis*', *Plant Journal*, 76(3), pp. 466–480. doi:
2506 10.1111/tpj.12311.

2507 Marti, M. C., Stancombe, M. A. and Webb, A. A. R. (2013) 'Cell- and Stimulus Type-Specific
2508 Intracellular Free Ca^{2+} Signals in Arabidopsis', *Plant Physiology*, 163(2), pp. 625–634. doi:
2509 10.1104/pp.113.222901.

2510 Martinoia, E. *et al.* (2012) 'Vacuolar Transporters in Their Physiological Context', *Annual Review of*
2511 *Plant Biology*, 63(1), pp. 183–213. doi: 10.1146/annurev-arplant-042811-105608.

2512 Mazars, C. *et al.* (2010) 'Cross-talk between ROS and calcium in regulation of nuclear activities',
2513 *Molecular Plant*, 3(4), pp. 706–718. doi: 10.1093/mp/ssq024.

2514 McAinsh, M. R. and Pittman, J. K. (2009) 'Shaping the calcium signature', *New Phytologist*, 181(2),
2515 pp. 275–294. doi: 10.1111/j.1469-8137.2008.02682.x.

2516 Meyerhoff, O. *et al.* (2005) 'AtGLR3.4, a glutamate receptor channel-like gene is sensitive to touch
2517 and cold', *Planta*, 222(3), pp. 418–427. doi: 10.1007/s00425-005-1551-3.

2518 Michael M. Wudick, Erwan Michard, Custódio Oliveira Nunes, J. A. F. (2018b) 'Comparing plant and
2519 animal glutamate receptors: Common traits but different fates?', *Journal of Exp. Bot.*, pp. 1–13. doi:
2520 10.1038/pr.2015.58.

2521 Michard, E. *et al.* (2011) 'Glutamate Receptor – Like Genes Form Ca^{2+} Channels in Pollen Tubes and
2522 Are Regulated by Pistil', *Science*, 332, pp. 434–437. doi: 10.1126/science.1201101.

2523 Mills, R. F. *et al.* (2007) 'ECA3, a Golgi-Localized P2A-Type ATPase, Plays a Crucial Role in Manganese
2524 Nutrition in Arabidopsis', *Plant Physiology*, 146(1), pp. 116–128. doi: 10.1104/pp.107.110817.

2525 Mithöfer, A. and Mazars, C. (2002) 'Aequorin-based measurements of intracellular Ca^{2+}-signatures
2526 in plant cells', *Biological Procedures Online*, 4(1), pp. 105–118. doi: 10.1251/bpo40.

2527 Mittler, R. *et al.* (2011) 'ROS signaling: The new wave?', *Trends in Plant Science*. Elsevier Ltd, 16(6),
2528 pp. 300–309. doi: 10.1016/j.tplants.2011.03.007.

2529 Miyawaki, a *et al.* (1997) 'Fluorescent indicators for Ca^{2+} based on green fluorescent proteins and
2530 calmodulin.', *Nature*, 388(6645), pp. 882–887. doi: 10.1038/42264.

2531 Monshausen, G. B. (2012) 'Visualizing Ca^{2+} signatures in plants', *Current Opinion in Plant Biology*,
2532 15, pp. 677–682. doi: 10.1016/j.pbi.2012.09.014.

Mousavi, S. A. R. *et al.* (2013) 'GLUTAMATE RECEPTOR-LIKE genes mediate leaf-to-leaf wound signalling', *Nature*. Nature Publishing Group, 500(7463), pp. 422–426. doi: 10.1038/nature12478.

Mravec, J. *et al.* (2017) 'An oligogalacturonide-derived molecular probe demonstrates the dynamics of calcium-mediated pectin complexation in cell walls of tip-growing structures', *Plant Journal*, 91(3), pp. 534–546. doi: 10.1111/tpj.13574.

Murashige, T. and Skoog, F. (1962) 'A revised medium for rapid growth and bio assays with tobacco tissue culture', *Physiologia plantarum*.

Nagai, T. *et al.* (2004) 'Expanded dynamic range of fluorescent indicators for Ca^{2+} by circularly permuted yellow fluorescent proteins', *Proceedings of the National Academy of Sciences*, 101(29), pp. 10554–10559. doi: 10.1073/pnas.0400417101.

Navazio, L. *et al.* (2000) 'Calcium release from the endoplasmic reticulum of higher plants elicited by the NADP metabolite nicotinic acid adenine dinucleotide phosphate.', *Proceedings of the National Academy of Sciences of the United States of America*, 97(15), pp. 8693–8698. doi: 10.1073/pnas.140217897.

Navazio, L. (2001) 'Mobilization of Ca^{2+} by Cyclic ADP-Ribose from the Endoplasmic Reticulum of Cauliflower Florets', *Plant Physiology*, 125(4), pp. 2129–2138. doi: 10.1104/pp.125.4.2129.

Navazio, L. *et al.* (2002) 'Monitoring endoplasmic reticulum-to-Golgi traffic of a plant calreticulin by protein glycosylation analysis', *Biochemistry*, 41(48), pp. 14141–14149. doi: 10.1021/bi0204701.

Nguyen, C. T. *et al.* (2018) 'Identification of cell populations necessary for leaf-to-leaf electrical signaling in a wounded plant', *Proceedings of the National Academy of Sciences*, p. 201807049. doi: 10.1073/pnas.1807049115.

Ni, J. *et al.* (2016) 'Heterologous Expression and Functional Analysis of Rice GLUTAMATE RECEPTOR-LIKE Family Indicates its Role in Glutamate Triggered Calcium Flux in Rice Roots', *Rice*. Rice, 9(1), pp. 1–14. doi: 10.1186/s12284-016-0081-x.

Nomura, H. *et al.* (2012) 'Chloroplast-mediated activation of plant immune signalling in Arabidopsis', *Nature Communications*. Nature Publishing Group, 3(May), pp. 910–926. doi: 10.1038/ncomms1926.

Ordenes, V. R. *et al.* (2012) '*In vivo* analysis of the calcium signature in the plant Golgi apparatus

reveals unique dynamics', *Cell Calcium*. Elsevier Ltd, 52(5), pp. 397–404. doi: 10.1016/j.ceca.2012.06.008.

Ortiz-Ramírez, C. *et al.* (2017) 'GLUTAMATE RECEPTOR-LIKE channels are essential for chemotaxis and reproduction in mosses', *Nature*, pp. 91–95. doi: 10.1038/nature23478.

Palmer, A. E. *et al.* (2006) 'Ca*2+* Indicators Based on Computationally Redesigned Calmodulin-Peptide Pairs', *Chemistry and Biology*, 13(5), pp. 521–530. doi: 10.1016/j.chembiol.2006.03.007.

Peña-Cortés, H., Fisahn, J. and Willmitzer, L. (1995) 'Signals involved in wound-induced proteinase inhibitor II gene expression in tomato and potato plants.', *Proceedings of the National Academy of Sciences of the United States of America*, 92(10), pp. 4106–13. doi: 10.1073/pnas.92.10.4106.

Pérez Koldenkova, V. and Nagai, T. (2013) 'Genetically encoded Ca^{2+} indicators: Properties and evaluation', *Biochimica et Biophysica Acta - Molecular Cell Research*. Elsevier B.V., 1833(7), pp. 1787–1797. doi: 10.1016/j.bbamcr.2013.01.011.

Pittman, J. K. and Hirschi, K. D. (2016) 'CAX-ing a wide net: Cation/H(+) transporters in metal remediation and abiotic stress signalling', *Plant biology (Stuttgart, Germany)*, 18(5), pp. 741–749. doi: 10.1111/plb.12460.

Pittman, J. K., Shigaki, T. and Hirschi, K. D. (2005) 'Evidence of differential pH regulation of the Arabidopsis vacuolar Ca^{2+}/H^{+} antiporters CAX1 and CAX2', *FEBS Letters*, 579(12), pp. 2648–2656. doi: 10.1016/j.febslet.2005.03.085.

Pizzo, P. *et al.* (2011) 'Ca^{2+} signalling in the Golgi apparatus', *Cell Calcium*. Elsevier Ltd, 50(2), pp. 184–192. doi: 10.1016/j.ceca.2011.01.006.

Pottosin, I. I., Muñiz, J. and Shabala, S. (2005) 'Fast-activating channel controls cation fluxes across the native chloroplast envelope', *Journal of Membrane Biology*, 204(3), pp. 145–156. doi: 10.1007/s00232-005-0758-3.

Price, M. B., Jelesko, J. and Okumoto, S. (2012) 'Glutamate Receptor Homologs in Plants: Functions and Evolutionary Origins', *Frontiers in Plant Science*, 3(October), pp. 1–10. doi: 10.3389/fpls.2012.00235.

Qi, Z., Stephens, N. R. and Spalding, E. P. (2006) 'Calcium Entry Mediated by GLR3.3, an Arabidopsis Glutamate Receptor with a Broad Agonist Profile', *Plant Physiology*, 142(3), pp. 963–971. doi:

10.1104/pp.106.088989.

Ranf, S. *et al.* (2008) 'Loss of the vacuolar cation channel , AtTPC1 , does not impair Ca^{2+} signals induced by abiotic and biotic stresses', pp. 287–299. doi: 10.1111/j.1365-313X.2007.03342.x.

Rhodes, J. D., Thain, J. F. and Wildon, D. C. (1999) 'Evidence for physically distinct systemic signalling pathways in the wounded tomato plant', *Annals of Botany*, 84(1), pp. 109–116. doi: 10.1006/anbo.1999.0900.

Rienmller, F. *et al.* (2010) 'Guard cell-specific calcium sensitivity of high density and activity SV/TPC1 channels', *Plant and Cell Physiology*, 51(9), pp. 1548–1554. doi: 10.1093/pcp/pcq102.

Robinson, D. G. *et al.* (2015) 'Vesicles versus Tubes: Is Endoplasmic Reticulum-Golgi Transport in Plants Fundamentally Different from Other Eukaryotes?', *Plant Physiology*, 168(2), pp. 393–406. doi: 10.1104/pp.15.00124.

Ross, M. T. *et al.* (2005) 'The DNA sequence of the human X chromosome', *Nature*, 434(7031), pp. 325–337. doi: 10.1038/nature03440.

Roy, S. J. *et al.* (2008) 'Investigating glutamate receptor-like gene co-expression in *Arabidopsis thaliana*', *Plant, Cell and Environment*, 31(6), pp. 861–871. doi: 10.1111/j.1365-3040.2008.01801.x.

Ruge, H. *et al.* (2016) 'The calmodulin-like proteins AtCML4 and AtCML5 are single-pass membrane proteins targeted to the endomembrane system by an N-terminal signal anchor sequence', *Journal of Experimental Botany*, 67(13), pp. 3985–3996. doi: 10.1093/jxb/erw101.

Salvador-Recatalï¿½, V. (2016) 'New roles for the GLUTAMATE RECEPTOR-LIKE 3.3, 3.5, and 3.6 genes as on/off switches of wound-induced systemic electrical signals', *Plant Signaling and Behavior*, 11(4). doi: 10.1080/15592324.2016.1161879.

Sammels, E. *et al.* (2010) 'Intracellular Ca^{2+} storage in health and disease: A dynamic equilibrium', *Cell Calcium*. Elsevier Ltd, 47(4), pp. 297–314. doi: 10.1016/j.ceca.2010.02.001.

Schilmiller, A. L. and Howe, G. A. (2005) 'Systemic signaling in the wound response', *Current Opinion in Plant Biology*, 8(4), pp. 369–377. doi: 10.1016/j.pbi.2005.05.008.

Selles, B. *et al.* (2018) 'Arabidopsis pollen tube germination and growth depend on the mitochondrial calcium uniporter complex', *New Phytologist*, 219(1), pp. 58–65. doi: 10.1111/nph.15189.

Sello, S. *et al.* (2018) 'Chloroplast Ca^{2+} fluxes into and across thylakoids revealed by thylakoid-targeted aequorin probes', *Plant Physiology*, 177(May), p. pp.00027.2018. doi: 10.1104/pp.18.00027.

Shinoda, H., Shannon, M. and Nagai, T. (2018) 'Fluorescent Proteins for Investigating Biological Events in Acidic Environments', *International Journal of Molecular Sciences*, 19, p. 1548. doi: 10.3390/ijms19061548.

Shkolnik, D. *et al.* (2013) 'MIZ1 regulates ECA1 to generate a slow, long-distance phloem-transmitted Ca^{2+} signal essential for root water tracking in Arabidopsis', *PNAS*, pp. 6–11. doi: 10.1073/pnas.1804130115.

Sivankalyani, V. *et al.* (2012) 'Coping with stresses: roles of calcium- and calcium/calmodulin-regulated gene expression.', *The Plant cell*, 8(1), pp. 435–466. doi: 10.1105/tpc.111.084988.

Sobolevsky, A. I. (2015) 'Structure and gating of tetrameric glutamate receptors', *J. Physiology*, pp. 29–38. doi: 10.1113/jphysiol.2013.264911.

Stael, S. *et al.* (2012) 'Plant organellar calcium signalling: An emerging field', *Journal of Experimental Botany*, 63(4), pp. 1525–1542. doi: 10.1093/jxb/err394.

Stahlberg, R. and Cosgrove, D. J. (1997) 'The Propagation of Slow Wave Potentials in Pea Epicotyls', *Plant Physiology*, 113(1), pp. 209–217. doi: 10.1104/pp.113.1.209.

De Stefani, D. *et al.* (2011) 'A forty-kilodalton protein of the inner membrane is the mitochondrial calcium uniporter', *Nature*, 476(7360), pp. 336–340. doi: 10.1038/nature10230.

Stephan, A. B. *et al.* (2016) 'Rapid hyperosmotic-induced Ca^{2+} responses in *Arabidopsis thaliana* exhibit sensory potentiation and involvement of plastidial KEA transporters', *Proceedings of the National Academy of Sciences*, 113(35), pp. E5242–E5249. doi: 10.1073/pnas.1519555113.

Stephens, N. R., Qi, Z. and Spalding, E. P. (2007) 'Glutamate Receptor Subtypes Evidenced by Differences in Desensitization and Dependence on the GLR3.3 and GLR3.4 Genes', *Plant Physiology*, 146(2), pp. 529–538. doi: 10.1104/pp.107.108134.

Storti, M. *et al.* (2018) 'Systemic calcium wave propagation in *Physcomitrella patens*', *Plant and Cell Physiology*, 59(July), pp. 1377–1384. doi: 10.1093/pcp/pcy104/5033790.

Sukhov, V. *et al.* (2012) 'Analysis of the photosynthetic response induced by variation potential in

geranium', *Planta*, 235(4), pp. 703–712. doi: 10.1007/s00425-011-1529-2.

Sukhov, V. *et al.* (2013) 'Simulation of variation potential in higher plant cells', *Journal of Membrane Biology*, 246(4), pp. 287–296. doi: 10.1007/s00232-013-9529-8.

Sukhov, V. *et al.* (2014) 'Proton cellular influx as a probable mechanism of variation potential influence on photosynthesis in pea', *Plant Cell and Environment*, 37(11), pp. 2532–2541. doi: 10.1111/pce.12321.

Swarbreck, S. M., Colaco, R. and Davies, J. M. (2013) 'Plant Calcium-Permeable Channels', *Plant Physiology*, 163(2), pp. 514–522. doi: 10.1104/pp.113.220855.

Tang, R. J. and Luan, S. (2017) 'Regulation of calcium and magnesium homeostasis in plants: from transporters to signaling network', *Current Opinion in Plant Biology*. Elsevier Ltd, 39, pp. 97–105. doi: 10.1016/j.pbi.2017.06.009.

Tapken, D. *et al.* (2013) 'A Plant Homolog of Animal Glutamate Receptors Is an Ion Channel Gated by Multiple Hydrophobic Amino Acids', *Science Signalling*, pp. 1–11.

Tapken, D. and Hollmann, M. (2008) '*Arabidopsis thaliana* Glutamate Receptor Ion Channel Function Demonstrated by Ion Pore Transplantation', *Journal of Molecular Biology*, 383(1), pp. 36–48. doi: 10.1016/j.jmb.2008.06.076.

Teardo, E. *et al.* (2011) 'Dual localization of plant glutamate receptor AtGLR3.4 to plastids and plasmamembrane', *Biochimica et Biophysica Acta - Bioenergetics*. Elsevier B.V., 1807(3), pp. 359–367. doi: 10.1016/j.bbabio.2010.11.008.

Teardo, E. *et al.* (2015) 'Alternative Splicing-Mediated Targeting of the Arabidopsis GLUTAMATE RECEPTOR3.5 to Mitochondria Affects Organelle Morphology', *Plant Physiology*, 167(1), pp. 216–227. doi: 10.1104/pp.114.242602.

Teardo, E. *et al.* (2017) 'Physiological Characterization of a Plant Mitochondrial Calcium Uniporter *in Vitro* and *in Vivo*', *Plant Physiology*, 173(2), pp. 1355–1370. doi: 10.1104/pp.16.01359.

The Arabidopsis Genome Initiative (2000) 'Analysis of the genome sequence of the flowering plant *Arabidopsis thaliana*', *Nature*, 408(6814), pp. 796–815. doi: 10.1038/35048692.

Toyota, M. *et al.* (2018) 'Glutamate triggers long-distance, calcium-based plant defense signalling', *Science*, pp. 1112–1115.

Traynelis, S. F. *et al.* (2014) 'Glutamate Receptor Ion Channels : Structure , Regulation , and Function'. *Pharmacological Reviews*, doi: 10.1124/pr.109.002451.405.

Trewavas, A. *et al.* (1996) 'Transduction of Ca $^{2+}$ signals in plant cells and compartmentalization of the Ca^{2+} signal', *Biochemical Society Transactions*, 24(4), pp. 971–974. doi: 10.1042/bst0240971.

Turano, F. J. *et al.* (2001) 'The putative glutamate receptors from plants are related to two superfamilies of animal neurotransmitter receptors via distinct evolutionary mechanisms', *Molecular Biology and Evolution*, 18(7), pp. 1417–1420. doi: 10.1093/oxfordjournals.molbev.a003926.

Twomey, E. C. and Sobolevsky, A. I. (2018) 'Structural Mechanisms of Gating in Ionotropic Glutamate Receptors', *Biochemistry*, 57(3), pp. 267–276. doi: 10.1021/acs.biochem.7b00891.

Valerio, C. *et al.* (2011) 'Thioredoxin-regulated β-amylase (BAM1) triggers diurnal starch degradation in guard cells, and in mesophyll cells under osmotic stress', *Journal of Experimental Botany*, 62(2), pp. 545–555. doi: 10.1093/jxb/erq288.

Vanderauwera, S. *et al.* (2012) 'AtWRKY15 perturbation abolishes the mitochondrial stress response that steers osmotic stress tolerance in Arabidopsis', *Proceedings of the National Academy of Sciences*, 109(49), pp. 20113–20118. doi: 10.1073/pnas.1217516109.

Very, A.-A. and Davies, J. M. (2000) 'Hyperpolarization-activated calcium channels at the tip of Arabidopsis root hairs', *Proceedings of the National Academy of Sciences*, 97(17), pp. 9801–9806. doi: 10.1073/pnas.160250397.

Vincent, T. R. *et al.* (2017) 'Interplay of Plasma Membrane and Vacuolar Ion Channels, Together with BAK1, Elicits Rapid Cytosolic Calcium Elevations in Arabidopsis during Aphid Feeding', *The Plant Cell*, 29(June), p. tpc.00136.2017. doi: 10.1105/tpc.17.00136.

Vincill, E. D. *et al.* (2013) 'Interacting Glutamate Receptor-Like Proteins in Phloem Regulate Lateral Root Initiation in Arabidopsis', *The Plant Cell*, 25(4), pp. 1304–1313. doi: 10.1105/tpc.113.110668.

Vincill, E. D., Bieck, A. M. and Spalding, E. P. (2012) 'Ca^{2+} Conduction by an Amino Acid-Gated Ion Channel Related to Glutamate Receptors', *Plant Physiology*, 159(1), pp. 40–46. doi: 10.1104/pp.112.197509.

Vitale, A. (2001) 'The Endomembrane System and the Problem of Protein Sorting', *Plant Physiology*,

125(1), pp. 115–118. doi: 10.1104/pp.125.1.115.

Vodeneev, V. *et al.* (2012) 'The mechanism of propagation of variation potentials in wheat leaves', *Journal of Plant Physiology*. Elsevier GmbH., 169(10), pp. 949–954. doi: 10.1016/j.jplph.2012.02.013.

Vodeneev, V. A. *et al.* (2011) 'The role of Ca^{2+}, H^{+}, and Cl^{-} ions in generation of variation potential in pumpkin plants', *Russian Journal of Plant Physiology*, 58(6), pp. 974–981. doi: 10.1134/S1021443711050256.

Vodeneev, V. A., Opritov, V. A. and Pyatygin, S. S. (2006) 'Reversible changes of extracellular pH during action potential generation in a higher plant *Cucurbita pepo*', *Russian Journal of Plant Physiology*, 53(4), pp. 481–487. doi: 10.1134/S102144370604008X.

Vodeneev, V., Akinchits, E. and Sukhov, V. (2015) 'Variation potential in higher plants : Mechanisms of generation and propagation', (September), pp. 1–7.

Waadt, R. *et al.* (2017) 'Multiparameter imaging of calcium and abscisic acid and high-resolution quantitative calcium measurements using R-GECO1-mTurquoise in Arabidopsis', *New Phytologist*, 216(1), pp. 303–320. doi: 10.1111/nph.14706.

Waadt, R. and Kudla, J. (2008) 'In plant visualization of protein interactions using bimolecular fluorescence complementation (BiFC)', *Cold Spring Harbor Protocols*, 3(4). doi: 10.1101/pdb.prot4995.

Wagner, S. *et al.* (2015) 'The EF-Hand Ca^{2+} Binding Protein MICU Choreographs Mitochondrial Ca^{2+} Dynamics in Arabidopsis', *The Plant Cell*. doi: 10.1105/tpc.15.00509.

Wagner, S. *et al.* (2016) 'Regulation of mitochondrial calcium in plants versus animals', *Journal of Experimental Botany*, 67(13), pp. 3809–3829. doi: 10.1093/jxb/erw100.

Wang, W. H. *et al.* (2012) 'Calcium-sensing receptor regulates stomatal closure through hydrogen peroxide and nitric oxide in response to extracellular calcium in Arabidopsis', *Journal of Experimental Botany*, 63(1), pp. 177–190. doi: 10.1093/jxb/err259.

Wang, Y. *et al.* (2015) 'Cytosolic Ca^{2+} Signals Enhance the Vacuolar Ion Conductivity of Bulging Arabidopsis Root Hair Cells', *Molecular Plant*, 8(11), pp. 1665–1674. doi: 10.1016/j.molp.2015.07.009.

Wang, Y. *et al.* (2017) 'CNGC2 Is a Ca^{2+} Influx Channel That Prevents Accumulation of Apoplastic Ca^{2+} in the Leaf', *Plant Physiology*, 173(2), pp. 1342–1354. doi: 10.1104/pp.16.01222.

Winter, D. *et al.* (2007) 'An "electronic fluorescent pictograph" Browser for exploring and analyzing large-scale biological data sets', *PLoS ONE*, 2(8), pp. 1–12. doi: 10.1371/journal.pone.0000718.

Wu, Z. *et al.* (2002) 'An Endoplasmic Reticulum-Bound Ca^{2+}/Mn^{2+} Pump, ECA1, Supports Plant Growth and Confers Tolerance to Mn^{2+} Stress, *Plant Physiology*, pp. 128–137. doi: 10.1104/pp.004440.

Wudick, M. M. *et al.* (2018) 'CORNICHON sorting and regulation of GLR channels underlie pollen tube Ca^{2+} homeostasis', *Science*, pp. 533–536. doi: 10.1126/science.aar6464.

Xiong, T. C. *et al.* (2006) 'Calcium signaling in plant cell organelles delimited by a double membrane', *Biochimica et Biophysica Acta - Molecular Cell Research*, 1763(11), pp. 1209–1215. doi: 10.1016/j.bbamcr.2006.09.024.

Xiong, T. C. *et al.* (2014) 'Imaging long distance propagating calcium signals in intact plant leaves with the BRET-based GFP-aequorin reporter', *Frontiers in Plant Science*, 5(February), pp. 1–13. doi: 10.3389/fpls.2014.00043.

Yoo, S. D., Cho, Y. H. and Sheen, J. (2007) 'Arabidopsis mesophyll protoplasts: A versatile cell system for transient gene expression analysis', *Nature Protocols*, 2(7), pp. 1565–1572. doi: 10.1038/nprot.2007.199.

Zhang, B. *et al.* (2012) 'LETM proteins play a role in the accumulation of mitochondrially encoded proteins in Arabidopsis thaliana and AtLETM2 displays parent of origin effects', *Journal of Biological Chemistry*, 287(50), pp. 41757–41773. doi: 10.1074/jbc.M112.383836.

Zhao, Y. *et al.* (2013) 'The Actin-Related Protein2/3 Complex Regulates Mitochondrial-Associated Calcium Signaling during Salt Stress in Arabidopsis', *The Plant Cell*, 25(11), pp. 4544–4559. doi: 10.1105/tpc.113.117887.

Zhu, S. and Gouaux, E. (2017) 'Neuropharmacology Structure and symmetry inform gating principles of ionotropic glutamate receptors', *Neuropharmacology*. Elsevier Ltd, 112, pp. 11–15. doi: 10.1016/j.neuropharm.2016.08.034.

Zimmermann, M. R. *et al.* (2009) 'System Potentials, a Novel Electrical Long-Distance Apoplastic

Signal in Plants, Induced by Wounding', *Plant Physiology*, 149(3), pp. 1593–1600. doi: 10.1104/pp.108.133884.

Chapter VII: Appendix

primer name	locus	gene	sequence (5'-3')	description	orientation
AC280		UBIQUITIN10	CATGGGTACCGTCGACGAGTCAGTAATAAACG	Used to screen pUBQ10::GLR3.7-mCherry	forward
AC332	At2g32400	AtGLR3.7	catgCCATGGGACTGGGCATTGACCCAT	NcoI - pGreen0029-2x35S-YFP	forward
AC333	At2g32400	AtGLR3.7	catgCCATGGcATTTCGTGGTACCTCAGTA	NcoI - pGreen0029-2x35S-YFP	reverse
AC348	At5g44340	AtTUBULIN4	AGGGAAACGAAGACAGCAAG	Real-Time PCR (housekeeping gene)	forward
AC349	At5g44340	AtTUBULIN4	GCTCGCTAATCCTACCTTTGG	Real-Time PCR (housekeeping gene)	reverse
AC355	At2g32400	AtGLR3.7	TCCCCACTGTTGAAAAATTTG	*glr3.7-1* T-DNA insertion screening (SALK_022757)	forward
AC356	At2g32400	AtGLR3.7	TTGGAGGTACCGTGACTGTTC	*glr3.7-1* T-DNA insertion screening (SALK_022757)	reverse
AC400	At1g42540	AtGLR3.3	GAAACCAAAAGTTGTGAAAATCGGT	*glr3.3-1* and *glr3.3-2* T-DNA insertion screening (SALK_040458 and SALK_066009)	forward
AC401	At1g42540	AtGLR3.3	GACACATTGTCTCTTAGGTGGGCCT	*glr3.3-1* and *glr3.3-2* T-DNA insertion screening (SALK_040458 and SALK_066009)	reverse
AC402	At1g42540	AtGLR3.3	ACGTTGGGAAAAAGCGGAAA	Real-Time PCR	forward
AC403	At1g42540	AtGLR3.3	ACCATACGCGTTCCGAGGAT	Real-Time PCR	reverse
AC413			CATGGCGGCCGCTTATTTATATAATTCATCCAT	Annealing on mCherry And used to screen pUBQ10::GLR3.7-mCherry	reverse
OS857	At2g32400	AtGLR3.7	TCCTACATTGCGGTTGAGAGA	Real-Time PCR	forward
0S859	At2g32400	AtGLR3.7	GAGTCATCGCTTCTTCTGAACA	Real-Time PCR	reverse
AC441 (Lb1.3)			ATTTTGCCGATTTCGGAAC	Salk specific	left border
AC451	At2g32400	AtGLR3.7	TCTTCTGTCCGGATGAGTTTG	*glr3.7-2* T-DNA insertion screening (SALK_103942)	reverse
AC452	At2g32400	AtGLR3.7	CGAAGAAAGAAGGGAAATTGG	*glr3.7-2* T-DNA insertion screening (SALK_103942)	forward
AC509	At1g42540	AtGLR3.3	TTTGTTCAGATCATCCGTCAGC	Used to screen p35S::GLR3.3-eGFP	forward
AC510		GFP	GTCGTCCTTGAAGAAGATGGTG	Used to screen p35S::GLR3.3-eGFP	reverse

Appendix Table 1. List of primers used in this work with corresponding locus, gene, nucleotide sequence, description and orientation.